NAZARBAYEV
UNIVERSITY

Black Hole/Moving Mirror correspondence in (1+1)-dimensions

by

Aizhan Myrzakul

Submitted in partial fulfillment of the requirements for the degree of Doctor of Philosophy in Science, Engineering and Technology

Date of Completion
November, 2023

Black Hole/Moving Mirror correspondence in (1+1)-dimensions

by
Aizhan Myrzakul

Submitted in partial fulfillment of the requirements for the degree of
Doctor of Philosophy in Science, Engineering and Technology

School of Engineering and Digital Sciences
School of Sciences and Humanities
Nazarbayev University

November, 2023

Supervised by
Prof. Michael R.R. Good
Prof. Daniele Malafarina
Prof. Yen Chin Ong

Declaration

I, Aizhan Myrzakul, declare that the research contained in this thesis, unless otherwise formally indicated within the text, is the author's original work. The thesis has not been previously submitted to this or any other university for a degree and does not incorporate any material already submitted for a degree.

Signature: Aizhan Myrzakul

Date: 10 November 2023

BLANK

Abstract

The Hawking effect predicts that black holes can emit particles and energy when quantum mechanical effects are taken into account in quantum atmosphere around the black hole. However, certain models of black holes emit infinite energy and infinite particles that are contradictory to both classical and quantum theories' laws. These and other black hole evaporation problems along with the need to get experimental verification have underscored the need for analog and toy models that can solve the issues without losing the essential physical properties of the black hole radiation processes.

The significance of studying moving mirrors is that they are accelerated boundaries that create energy, particles, and entropy similar to black holes. In fact, moving mirrors, which are simplified (1+1)-dimensional versions of the dynamical Casimir effect, act as toy models for black hole evaporation, in some cases, with an exact correspondence to the amount of particle production. Moreover, the dynamical Casimir effect has been measured in the laboratory within the framework of moving mirror model providing experimental observations and insight into the effect, whereas Hawking radiation from black holes effectively can not be measured because the effect is too small.

The general and physically relevant connections of moving mirrors to black hole physics is a prime focus of this thesis. Here black holes and some cosmological models are approximated by (1+1)-dimensional moving mirrors. The detailed and complete investigation of all existing moving mirror models, their classifications and specific characters are the main objectives. This extensive study allows one to distinguish the moving mirror solutions that most physically describe black hole evaporation. They have proven capability to solve specific issues related to Hawking radiation. A new model related to the Schwarzschild black hole that solves the issue of finite energy with respect to Hawking radiation is developed. Also, it is established that Callan-Giddings-Harvey-Strominger (CGHS) black hole model has a correspondence to the exponentially accelerated moving mirror in coordinate time for the particle production. In addition, the mirror radiation power and radiation reaction force, that have recently been derived, have been applied to the specific moving mirror model of the CGHS correspondence. As a result, it is shown that Larmor power and self-force for the mirror describe quantum radiation. Furthermore, two distinct methods of deriving the stress tensor for the quantum radiation of the moving mirror are analyzed and a comparison analysis is made. Finally, while extensively studying all the known moving

mirror solutions and trying to compile collective results, some new results have been found, including some trajectories in null and spacetime coordinates, particle count for the mirrors that have finite particle production, fluxes for some mirrors in certain coordinates that have interesting physical effect, and etc.

All existing moving mirror solutions are studied by classification into several types based on their dynamics. Then, each mirror is extensively reviewed from four perspectives: dynamics, flux & energy, particles, and entropy. These methodologies enable one to obtain a complete set of solutions, understand their behavior, and unveil particular implications and physical features of the moving mirror model as a whole.

Acknowledgments

I would like to express deep gratitude to my main supervisor, Prof. Michael Good, for his great supervision. Particularly, I am thankful for his clear guidance, constant support and patience during my PhD study.

Contents

List of Figures

Chapter 1

Introduction

Exotic circumstances often surround those regions in nature where both gravity and quantum theories are required, such as the Big Bang and black hole singularities. It was long believed that at the classical level black holes can only absorb light and matter, and nothing could escape it after entering the event horizon. However, in the 1970s, Stephen Hawking proposed that black holes can also emit particles and energy when quantum mechanical effects are taken into account near the black hole event horizon region [1]. Such radiation of particles and energy from the black hole is called *Hawking radiation* or black hole evaporation. This discovery led to massive interest among researchers in black holes and related areas. However, there is a problem associated with the Hawking effect: information about the content of the black hole is dissipated during its evaporation, i.e. the radiation emitted by the black hole is random having no relation with information on absorbed light and matter. This is mostly referred to as *the black hole information loss paradox*. To be specific, certain models of black holes emit infinite energy and infinite particles that are contradictory to both classical and quantum theories' laws. These and other black hole evaporation problems along with the need to get experimental verification caused scientists to think of analog or toy models that can solve the issues without losing the essential physical properties of the black hole radiation process.

It was shown that moving mirrors can be treated as toy models for black hole evaporation since they are accelerated boundaries that create energy, particles, and entropy [2, 3]. Interesting in their own right, moving mirrors are simplified (1+1)-dimensional versions of the dynamical Casimir effect, that is considered to be the main starting point in the elaboration of the moving mirror model. For the historical purpose, the static case of the Casimir effect, that was proposed first, can be found in [4].

The development of the moving mirror model and its relationship to black holes evaporation are briefly reviewed here following some main works mostly in chronological order to make the understanding smooth.

1970s: One of the first works exploring particle emission caused by the moving mirrors was done by Moore [5]. This work studies propagation of light in one dimensional cavity bounded by two perfectly conducting parallel mirrors moving with timelike trajectories $z = f_1(t)$ and $z = f_2(t)$. The prime field of concern is a scalar field that is considered to be free in the sense that there is interaction only between propagating light and a mirror, i.e. no other external interactions. The number of created

photons is finite but very small.

Afterwards, Fulling considered quantization of the neutral scalar field in two-dimensional flat spacetime using specific notion of static metrics as described in [6]. As a result, it was demonstrated that when an external gravitational field is taken into account, Quantum field theory (QFT) has a specific problem with a definition of particles, i.e. it is different from the definition obtained in the Fock space. This difference has a direct consequence on the definition of the energy-momentum stress tensor, playing a significant role in quantum theory of matter near the Schwarzchild black hole horizon. Addressing the change of the energy-momentum tensor definition, Fulling also made a comparison with the results obtained by Casimir on electromagnetic field vacuum energy at different configurations of plates (mirrors) [4].

Quantum field theory in curved spacetime and black hole evaporation, since its inception in the 1970s, has matured to the level of well-known textbooks [7, 8], one of which is the book by DeWitt [9], who was the first to suggest the moving mirror model from a black hole prospective. This book significantly influenced how the moving mirror model was developed. DeWitt offered a very thorough work that is devoted to radiation emission and particle production processes by accelerating boundaries and black holes. Specifically, it is claimed that currents play a significant role in all field theories as they characterize interaction. The components of the stress tensor, in particular, have a role in such currents in the context of general relativity. Building the QFT in curved spacetime that enables better comprehension of the stress tensor is therefore the primary challenge. The main issue with the stress energy tensor here is occurrence of diverging terms, that are analyzed and addressed using some regularization techniques.

Thereafter, Fulling and Davies derived the mirror energy-momentum tensor using a point splitting method [2]. The non-diverging term in the derived expectation value of the stress tensor corresponds to the mirror energy flux, expressed in terms of the mirror trajectory. Another essential part of this work is devoted to the study of the mirror model that travels with constant acceleration through time. This mirror is found to have zero energy flux, i.e. no energy radiation.

Numerous facets of black holes evaporation are examined by Unruh in [10]. Particularly, he investigated a particle detector behavior and demonstrated that an accelerated observer will detect particles in the vacuum even in flat spacetime. This process is mainly referred to as the Unruh effect, where particles are created with the temperature similar to the moving mirror effect.

Following their previous work mentioned above, Davies and Fulling calculated the beta Bogolubov coefficient for the uniformly accelerated mirror [3]. The non-zero value of the coefficient indicates particles creation by the mirror. Also, another class of moving mirror trajectories that contain null asymptotes was investigated in this paper, where the associated energy flux was found to have constant thermal behavior.

1980s: In 1982, two types of asymptotically null trajectories were introduced: one produces the Planck spectrum at late times, whereas the another trajectory yields Bessel function distribution and results in vanishing energy flux, demonstrating unusual particle-energy relationship [11]. However, both of these models work only at certain time limits, and the second trajectory has additional requirements to be a physical model. Addressing some obstacles related to these mirror types, Walker and Davies proposed the moving mirror model that moves along an asymptotically static trajectory that has non-trivial radiation and is exactly solvable. The corresponding flux has a negative value at some point in time that, later on, was understood to be a requirement to have finite emitted energy. Also, the total number of created particles is found to be finite.

The further work providing some insight into particle-energy relationship within the moving mirror framework is given in [12]. Here other representations of the Bogolubov coefficients were provided, and their behavior at the high-frequency limit is studied. In addition, several mirror model examples were considered to show that even having non-trivial particle production, some of the trajectories might give zero or even negative energies. Moreover, Walker derived the formula for calculating the mirror energy using Bogolubov coefficient, that is consistent with the energy via the formula proposed by Fulling and Davies using mirror trajectory straightforwardly [2].

Continuing the work by Unruh and Wald [13], Walker also investigated negative energy flux radiated by the moving mirrors in curved spacetime [14]. He concluded that the flux as a function has the same dependence on the mirror trajectory in both flat and curved spaces. Namely, in this work the energy momentum tensor is derived in the form that allows to see what kind of mirror trajectories produce negative total energy. As an example, a moving mirror in the vacuum corresponding to a black hole in thermal equilibrium, i.e. the Hartle-Hawking vacuum, is considered.

Later on, Carlitz and Willey suggested a specific moving mirror trajectory that creates constant thermal flux over time and has exactly solvable Bogolubov coefficients [15]. This new trajectory allows to get the final quantum pure state without further approximations. The correlation functions of the energy momentum tensor are computed. Some properties of these correlation functions, including their relation to the Einstein-Podolsky-Rosen effect, are emphasized.

Another method of finding energy flux emitted by the moving mirrors is studied by Reuter in [16]. When the gravitational field is turned off, it is recognized that the central charge could be considered as a residue of the trace anomaly in some ways. Hawking radiation and the trace anomaly are comparable in the context of 2D gravitational collapse models utilizing the curved spacetime background [17]. Analogously, for flat spacetime Reuter proved that the radiation emitted by the moving mirror corresponds to the central charge that is not zero. So, the quantum stress-energy tensor of the mirror radiation is derived using Virasoro algebra with central charge, or Schwinger term.

However, it seems that this work has not received enough attention since its inception in 1989.

1990s: A general discussion on how the moving mirror can mimic black hole radiation is also provided by Wilczek in [18]. Specifically, he proposed a significant notion that the mirror corresponds to the center of the black hole, i.e. to $r = 0$ origin of space. Three possible scenarios of the mirror travel are explained. In addition, a precise mathematical relationship between the moving mirror model and collapse geometry is shown. In fact, this paper played a crucial role in the investigation of the possible moving mirror models and their analogies.

In 1994, a group of scientists found a specific mirror model that has event horizon and approaches a null infinity at an exponential rate [19]. This solution, later on referred to as the Arcx moving mirror, asymptotically attains the speed of light at some point in its' dynamics, emits corresponding thermal radiation with infinite energy and infinite particle production.

2000s: The generalization of the Davies-Fulling mirror addressing some issues related to this model was further investigated by Obadia and Parentani in [20]. Here two ways of solving the problems are considered. In the first approach, the Davies-Fulling model is expressed using kinematic terms. In the second approach, an alternative model derived using the action principle is proposed. The work in this direction was continued by the same authors in their following papers [21, 22].

2010s: Starting from 2010s, a considerable number of works investigating concrete moving mirror models, related aspects and some quantities of interest have been done by Good and et. al. In [23], authors, first, analyzed a well-known class of trajectories proposed by Carlitz-Willey and Walker-Davies, and then introduced some new mirror solutions such as Arctx, Darcx, Proex and Modified Carlitz-Willey. In [24], a temperature of the Kerr black hole is expressed in terms of the Schwarzschild black hole surface gravity and harmonic spring constant. This result plays a significant role in the further investigation of the Kerr black hole analog moving mirror model. Another new mirror model, originally called black mirror or black hole collapse mirror, corresponding to the black hole formation is proposed in [25, 26, 27, 28]. The drifting counterpart of this mirror is investigated in [29, 30, 31]. Asymptotically static mirror solutions such as self-dual and Good-Linder mirrors are introduced in [32] and [33], respectively. Furthermore, the drifting case of some mirror models are studied in [34, 35, 32].

The connection between black hole radiation and accelerating boundary radiation is especially evident for mirror trajectories that provide a continuous thermal flux of particles. In [36], novel methods for creating such thermal plateaus are explained. Also, straightforward formulas for the energy flux in terms of proper and null times are obtained.

The first analysis of entanglement harvesting between two detectors in the presence of mirrors in (1+1)D is conducted by Cong, Tjoa and Mann in [37]. They examined both static and non-inertial trajectories, with a focus on the Carlitz-Willey and black hole collapse mirrors, and offered a theoretical prediction of what to anticipate from entanglement detection in the presence of the dynamical Casimir effect.

2020s: There have been a number of studies in recent years investigating the relationship between certain black hole models and their analog moving mirrors, including Schwarzschild [27], Reissner-Nordström [38, 39], Kerr [40], their extremal limits [41, 42], Taub-NUT [43], CGHS [44]. A moving mirror is also used to represent de Sitter, anti-de Sitter [45] and Schwarzschild-de-Sitter [46] cosmologies. Moreover, there have been introduced some new types of moving mirrors with interesting features. These new models include Schwarzschild-Planck [47, 48, 49], Inertial Horizon [50], Dual-Temperature [51], and Light-Airy [52] mirrors.

Objective & methodology of the research. The detailed and complete investigation of the above mentioned moving mirror models, their classifications and specific characters are the prime objectives of the current dissertation. This extensive study allows us to distinguish the moving mirror solutions that most physically describe black hole evaporation process and can solve some issues related to Hawking radiation.

The methodology used is, first, all existing moving mirrors will be classified into several types: canonical, static, null, black hole null, extremal null, cosmo null, inertial null, and drifting ones. This classification is done based on the dynamics of the mirrors. After that, each mirror will be extensively reviewed from four perspectives: dynamics, flux & energy, particles, and entropy. These methodologies enable to obtain a complete set of quantities of interest, understand the behavior, and unveil particular implication and features of each mirror model.

Organization of the thesis. The dissertation is organized as follows: In Ch. (2) the basic elements of the quantum field theory in both flat and curved spacetimes are briefly reviewed. In Ch. (3) the general quantities of interest, that are used to investigate each mirror model in detail in the main part of the thesis, are derived. The basic derivations include dynamical quantities, quantum stress energy tensor (flux) via point-splitting and conformal anomaly methods, energy, particles, entropy, mirror Larmor power and self-force. In the main part of the thesis, Ch. (4), all existing moving mirror models are studied comprehensively using the methodologies mentioned above. The summary of the thesis work, and some insights into future directions are provided in conclusion, Ch. (5).

BLANK

Chapter 2

Elements of Quantum Field Theory

In this chapter, the basic notions of quantization of the field in flat and curved spacetimes are briefly reviewed. The flat spacetime case is discussed first in order to better understand the quantization in the curved background.

2.1 Quantization in flat spacetime

Let us start from the simplest action with a massless scalar field [8],

$$S = -\frac{1}{2}\int d^4x \partial_\mu\phi\partial^\mu\phi, \tag{2.1}$$

whose corresponding equation of motion is the Klein-Gordon equation,

$$\partial_\mu\partial^\mu\phi = 0. \tag{2.2}$$

In order to perform a quantization, a solution to the above equation of motion is written as a sum of frequency modes of the field ϕ,

$$\phi(t,\vec{x}) = \sum_i \left[a_i\phi_i(t,\vec{x}) + a_i^\dagger\phi_i^*(t,\vec{x})\right]. \tag{2.3}$$

Here t is a global inertial time of Minkowski background, which means

$$\frac{\partial}{\partial t}\phi_j(t,\vec{x}) = -i\omega_j\phi_j(t,\vec{x}), \tag{2.4}$$

where ω_j is positive. The solutions $\phi_i(t,\vec{x})$ form orthonormal basis such that the scalar product is,

$$(\phi_1,\phi_2) = -i\int d^3\vec{x}\left(\phi_1\partial_t\phi_2^* - \phi_2^*\partial_t\phi_1\right). \tag{2.5}$$

Eq. (2.5) enables one to perform one-particle Hilbert space as the above scalar product is positively defined on the positive frequency solutions space. Then it is possible to construct many-particle Fock space. To demonstrate that, one starts from the commutation relations between creation and annihilation operators,

$$[a_i, a_j^\dagger] = (\phi_i,\phi_j)\hbar = \delta_{ij}\hbar, \tag{2.6}$$

$$[a_i, a_j] = [a_i^\dagger, a_j^\dagger] = 0. \tag{2.7}$$

For the quantum case similar commutation relations read as,

$$[\psi(t,\vec{x}),\pi(t,\vec{x})] = i\hbar\delta^3(\vec{x}-\vec{x}'), \tag{2.8}$$

$$[\psi(t,\vec{x}),\psi(t,\vec{x}')] = [\pi(t,\vec{x}),\pi(t,\vec{x}')] = 0. \tag{2.9}$$

where ψ is a quantum field operator now and $\pi = \partial_t\psi$. Acting on the vacuum state with the annihilation operators results in building the Fock space,

$$a_i|0\rangle = 0, \tag{2.10}$$

whereas acting on the vacuum with the creation operators spans one-particle Hilbert space,

$$\hbar^{-\frac{1}{2}}a_i^\dagger|0\rangle = |1_i\rangle. \tag{2.11}$$

Then, the many-particle states are performed as,

$$\left(n^{(1)}!n^{(2)}!...n^{(k)}!\right)^{-\frac{1}{2}}\left(\hbar^{-\frac{1}{2}}a_{i1}^\dagger\right)^{n^{(1)}}\left(\hbar^{-\frac{1}{2}}a_{i2}^\dagger\right)^{n^{(2)}}...\left(\hbar^{-\frac{1}{2}}a_{ik}^\dagger\right)^{n^{(k)}}|0\rangle = |n_{i1}^{(1)},n_{i2}^{(2)},...,n_{ik}^{(k)}\rangle. \tag{2.12}$$

The plane wave modes in solution (2.3) are chosen such that they form the orthonormal basis,

$$\phi_{\vec{\kappa}} \equiv \frac{1}{\sqrt{16\pi^3\omega}}e^{-i\omega t+i\vec{\kappa}\vec{x}}, \tag{2.13}$$

where $\omega = |\vec{\kappa}|$. Then the commutation relations (2.6) and (2.7) are written in terms of the vector $\vec{\kappa}$ as,

$$[a_{\vec{\kappa}},a_{\vec{\kappa}'}^\dagger] = \hbar\delta^3(\vec{\kappa}-\vec{\kappa}'), \tag{2.14}$$

$$[a_{\vec{\kappa}},a_{\vec{\kappa}'}] = [a_{\vec{\kappa}}^\dagger,a_{\vec{\kappa}'}^\dagger] = 0. \tag{2.15}$$

So, quantization has a key feature: it does not depend on time. This means Eq. (2.3), i.e. splitting the solution into positive and negative modes, is invariant with respect to time. As a result, the vacuum state and the corresponding Fock space are also invariant.

2.2 Quantization in curved spacetime

Adopting the notation in [8], the quantization in curved spacetime is implemented by generalising the concepts introduced in the previous section. The generalization is needed as the Poincare symmetry does not work in the curved spacetime case, so the steps given in the Minkowski case can not be applied directly. For this reason, the following extensions are done:

- The equation of motion now reads as,

$$\Box\phi = 0, \tag{2.16}$$

  where $\Box \equiv \nabla_\mu\nabla^\mu$ is a d'Alembertian operator.

- The scalar product is written as,

$$(\phi_1, \phi_2) = -i \int\limits_{\sum} d\sum (\phi_1 \partial_\mu \phi_2^* - \phi_2^* \partial_\mu \phi_1) \,. \tag{2.17}$$

  Here $\sum$ is a Cauchy hypersurface.

In quantization for the curved background, one can not easily split the solution into positive and negative frequency modes as in the flat spacetime case. In the curved spacetime, choosing different positive frequency solutions results in different vacuum state and, as a consequence, also in different Fock space. Nevertheless, there exist situations when it becomes possible to naturally choose positive frequency solutions. This happens when the curved background is stationary, or is asymptotically stationary in the early or late times. Such places in space are denoted as "in" and "out" regions. Then the corresponding solutions with positive frequencies are denoted as u_i^{in} and u_i^{out}.

Apparently, the initial vacuum state is in the "in" region, so it is denoted as $|in\rangle$. The final vacuum state is reached when the geometry of the system finally settles down to the static configuration again. It is crucial to note that in the Fock space the $|in\rangle$ vacuum state is not typically considered to be the same vacuum state as in the "out" region. The mathematical formalism of this phenomenon is given via the Bogolubov transformations that are discussed below.

Let us start from the expansion of the massless field ϕ for the initial state as,

$$\phi = \sum_i \left[a_i^{in} \phi_i^{in} + a_i^{in\dagger} \phi_i^{in*} \right]. \tag{2.18}$$

Alternatively, for the final stationary state the field can be expanded as,

$$\phi = \sum_i \left[a_i^{out} \phi_i^{out} + a_i^{out\dagger} \phi_i^{out*} \right]. \tag{2.19}$$

The positive frequency modes u_i^{in} obey orthonormality relations,

$$\left(\phi_i^{in}, \phi_j^{in} \right) = \delta_{ij}, \tag{2.20}$$

$$\left(\phi_i^{in*}, \phi_j^{in*} \right) = -\delta_{ij}, \tag{2.21}$$

$$\left(\phi_i^{in}, \phi_j^{in*} \right) = 0. \tag{2.22}$$

Similar to the commutation relations (2.6) and (2.7), for the operators in the initial stationary state one has,

$$[a_i^{in}, a_j^{in\dagger}] = \hbar \delta_{ij}, \tag{2.23}$$

$$[a_i^{in}, a_j^{in}] = [a_i^{in\dagger}, a_j^{in\dagger}] = 0. \tag{2.24}$$

The same relations are applied to the u_i^{out} modes. So, it is possible now to define one mode in terms of another one as,

$$\phi_j^{out} = \sum_i (\alpha_{ji} \phi_i^{in} + \beta_{ji} \phi_i^{in*}), \tag{2.25}$$

$$\phi_i^{in} = \sum_j (\alpha_{ji}^* \phi_j^{out} - \beta_{ji} \phi_j^{out*}), \tag{2.26}$$

where α_{ij} and β_{ij} are the Bogolubov coefficients, and Eqs. (2.25) and (2.26) are called the Bogolubov transformations. Here Eq. (2.26) is obtained by inverting Eq. (2.25). In terms of the scalar product between different frequency modes, the Bogolubov coefficients are defined as,

$$\alpha_{ij} = \left(\phi_i^{out}, \phi_j^{in}\right), \tag{2.27}$$

$$\beta_{ij} = -\left(\phi_i^{out}, \phi_j^{in*}\right), \tag{2.28}$$

where the matrices α_{ij} and β_{ij} satisfy the relations,

$$\sum_\kappa (\alpha_{i\kappa} \alpha_{j\kappa}^* - \beta_{i\kappa} \beta_{j\kappa}^*) = \delta_{ij}, \tag{2.29}$$

$$\sum_\kappa (\alpha_{i\kappa} \beta_{j\kappa} - \beta_{i\kappa} \alpha_{j\kappa}) = 0. \tag{2.30}$$

Using $a_i^{in} = (\phi, u_i^{in})$ and $a_i^{out} = (\phi, u_i^{out})$, it is possible now to express one ladder operator in terms of another one as,

$$a_i^{in} = \sum_j (\alpha_{ji} a_j^{out} + \beta_{ji}^* a_j^{in\dagger}), \tag{2.31}$$

$$a_i^{out} = \sum_j (\alpha_{ij}^* a_j^{in} - \beta_{ij}^* a_j^{in\dagger}), \tag{2.32}$$

where

$$a_i^{in} |in\rangle = 0, \tag{2.33}$$

$$a_i^{out} |out\rangle = 0. \tag{2.34}$$

Here the initial $|in\rangle$ and final $|out\rangle$ vacuum states are not the same, as long as the β_{ij} Bogolubov coefficients do not vanish. This can be verified by evaluating the expectation value of the particle count operator in the "out" region,

$$N_i^{out} \equiv \frac{1}{\hbar} a_i^{out\dagger} a_i^{out}. \tag{2.35}$$

Then for the initial vacuum state the expectation value is defined as,

$$\langle in | N_i^{out} | in \rangle = \frac{1}{\hbar} \langle in | a_i^{out\dagger} a_i^{out} | in \rangle = \frac{1}{\hbar} \langle in | \sum_j (-\beta_{ij} a_j^{in}) \sum_\kappa (-\beta_{i\kappa}^* a_\kappa^{in\dagger}) | in \rangle = \sum_j |\beta_{ij}|^2. \tag{2.36}$$

So, the non-trivial particle content of the $|in\rangle$ state is determined in the "out" Fock space if the beta Bogolubov coefficients do not vanish. Otherwise, if all β_{ij} are zero, then Eq. (2.29) reduces to,

$$\sum_\kappa \alpha_{i\kappa} \alpha_{j\kappa}^* = \delta_{ij}. \tag{2.37}$$

This condition means that $|in\rangle = |out\rangle$, i.e. the initial and final vacuum states are the same since the modes u_i^{in} and u_i^{out} are related via unitary matrix α_{ij}.

So, one way of describing particle emission resulting from the moving mirror is done via using the Bogolubov transformation. The exact integrals for calculating the beta Bogolubov coefficients $\beta_{\omega\omega'}$ for the moving mirror model are provided in the next chapter, Sec. (3.5).

BLANK

Chapter 3

Basics of Moving Mirror Model

Starting from this chapter, we use natural units $G = \hbar = c = 1$ throughout the thesis.

3.1 Dynamics

The dynamics of the moving mirror is described via several important quantities such as trajectories in different coordinates, i.e. spacetime (x, t) and null (u, v), velocity of the mirror, corresponding proper acceleration, and rapidity. The relation between spacetime and null coordinates are given as follows [8, 29],

$$u \equiv t - x(t), \tag{3.1}$$

$$v \equiv t + x(t), \tag{3.2}$$

where $x(t)$ is trajectory of a mirror in t time coordinate, u is retarded time, and v is advanced time. The inverse function of $x(t)$, which is $t(x)$, gives the trajectory in space coordinate x. These trajectories are also related as,

$$\dot{x}(t) = \frac{dx}{dt} = \left[\frac{dt}{dx}\right]^{-1} = (t')^{-1}, \tag{3.3}$$

where the prime represents a derivative with respect to x coordinate. The ray-tracing or shock functions of the mirror are defined as,

$$p(u) = 2t(u) - u, \tag{3.4}$$

$$f(v) = 2t(v) - v. \tag{3.5}$$

Here $t(u)$ and $t(v)$ are found from inverting t in terms of (u, v) in Eqs. (3.1) and (3.2). On the other hand, the ray-tracing functions and null coordinates are related as,

$$p(u) \equiv v, \tag{3.6}$$

$$f(v) \equiv u, \tag{3.7}$$

from which one can deduce that,

$$\frac{dp}{du} = \frac{dv}{df} = (f')^{-1}, \tag{3.8}$$

where the prime in this case represents a derivative with respect to v coordinate.

Another significant coordinate to describe the moving mirror is proper time τ, which is defined as,

$$d\tau^2 = dt^2 - dx^2. \tag{3.9}$$

The procedure of defining $x(\tau)$ trajectory is given in [36]. First, let us start from the $x(t)$ trajectory of the mirror, then find the Lorentz factor,

$$\gamma(t) = \frac{1}{\sqrt{1-\dot{x}^2}}. \tag{3.10}$$

Next, using the relation between proper and coordinate times, the $\tau(t)$ function is obtained,

$$\tau(t) = \int \frac{dt}{\gamma(t)}, \tag{3.11}$$

where the inverse of Eq. (3.11) yields $t(\tau)$. Applying it to $x(t)$ function leads to the trajectory in proper time, $x(\tau)$.

Let us now derive the rapidity of the mirror in different coordinates [34, 36]. In terms of t coordinate it is defined as,

$$\eta(t) = \tanh^{-1}\dot{x}(t). \tag{3.12}$$

Using this and Eq. (3.3), the expression for $\eta(x)$ is found trivially. More interesting is to find the rapidity in null coordinates. For that, one needs to use the definition of the inverse hyperbolic tangent function,

$$\tanh^{-1} z = \frac{1}{2}\ln\frac{1+z}{1-z}, \tag{3.13}$$

and find the first derivative of the $p(u)$ trajectory as,

$$p' = \frac{dp}{du} = \frac{d(t+x)}{d(t-x)} = \frac{d(t+x)}{dt}\frac{dt}{d(t-x)} = \frac{1+\dot{x}}{1-\dot{x}}. \tag{3.14}$$

Then applying these definitions into Eq. (3.12) yields the rapidity in terms of u coordinate,

$$\eta(u) = \frac{1}{2}\ln p'(u). \tag{3.15}$$

Using this and Eq. (3.8), the rapidity in terms of v coordinate is defined as,

$$\eta(v) = -\frac{1}{2}\ln f'(v). \tag{3.16}$$

In order to find the rapidity in proper time, $\eta(\tau)$, we first need to find proper velocity, or celerity, as $w(\tau) \equiv \frac{dx(\tau)}{d\tau}$, then

$$\eta(\tau) = \sinh^{-1} w(\tau). \tag{3.17}$$

The expressions (3.15) and (3.16) can also be derived using the Lorentz transformations in null coordinates, i.e.

$$u' = e^{-\eta}u, \tag{3.18}$$

$$v' = e^{\eta} v. \tag{3.19}$$

Next, expressing $p'(u)$ and $f'(v)$ in terms of η gives,

$$\frac{dp(u)}{du} = e^{2\eta} \tag{3.20}$$

$$\frac{df(v)}{dv} = e^{-2\eta}. \tag{3.21}$$

Now defined for both spacetime and null coordinates, the rapidity can be written in terms of general mirror velocity as,

$$\eta = \tanh^{-1}(V). \tag{3.22}$$

Another important quantity of interest is proper acceleration. In time coordinate, it is defined as,

$$\alpha(t) = \gamma^3 \ddot{x}(t), \tag{3.23}$$

where $\gamma(t)$ is the Lorentz factor, and $\ddot{x}(t)$ is a coordinate acceleration. Using Eq. (3.3), the proper acceleration in space coordinate x is defined as,

$$\alpha(x) = \gamma'(x), \tag{3.24}$$

where $\gamma(x) = \frac{t'}{\sqrt{t'^2 - 1}}$ now is a Lorentz factor of space. The proper accelerations in null and proper time coordinates are,

$$\alpha(u) = \eta'(u) e^{-\eta(u)}, \tag{3.25}$$

$$\alpha(v) = \eta'(v) e^{\eta(v)}, \tag{3.26}$$

and

$$\alpha(\tau) = \frac{d\eta(\tau)}{d\tau}. \tag{3.27}$$

It is worth mentioning that some moving mirror models are well defined in both spacetime and null coordinates. However, some trajectories might not be tractable in certain coordinates, or it is very complicated to do so.

Geometrically, the dynamics of the moving mirrors is demonstrated with the help of the Penrose (conformal) and spacetime diagrams. The spacetime diagram is a usual interpretation of the trajectory that might not give sufficient information about the behavior of the mirror. In this regard, the Penrose diagram [53, 8] is an elegant way of demonstrating the trajectory that, in turn, could provide more information on the dynamics of the mirror.

3.2 Quantum stress tensor via regularization

In this section the quantum energy-momentum tensor of the moving mirror is reviewed following the method by Fulling and Davies [2, 3]. The stress energy tensor in (1+1)-dimensional flat spacetime is defined by the following 2×2 matrix,

$$T_{\mu\nu} = \frac{1}{2}\begin{bmatrix} \left(\frac{\partial\phi}{\partial t}\right)^2 + \left(\frac{\partial\phi}{\partial x}\right)^2 & \frac{\partial\phi}{\partial x}\frac{\partial\phi}{\partial t} + \frac{\partial\phi}{\partial t}\frac{\partial\phi}{\partial x} \\ \frac{\partial\phi}{\partial t}\frac{\partial\phi}{\partial x} + \frac{\partial\phi}{\partial x}\frac{\partial\phi}{\partial t} & \left(\frac{\partial\phi}{\partial t}\right)^2 + \left(\frac{\partial\phi}{\partial x}\right)^2 \end{bmatrix}. \tag{3.28}$$

Here $\phi(t, x)$ is the massless scalar field which obeys the following wave equation,

$$\frac{\partial^2\phi}{\partial t^2} - \frac{\partial^2\phi}{\partial x^2} = 0, \tag{3.29}$$

as well as satisfies the following boundary condition,

$$\phi(t, x)|_{x=x(t)} = 0, \tag{3.30}$$

where $x = x(t)$ is the mirror ray-tracing function. In the usual quantum field theory, $\phi(t, x)$ is an operator determined by field modes as,

$$\phi(t, x) = \int_0^\infty \left[\hat{a}_\omega^{in}\phi_\omega + \hat{a}_\omega^{in\dagger}\phi_\omega^*\right] d\omega. \tag{3.31}$$

Here $\hat{a}_\omega$, $\hat{a}_\omega^\dagger$ are annihilation and creation operators, respectively, and ϕ_ω^* is a complex conjugate of ϕ_ω. After inserting Eq. (3.31) into the matrix Eq. (3.28), the energy-momentum tensor can be written as,

$$T_{\mu\nu} =: T_{\mu\nu} : + \langle T_{\mu\nu}|T_{\mu\nu}\rangle\,, \tag{3.32}$$

where the first term has normal ordering of the ladder operators, i.e.

$$: \hat{a}_\omega^{in}\hat{a}_\omega^{in\dagger} := \hat{a}_\omega^{in\dagger}\hat{a}_\omega^{in}. \tag{3.33}$$

The second term in Eq. (3.32) is the expectation value of the operator in vacuum, which is determined as follows,

$$\langle T_{\mu\nu}|T_{\mu\nu}\rangle = \int_0^\infty T_{\mu\nu}(\phi_\omega, \phi_\omega^*)d\omega. \tag{3.34}$$

As it is, the stress energy tensor is of crucial interest. However, the aforementioned integral is divergent. To make it finite and retrieve significant information about the emitted radiation, point-splitting regularization is used. The main aim is to evaluate the field modes at different times: ϕ at (t, x) and ϕ^* at $(t+\epsilon, x)$, where ϵ is an infinitesimally small quantity. Then the field modes at these points:

$$\begin{cases} \frac{\partial\phi_\omega}{\partial t} \\ \frac{\partial\phi_\omega}{\partial x} \end{cases} = \sqrt{\frac{\omega}{4\pi}}\left[e^{-i\omega v} \mp p'(u)e^{-i\omega p(u)}\right], \tag{3.35}$$

$$\begin{cases} \frac{\partial\phi^*_\omega}{\partial t} \\ \frac{\partial\phi^*_\omega}{\partial x} \end{cases} = \sqrt{\frac{\omega}{4\pi}}\left[e^{i\omega(v+\epsilon)} \mp p'(u+\epsilon)e^{i\omega p(u+\epsilon)}\right], \tag{3.36}$$

where $p(u) \equiv 2t(u) - u$ and $u \equiv t - x(t)$. Inserting Eqs. (3.35) and (3.36) into Eq. (3.34) leads to,

$$\begin{cases} \langle T_{00}|T_{00}\rangle = \langle T_{11}|T_{11}\rangle \\ \langle T_{10}|T_{10}\rangle = \langle T_{01}|T_{01}\rangle \end{cases} = \frac{1}{4\pi}\int_0^\infty \omega\left[e^{i\omega\epsilon} \pm \frac{p'(u)p'(u+\epsilon)}{e^{-i\omega(p(u+\epsilon)-p(u))}}\right]d\omega. \tag{3.37}$$

Calculation of the above integrals results in,

$$\begin{cases} \langle T_{00}|T_{00}\rangle \\ \langle T_{01}|T_{01}\rangle \end{cases} = -\frac{1}{4\pi\epsilon^2} \mp \frac{1}{4\pi}\frac{p'(u)p'(u+\epsilon)}{[p(u)-p(u+\epsilon)]^2}. \tag{3.38}$$

Consequently,

$$\langle T_{00}|T_{00}\rangle = -\frac{1}{2\pi\epsilon^2} - \langle T_{01}|T_{01}\rangle. \tag{3.39}$$

The result for $\langle T_{01}|T_{01}\rangle$ in Eq. (3.38) is Taylor expanded in ϵ to give,

$$\langle T_{01}|T_{01}\rangle = \frac{1}{24\pi}\left[\frac{p'''}{p'} - \frac{3}{2}\left(\frac{p''}{p'}\right)^2\right] + O(\epsilon). \tag{3.40}$$

When $\epsilon \to 0$, the first term in Eq. (3.39) becomes divergent, whereas the second term does not vanish like the higher order terms as it is independent of ϵ. So, the second term has special physical meaning: it corresponds to the energy flux radiated by the mirror into the vacuum,

$$\langle T_{00}|T_{00}\rangle = F(u) = -\frac{1}{24\pi}\left[\frac{p'''}{p'} - \frac{3}{2}\left(\frac{p''}{p'}\right)^2\right], \tag{3.41}$$

which characterizes the amplified quantum fluctuations due to the presence of the moving mirror.

Using the relations between spacetime and null coordinates, Eqs. (3.1)-(3.5), as well as Eq. (3.14), the energy flux can also be expressed with care, using straightforward differential algebra,

$$F(t) = \frac{\dddot{x}(\dot{x}^2-1) - 3\dot{x}\ddot{x}^2}{12\pi(\dot{x}+1)^2(\dot{x}-1)^4}, \tag{3.42}$$

$$F(x) = \frac{t'''(t'^2-1) - 3t't''^2}{12\pi(t'+1)^2(t'-1)^4}, \tag{3.43}$$

$$F(v) = \frac{1}{24\pi}\left[\frac{f'''}{f'} - \frac{3}{2}\left(\frac{f''}{f'}\right)^2\right]\frac{1}{f'^2}. \tag{3.44}$$

Using Eq. (3.20) and inserting it into Eq. (3.41), it is also possible to express the flux in terms of rapidity as [36],

$$F(u) = \frac{1}{12\pi}\left[\eta'(u)^2 - \eta''(u)\right]. \tag{3.45}$$

Using Eqs. (3.25) and (3.27), one can deduce the relation between u and τ coordinates, $\frac{d\tau}{du} = e^{\eta}$, which allows rewriting Eq. (3.45) in terms of proper time,

$$F(\tau) = -\frac{1}{12\pi}\eta''(\tau)e^{2\eta(\tau)}. \tag{3.46}$$

Overall, the above defined fluxes are used to find the total emitted energy by mirrors. Also, a graphical illustration of the energy flux can tell us if the mirror is in thermal equilibrium or has dynamical behavior.

3.3 Quantum stress tensor via conformal anomaly

In this section, another method of finding particle flux emitted by the moving mirror is studied. When the gravitational field is turned off, it is recognized that the central charge could be considered as a residue of the trace anomaly in some ways. Hawking radiation and trace anomaly are comparable in the context of 2D gravitational collapse models utilizing a curved spacetime background [17]. Analogously, for the flat spacetime, Reuter proved that the radiation emitted by the moving mirror corresponds to the central charge that is not zero. So, here the quantum stress-energy tensor of the mirror radiation is derived using the Virasoro algebra with central charge, or Schwinger term [16].

Following notations by Fabbri [8], let us start with the massless scalar field ϕ that is expanded in terms of plane wave modes as,

$$\phi(u,v) = \int_0^\infty \left(\hat{a}_\omega \phi_\omega + \hat{a}_\omega^\dagger \phi_\omega^*\right) d\omega, \tag{3.47}$$

where

$$\phi_\omega(u,v) = \frac{1}{\sqrt{4\pi\omega}}\left(e^{-i\omega v} + e^{-i\omega u}\right). \tag{3.48}$$

The two-point function then is,

$$\langle 0|\phi(u,v)\phi(u',v')|0\rangle = \int_0^\infty \frac{d\omega}{4\pi\omega}\left[e^{-i\omega(v-v')} + e^{-i\omega(u-u')}\right], \tag{3.49}$$

where $\left[\hat{a}_\omega, \hat{a}_{\omega'}^\dagger\right] = \delta(\omega-\omega')$, $[\hat{a}_\omega, \hat{a}_{\omega'}] = \left[\hat{a}_\omega^\dagger, \hat{a}_{\omega'}^\dagger\right] = 0$, and Eq. (3.49) is divergent. This infrared (IR) divergence is removed by introducing a small cut-off as,

$$\langle 0|\phi(u,v)\phi(u',v')|0\rangle = \int_\lambda^\infty \frac{d\omega}{4\pi\omega}\left[e^{-i\omega(v-v')} + e^{-i\omega(u-u')}\right]. \tag{3.50}$$

The solution of Eq. (3.50) then is,

$$\langle 0|\phi(u,v)\phi(u',v')|0\rangle = -\frac{1}{4\pi}\left(2\gamma + \ln\lambda^2\,|(u-u')(v-v')|\right). \tag{3.51}$$

Here γ - Euler constant. The IR cut-off λ in Eq. (3.51) vanishes when considering the correlation of the field ϕ, i.e. $\partial_u\phi \equiv \partial_u\phi(u)$ and $\partial_v\phi \equiv \partial_v\phi(v)$. As a result,

$$\langle 0|\partial_u\phi(u)\partial_u\phi(u')|0\rangle = -\frac{1}{4\pi}\frac{1}{(u-u')^2}, \tag{3.52}$$

and

$$\langle 0|\partial_v\phi(v)\partial_v\phi(v')|0\rangle = -\frac{1}{4\pi}\frac{1}{(v-v')^2}. \tag{3.53}$$

From the definition of the quantum energy momentum tensor operator, Eq. (3.32), one needs to find normal ordered stress tensor operator,

$$: T_{\mu\nu} := T_{\mu\nu} - \langle T_{\mu\nu}\rangle. \tag{3.54}$$

Here $T_{\mu\nu}$ is determined as,

$$T_{uu} = \left(\frac{\partial\phi}{\partial u}\right)^2 = (\partial_u\phi)^2\,, \qquad T_{vv} = \left(\frac{\partial\phi}{\partial v}\right)^2 = (\partial_v\phi)^2\,. \tag{3.55}$$

Since the procedures for both u and v are the same, from now on let us focus on u component of the field. Note that Eq. (3.52) is, in turn, the quantum energy momentum tensor operator expectation value in the state $|0\rangle$. So, substituting Eq. (3.52) and Eq. (3.55a) into Eq. (3.54), one gets

$$: T_{uu}(u) :\equiv \lim_{u'\to u}\partial_u\phi(u)\partial_u\phi(u') + \frac{1}{4\pi}\frac{1}{(u-u')^2}. \tag{3.56}$$

Let us now introduce the conformal transformation $u \to p(u)$. Analogously, for a new coordinate $p(u)$ Eq. (3.56) can be rewritten as,

$$: T_{uu}(p(u)) :\equiv \lim_{p'\to p}\partial_u\phi(p)\partial_u\phi(p') + \frac{1}{4\pi}\frac{1}{(p-p')^2}. \tag{3.57}$$

The relation between Eqs. (3.56) and (3.57) is found as,

$$: \partial_u\phi(p(u))\partial\phi(p'(u)) := \frac{du}{dp}(p)\frac{du}{dp}(p')\partial_u\phi(u)\partial_u\phi(u') + \frac{1}{4\pi}\frac{1}{(p-p')^2}. \tag{3.58}$$

Inserting Eq. (3.58) into Eq. (3.57) gives,

$$: T_{uu}(p) := \left(\frac{du}{dp}(p)\right)^2 : T_{uu}(u) : -\frac{1}{4\pi}\left(\lim_{p'\to p}\frac{\frac{du}{dp}(p)\frac{du}{dp}(p')}{(u(p)-u(p'))^2} - \frac{1}{(p-p')^2}\right). \tag{3.59}$$

The limit in the above equation can be calculated by expanding $u(p)$ in the Taylor series as,

$$u(p') = u(p) + \frac{du}{dp}(p)(p'-p) + \frac{1}{2!}\frac{d^2u}{dp^2}(p)(p'-p)^2 + \frac{1}{3!}\frac{d^3u}{dp^3}(p)(p'-p)^3 + ... \tag{3.60}$$

Inserting this finite expansion into Eq. (3.59) and using some algebraic manipulations, one has

$$: T_{uu}(p) := \left(\frac{du}{dp}\right)^2 : T_{uu}(u) : -\frac{1}{24\pi}\{u,p\}\,. \tag{3.61}$$

Here

$$\{u,p\} = \frac{d^3u}{dp^3}/\frac{du}{dp} - \frac{3}{2}\left(\frac{d^2u}{dp^2}/\frac{du}{dp}\right)^2 \tag{3.62}$$

is the Schwarzian derivative that can also be rewritten as,

$$\{p,u\} = -\left(\frac{dp}{du}\right)^2 \{u,p\}. \tag{3.63}$$

It is worth mentioning that under conformal transformations, the stress tensor transforms covariantly as,

$$T_{uu}(p) = \left(\frac{du}{dp}\right)^2 T_{uu}(u), \tag{3.64}$$

i.e. it obeys the classical transformation law, whereas the normal ordering violates this law, Eq. (3.61). The second term in Eq. (3.61), which is responsible for conformal symmetry breaking, is called the Virasoro anomaly. This is the reason why static and accelerating mirrors are not invariant under conformal transformations [16].

Alternatively, Eq. (3.61) can also be rewritten in terms of unitary operator as,

$$UT_{uu}(p)U^\dagger = \left(\frac{du}{dp}\right)^2 T_{uu}(u) - \frac{1}{24\pi}\{u,p\}, \tag{3.65}$$

where for an infinitesimal conformal transformation $u \to u + \epsilon(\epsilon)$, the unitary operator is defined as,

$$U = \exp\left(-i\int du\epsilon(u)T_{uu}(u)\right). \tag{3.66}$$

Under this unitary transformation the stress energy tensor transforms as,

$$UT_{uu}(u)U^\dagger = T_{uu}(u) + \delta T_{uu}(u), \tag{3.67}$$

where

$$\delta T_{uu}(u) = \epsilon(u)T'_{uu}(u) + 2\epsilon'(u)T_{uu}(u) + \frac{1}{24\pi}\epsilon'''(u). \tag{3.68}$$

In order to derive the quantum energy momentum tensor or energy flux using the above mentioned conformal transformation anomaly, one needs to evaluate the expectation value of the stress tensor operator of the static mirror with trajectory $p(u) = u$ or $x(t) = 0$ at all times t in vacuum, i.e. $\langle vac|T^0_{uu}|vac\rangle$, where $T^0_{uu} \equiv (\partial_u\phi_0)^2$. So, if for a general mirror trajectory $p(u)$ one has,

$$\frac{\partial\phi(u)}{\partial u} = ip'(u)\int_0^\infty \sqrt{\frac{\omega}{4\pi}}\left[\hat{a}_\omega e^{-i\omega p(u)} - \hat{a}^\dagger_\omega e^{i\omega p(u)}\right]d\omega, \tag{3.69}$$

then, for $p(u) = u$ trajectory, the above derivative reduces to,

$$\frac{\partial\phi_0(u)}{\partial u} = i\int_0^\infty \sqrt{\frac{\omega}{4\pi}}\left(\hat{a}_\omega e^{-i\omega u} - \hat{a}^\dagger_\omega e^{i\omega u}\right)d\omega. \tag{3.70}$$

Taking into account Eqs. (3.69) and (3.70), let us proceed to the evaluation of the vacuum expectation value of the stress energy tensor operator,

$$\langle vac|T_{uu}(u)|vac\rangle = (p'(u))^2\langle vac|T^0_{uu}(p(u))|vac\rangle = (p'(u))^2\langle 0|UT^0_{uu}(p(u))U^\dagger|0\rangle, \tag{3.71}$$

where $|0\rangle \equiv U|vac\rangle$. Using Eq. (3.65), one gets

$$UT^0_{uu}(p(u))U^\dagger = (p'(u))^{-2}\, T^0_{uu}(u) + \frac{1}{24\pi}\{u;p\}. \tag{3.72}$$

Substituting Eq. (3.72) into Eq. (3.71), and taking into account Eq. (3.63), one has

$$\langle vac|T_{uu}(u)|vac\rangle = \langle 0|T^0_{uu}(u)|0\rangle - \frac{1}{24\pi}\{p;u\}. \tag{3.73}$$

The first term in the above expression vanishes as it gives the vacuum expectation value of the stress tensor corresponding to the $p(u) = u$ trajectory, i.e. the static mirror case. As a result, Eq. (3.73) reduces to,

$$\langle vac|T_{uu}(u)|vac\rangle = -\frac{1}{24\pi}\{p;u\} = -\frac{1}{24\pi}\left[\frac{p'''}{p'} - \frac{3}{2}\left(\frac{p''}{p'}\right)^2\right], \tag{3.74}$$

which is exactly the same result that was obtained by Davies and Fulling using the point-splitting method, Eq. (3.41). So, Reuter derived the mirror quantum stress tensor using conformal anomaly of the corresponding tensor under conformal transformations, whereas Davies and Fulling used regularization or point-splitting technique. In both methods, there is a cost to pay: in the first case the infrared divergence is removed artificially by introducing a small cut-off, while in the second case the divergent terms in the pre-final expression for the stress tensor are neglected and only the term that does not have divergence is left.

3.4 Energy

The total emitted energy is calculated as a sum of the left and right moving mirrors. However, as in the most previously studied works on this topic, here we also assume that there is only one mirror moving to the left. So, the energy detected by the observer on the right side of the mirror, can be calculated analytically as [29],

$$E = \int_{-\infty}^{+\infty} F(u)du, \tag{3.75}$$

$$E = \int_{-\infty}^{+\infty} F(v)f'dv, \tag{3.76}$$

$$E = \int_{-\infty}^{+\infty} F(t)(1-\dot{z})dt, \tag{3.77}$$

$$E = \int_{+\infty}^{-\infty} F(x)(t'-1)dx. \tag{3.78}$$

After integrating by parts and ignoring boundary terms due to asymptotic inertial character, Eqs. (3.75)-(3.78) are reduced to,

$$E = \frac{1}{48\pi}\int_{-\infty}^{+\infty}\left(\frac{p"}{p'}\right)^2 du, \tag{3.79}$$

$$E = \frac{1}{48\pi}\int_{-\infty}^{+\infty}\frac{f''^2}{f'^3}dv, \tag{3.80}$$

$$E = \frac{1}{12\pi}\int_{-\infty}^{+\infty}\frac{\ddot{z}^2}{(1+\dot{z})^2(1-\dot{z})^3}dt, \tag{3.81}$$

$$E = \frac{1}{12\pi}\int_{-\infty}^{+\infty}\frac{t''^2}{(1+t')^2(1-t')^3}dx. \tag{3.82}$$

The total energy calculated via the flux using above integrals characterizes the radiation energy of the mirror. On the other hand, the energy of particles can be calculated using the beta Bogolubov coefficients, which is discussed in the following section. In both cases, the energy gives the same numerical result.

3.5 Particles

In this section, the exact integrals for calculating the beta Bogolubov coefficients for the moving mirror model are provided. Using the definitions (3.1) and (3.2), the line element in null coordinates reads as,

$$ds^2 = dudv. \tag{3.83}$$

Then the Klein-Gordon equation takes the form,

$$\partial_u\partial_v\phi = 0. \tag{3.84}$$

Since the massless sclar field ϕ satisfies the accelerating boundary condition, Eq. (3.30), the field mode solutions to the above plane wave equation are given as,

$$\phi_\omega^{in} = \frac{1}{\sqrt{4\pi\omega}}\left[e^{-i\omega v} - e^{-i\omega p(u)}\right], \tag{3.85}$$

$$\phi_\omega^{out} = \frac{1}{\sqrt{4\pi\omega}}\left[e^{-i\omega f(v)} - e^{-i\omega u}\right]. \tag{3.86}$$

For the null coordinates (u, v), the integral form of the beta Bogolubov coefficient, Eq. (2.28), reads as [8],

$$\beta_{\omega\omega'} = -i\int_{-\infty}^{\infty}\phi_{\omega'}^{in}\overleftrightarrow{\partial_u}\phi_\omega^{out}du, \tag{3.87}$$

$$\beta_{\omega\omega'} = -i\int_{-\infty}^{\infty}\phi_{\omega'}^{in}\overleftrightarrow{\partial_v}\phi_\omega^{out}dv. \tag{3.88}$$

Applying the modes (3.85) and (3.86) to Eqs. (3.87) and (3.88), one obtains the exact integrals for the beta Bogolubov coefficients in terms of different trajectories and coordinates as [29],

$$\beta_{\omega\omega'} = \frac{1}{4\pi\sqrt{\omega\omega'}}\int_{-\infty}^{\infty}e^{-i\omega u - i\omega' p(u)}\left(\omega'\frac{dp(u)}{du} - \omega\right)du, \tag{3.89}$$

$$\beta_{\omega\omega'} = -\frac{1}{4\pi\sqrt{\omega\omega'}}\int_{-\infty}^{\infty}e^{-i\omega' v - i\omega f(v)}\left(\omega\frac{df(v)}{dv} - \omega'\right)dv, \tag{3.90}$$

$$\beta_{\omega\omega'} = \frac{1}{4\pi\sqrt{\omega\omega'}} \int_{-\infty}^{\infty} e^{-i\omega_p t + i\omega_n z(t)} \left(\omega_p \frac{dz(t)}{dt} - \omega_n \right) dt, \tag{3.91}$$

$$\beta_{\omega\omega'} = -\frac{1}{4\pi\sqrt{\omega\omega'}} \int_{\infty}^{-\infty} e^{i\omega_n x - i\omega_p t(x)} \left(\omega_n \frac{dt(x)}{dx} - \omega_p \right) dx, \tag{3.92}$$

where $\omega_p \equiv \omega + \omega'$ and $\omega_n \equiv \omega - \omega'$. The last two integrals for the spacetime coordinates are obtained by substituting (u, v) coordinates using their definitions as in Eqs. (3.1) and (3.2). When the horizon is at $v_H = 0$, then the beta coefficients can be simplified as,

$$\beta_{\omega\omega'} = \frac{1}{2\pi} \sqrt{\frac{\omega'}{\omega}} \int_{-\infty}^{v_H} e^{-i\omega' v - i\omega f(v)} dv. \tag{3.93}$$

The particle spectrum is found through the following integration,

$$\left\langle N_\omega \right\rangle \equiv \left\langle 0_{in} | N_\omega^{out} | 0_{in} \right\rangle = \int_0^\infty |\beta_{\omega\omega'}|^2 d\omega'. \tag{3.94}$$

The energy emitted for the right and left sides is defined as,

$$E_R = \int_0^\infty \int_0^\infty \omega \cdot |\beta_{\omega\omega'}|^2 d\omega d\omega', \tag{3.95}$$

$$E_L = \int_0^\infty \int_0^\infty \omega' \cdot |\beta_{\omega\omega'}|^2 d\omega d\omega', \tag{3.96}$$

So, the total energy is the sum of energies from both right and left sides. The total particle count to the right is found as,

$$N_R = \int_0^\infty \int_0^\infty |\beta_R|^2 d\omega d\omega', \tag{3.97}$$

whereas for both right and left sides, its sum is calculated as,

$$N_T = \int_0^\infty \int_0^\infty |\beta_T|^2 d\omega d\omega'. \tag{3.98}$$

Note that the particle count can be evaluated only for the mirrors that have finite particle emission.

3.6 Entropy

There are different interpretations of the entropy of a system. In the framework of the moving mirror model, the entropy, or information defining quantity, is defined as the rapidity of the mirror. So, the von Neumann entanglement entropy for the mirror can be found from Bianchi-Smerlak's formula as [54, 32],

$$S(u) = -\frac{1}{12} \ln p'(u) = -\frac{1}{6} \eta(u). \tag{3.99}$$

Using Eq. (3.8), the entropy as a function of null advanced time coordinate is expressed as,

$$S(v) = \frac{1}{12} \ln f'(v) = \frac{1}{6} \eta(v). \tag{3.100}$$

In terms of the mirror trajectory in spacetime coordinate this is [34],

$$S(t) = -\frac{1}{6}\tanh^{-1}[\dot{z}(t)] = -\frac{1}{6}\eta(t). \tag{3.101}$$

The entropy in terms of space coordinate, $S(x)$, is found by applying Eq. (3.3) to Eq. (3.101). Obviously, the faster the mirror travels, the greater the entropy. The information is not lost when entropy is constant at early and late times, or does not diverge over all times. Another interesting method of deriving the mirror entropy, Eq. (3.99), can be found in [44].

3.7 Larmor power

In this section, the generalization of the classical relativistic Larmor power and radiation reaction from electrodynamics to the quantum relativistic radiation power and self-force of the moving mirror is derived. To do so, the radiation of the mirror for both sides is considered. The energy, emitted to the right and left sides, in terms of the acceleration, is [23],

$$E^R = \frac{1}{12\pi}\int_{-\infty}^{\infty}\alpha^2(1+\dot{z})dt, \tag{3.102}$$

$$E^L = \frac{1}{12\pi}\int_{-\infty}^{\infty}\alpha^2(1-\dot{z})dt, \tag{3.103}$$

where the energy radiated to the left is obtained by the symmetry $\dot{z} \to -\dot{z}$. Then the total energy is,

$$E = E^R + E^L = \frac{1}{6\pi}\int_{-\infty}^{\infty}\alpha^2 dt. \tag{3.104}$$

Using the classical relation between energy and power, $E = \int P dt$, and the right side of Eq. (3.104), the formula for the mirror radiation power is obtained,

$$P = \frac{\alpha^2}{6\pi}. \tag{3.105}$$

Using acceleration-rapidity relation, Eq. (3.27), and rapidity-entropy relations as given in Sec. (3.6), the mirror radiation power can also be expressed as,

$$P = \frac{\eta'^2(\tau)}{6\pi}, \tag{3.106}$$

and

$$P = \frac{6}{\pi}S'^2(\tau). \tag{3.107}$$

A comprehensive discussion on the mirror radiation power and its derivation can be found in [44, 55]. It is worth mentioning that Eq. (3.105), the mirror Larmor power, is given in natural units here for consistency with the whole discussions in the thesis. However, in SI units it is found that the mirror Larmor power has quantum relativistic nature, which is verified by applying Eq. (3.105) to the CGHS moving mirror model (see Sec. IX in [44]).

3.8 Self-force

In this section, the radiation reaction force, in other words, the self-force, is derived within the moving mirror framework by two distinct ways. The first method is based on using the mirror Larmor power defined in the previous section. The second method is based on using the energy flux of the moving mirror.

Let us start from the first approach, which uses the mirror radiation reaction power averaged over proper time [44],

$$\overline{F_{sf}} = -\frac{\overline{\eta'^2(\tau)}}{6\pi}, \tag{3.108}$$

where "-" sign indicates that the work done on the mirror is equal to the negative energy loss in the vacuum during radiation. Using the definition of the derivative, it is possible to write,

$$\eta'^2 = \frac{d}{d\tau}(\eta\eta') - \eta\eta''. \tag{3.109}$$

Here the first term that corresponds to the total derivative vanishes because of averaging procedure. Then Eq. (3.108) is rewritten as,

$$\overline{F_{sf}} = \frac{\overline{\eta\eta''(\tau)}}{6\pi}, \tag{3.110}$$

from which

$$F_{sf} = \frac{\eta''(\tau)}{6\pi}. \tag{3.111}$$

Using the definition of the proper acceleration as in Eq. (3.27), Eq. (3.111) is expressed as,

$$F_{sf} = \frac{\alpha'(\tau)}{6\pi}. \tag{3.112}$$

So, this mirror self-force is in accordance with the mirror radiation reaction force derived by Ford and Velenkin in [56].

Let us now turn to the second derivation of the mirror self-force by starting with the definition of energy in terms of flux in retarded time u for the right moving mirror,

$$E^R = \int_{-\infty}^{\infty} F(u)du, \tag{3.113}$$

where $F(u)$ is given as in Eq. (3.41). Inserting the flux in terms of proper time, Eq. (3.46), into Eq. (3.113), and using the Jacobian, $du = e^{-\eta}d\tau$, one gets,

$$E^R = -\frac{1}{12\pi}\int_{-\infty}^{\infty} \eta'' e^{\eta} d\tau. \tag{3.114}$$

Analogously, the energy for the left moving mirror is,

$$E^L = \frac{1}{12\pi}\int_{-\infty}^{\infty} \eta'' e^{-\eta} d\tau. \tag{3.115}$$

Using the difference in energy between left and right sides of the mirror and the time component of the flux, one obtains

$$\Delta U = U^L - U^R = \int_{-\infty}^{\infty} F^t d\tau, \tag{3.116}$$

where

$$F^t = \frac{dU}{d\tau} = \frac{dU}{dx}\frac{dx}{d\tau} = F \sinh\eta = F\omega. \tag{3.117}$$

Using the space component of the flux, the energy difference is,

$$\Delta \mathcal{U} = \mathcal{U}^L - \mathcal{U}^R = \int_{-\infty}^{\infty} F^x d\tau, \tag{3.118}$$

where

$$F^x = \frac{\eta^{''}}{12\pi}[e^{-\eta} - (-e^{\eta})] = \frac{\eta^{''}}{6\pi}\cosh\eta = F\gamma. \tag{3.119}$$

So, the 4-vector mirror self-force is,

$$F^\mu = (F^t, F^x) = (\omega F, \gamma F), \tag{3.120}$$

and the magnitude of the force is,

$$F = \sqrt{F^{t2} - F^{x2}} = \frac{\eta^{''}}{6\pi}, \tag{3.121}$$

which is the same as Eq. (3.111). More details on the derivation of the mirror self-force and related discussions can be found in [44].

Chapter 4

Specific Cases: Complete Solutions

There are 30 known moving mirror solutions at the moment with globally defined continuous trajectories and solved beta coefficients. These solutions are categorized into several distinct classifications based on their dynamical behavior and similar radiation scenarios. The main citations for all the moving mirror models are provided below for convenience.

Canonical mirrors

Davies-Fulling [2], [3], [7], [32], [36].

Uniform acceleration [2], [3], [20], [21], [22], [19], [7], [8], [57].

Carlitz-Willey [15], [23], [18], [19], [32], [27], [58].

Schwarzschild [57], [25], [26], [28], [27], [59], [29].

Asymptotically Static mirrors

Walker-Davies [11], [23], [57].

Arctx [23].

Self-dual [32], [36].

Good-Linder [33].

Schwarzschild-Planck [47, 60, 48, 49].

Asymptotically Null mirrors

Logex [34].

Evans [23].

Dual-Temperature [51].

Black Hole Null mirrors

CGHS [19], [61], [23], [44].

Reissner-Nordström [38, 39].

Kerr [40].

Taub-NUT [43].

Extremal Null mirrors

Reissner-Nordström [62], [41].

Kerr [63], [40].

Kerr-Newman [42].

Cosmo Null mirrors

de Sitter [45].

Anti de Sitter [45].

Schwarzschild de Sitter [46, 64, 65]

Inertial Null mirrors

Proex [23].

Inertial Horizon [50].

Light-Airy [52].

Asymptotically Drifting mirrors

Drifting Omex [29], [30], [31], [59].

Drifting Arcx [19], [23].

Drifting Proex [23], [35].

Drifting Logex [34].

Drifting Davies-Fulling [36].

4.1 Canonical

There are 4 beta-known canonical moving mirror models:

- Davies-Fulling
- Uniform acceleration
- Eternal thermal
- Schwarzschild

All four models are the first studied moving mirrors, which have demonstrated several significant physical insights.

The Davies-Fulling (DF) mirror produces thermal radiation in future time, confirming a strong relationship between black hole thermal emission at late time and moving mirror radiation.

The uniformly accelerated (UA) mirror reveals a weakening of the particle and energy definitions in evaporation, producing non-zero particle emission while emitting zero energy.

The Carlitz-Willey (CW), or eternal thermal, mirror emits constant energy flux over all times with Planck distribution of particles and constant temperature. It exemplifies the basic difference between moving mirrors and the Unruh phenomenon (constant acceleration with constant temperature).

The Schwarzschild mirror (Sch), or the black hole collapse mirror, has one-to-one correspondence with the black hole as some quantities, such as the beta Bogolubov coefficients, have the same form in both cases.

The first three mirrors in this case attain the speed of light in the asymptotic past and future. The exception is the Schwarzschild mirror that starts off its movement statically. And those mirrors that move to the speed of light have total particle and energy emission that is infinite. Thermal radiation occurs in the Davies-Fulling (late-times), Carlitz-Willey (all times) and Schwarzschild (late-times) cases, while the Uniform acceleration mirror has a unique non-Planckian spectrum. Moreover, the DF, CW and Sch mirrors go to infinite acceleration in the far future, while the UA mirror has constant acceleration over time.

Throughout the thesis, κ is a positively defined quantity within a mirror model that has a unit of acceleration in natural units, i.e. $\hbar = c = 1$. The graphs are plotted with $\kappa = 1$ since its value does not affect the general physical properties of the system.

4.1.1 Davies-Fulling

DF: Dynamics

One of the first moving mirror models, that was introduced by Davies and Fulling, is described by the following trajectory [2, 3, 36, 7],

$$x(t) = -\frac{1}{\kappa}\ln[\cosh(\kappa t)], \tag{4.1}$$

whose dynamics is depicted in Fig. (4.1). The trajectory has a symmetric behaviour

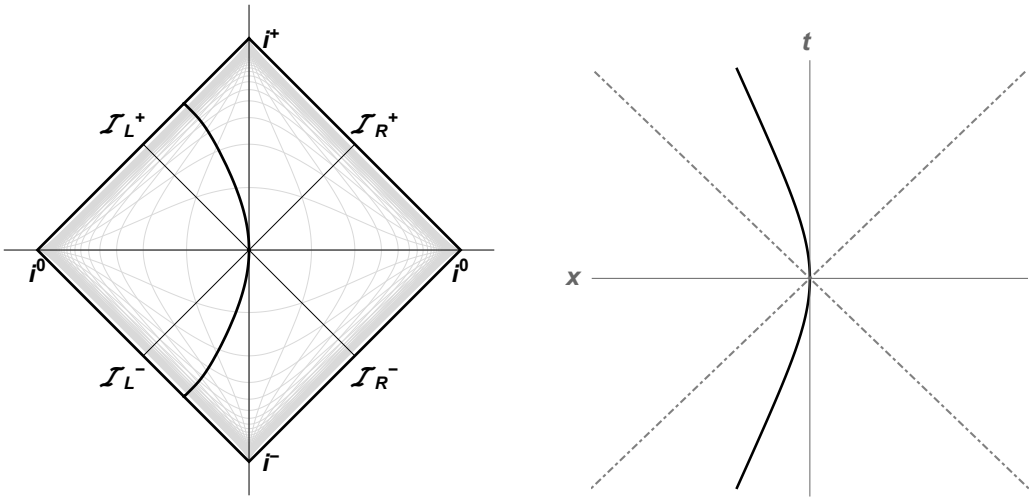

Figure 4.1: a) Penrose and b) Spacetime diagrams for the Davies-Fulling mirror trajectory.

with respect to the space coordinate x. The derivative of the trajectory with respect to time gives its velocity,

$$\dot{x}(t) = -\tanh(\kappa t), \tag{4.2}$$

which in the limit $t \to \pm\infty$ goes to the speed of light, i.e. $\dot{x}(t) = |V| \to 1$. Using Eqs. (4.1) and (3.1)-(3.7), the ray-tracing functions in null coordinates and proper time as well as the transcendental inversion are defined as,

$$p(u) = \frac{1}{\kappa}\ln\left(2 - e^{-\kappa u}\right), \tag{4.3}$$

$$f(v) = -\frac{1}{\kappa}\ln\left(2 - e^{\kappa v}\right), \tag{4.4}$$

$$t(x) = \frac{1}{\kappa}\cosh^{-1}\left(e^{-\kappa x}\right), \tag{4.5}$$

where $u > -\frac{\ln 2}{\kappa}$ and $v < \frac{\ln 2}{\kappa}$. Using Eqs. (4.1)-(4.5) and (3.23)-(3.27), the corresponding accelerations are,

$$\alpha(t) = -\kappa\cosh(\kappa t), \qquad \alpha(x) = -\kappa e^{-\kappa x}, \qquad \alpha(\tau) = -\kappa\sec(\kappa\tau). \tag{4.6}$$

The asymptotic expansion of Eq. (4.6c) around $\tau = \frac{\pi}{2\kappa}$ to the leading order yields $\alpha(\tau) = \frac{1}{\tau - \frac{\pi}{2\kappa}} + O\left(\tau - \frac{\pi}{2\kappa}\right)$. So, $\alpha(\tau)$ has scale dependent piece that is a function of where the horizon is located, i.e. if $v_H = 0$, then $\alpha(\tau) = 1/\tau$.

DF: Energy

Using Eqs. (4.1) and (3.42), the flux of the Davies-Fulling, or null-self-dual, mirror is found to be,

$$F(t) = \frac{\kappa^2}{12\pi} \frac{\tanh(\kappa t)}{[\tanh(\kappa t) + 1]^2}. \tag{4.7}$$

The graphical illustration of Eq. (4.7) is demonstrated in Fig. (4.2).

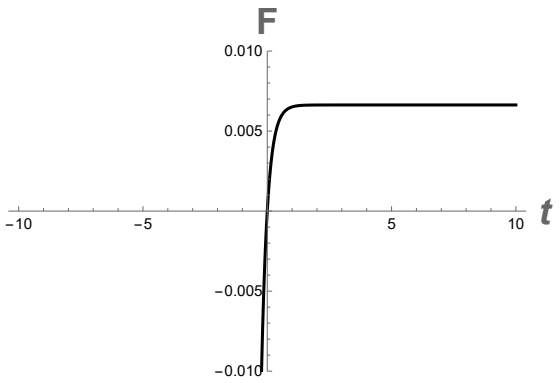

Figure 4.2: Davies-Fulling mirror energy flux.

The flux ascends at early times, then it becomes thermal at late times. The integration of the flux using Eqs. (3.75)-(3.78) gives divergent integral, meaning that the total energy emission is infinite.

DF: Particles

Using Eqs. (4.4a) and (3.89), the beta Bogolubov coefficient for the Davies-Fulling mirror is,

$$\beta_{\omega\omega'} = -\frac{2^{\frac{i\omega_n}{\kappa}}\sqrt{\omega\omega'}\,\mathrm{csch}\left(\frac{\pi\omega'}{\kappa}\right)}{2\kappa^2}\frac{\Gamma\left[\frac{i\omega}{\kappa}\right]}{\Gamma\left[1+\frac{i\omega_n}{\kappa}\right]\Gamma\left[1+\frac{i\omega'}{\kappa}\right]}, \tag{4.8}$$

where $\omega_n \equiv \omega - \omega'$, and $\Gamma[n]$ is the Gamma function. Taking complex conjugate squaring of Eq. (4.8) yields,

$$|\beta_{\omega\omega'}|^2 = \frac{\omega\omega'\,\mathrm{csch}^2\left(\frac{\pi\omega'}{\kappa}\right)}{4\kappa^4}\left|\frac{\Gamma\left[-\frac{i\omega}{\kappa}\right]}{\Gamma\left[1-\frac{i\omega_n}{\kappa}\right]\Gamma\left[1-\frac{i\omega'}{\kappa}\right]}\right|^2. \tag{4.9}$$

In the $\omega' \gg \omega$ limit (late times), Eq. (4.9) reduces to [3, 7],

$$|\beta_{\omega\omega'}|^2 = \frac{1}{2\pi\kappa\omega'}\frac{1}{e^{2\pi\omega/\kappa}-1}. \tag{4.10}$$

Using Eqs. (4.9) and (3.94), the numerical result for the DF mirror particle spectrum is demonstrated in Fig. (4.3).

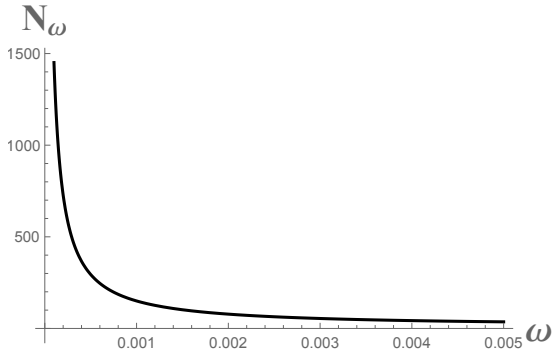

Figure 4.3: Davies-Fulling mirror particle spectrum.

The particle spectrum of the DF mirror obeys Planck distribution at late times and is infra-red divergent, i.e. there is infinite particle production.

DF: entropy

Using Eqs. (4.2) and (3.101), the entanglement entropy of the Davies-Fulling mirror simply is,

$$S(t) = \frac{\kappa t}{6}. \tag{4.11}$$

The graphical illustration of Eq. (4.11) is given in Fig. (4.4).

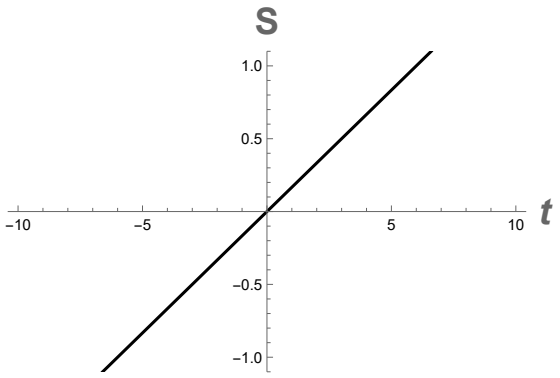

Figure 4.4: Davies-Fulling mirror entropy.

The entropy diverges in the $t \to \pm\infty$ limits, i.e. in both past and future times. This means that unitarity is not preserved.

The static and drifting cases of the Davies-Fulling mirror are investigated in further sections, Sec. (4.2.3) and Sec. (4.8.5).

4.1.2 Uniform acceleration

UA: Dynamics

Another class of firstly introduced moving mirrors is characterized by constant acceleration at all times, and travels along a hyperbolic path. A particular such model is described by the following trajectory [2, 3, 7, 57],

$$x(t) = \frac{1}{\kappa} - \sqrt{t^2 + \frac{1}{\kappa^2}}, \tag{4.12}$$

whose dynamics is depicted in Fig. (4.5). Similar to the Davies-Fulling mirror case,

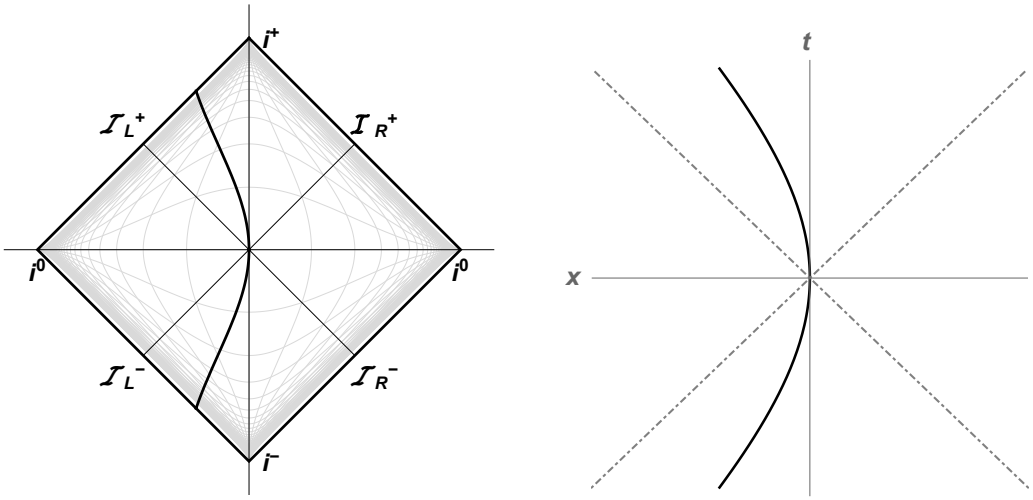

Figure 4.5: a) Penrose and b) Spacetime diagrams for the uniformly accelerated mirror trajectory.

the trajectory of the UA mirror has a symmetric behaviour with respect to the space coordinate x. The derivative of the trajectory with respect to time gives its velocity,

$$\dot{x}(t) = -\frac{\kappa t}{\sqrt{\kappa^2 t^2 + 1}}, \tag{4.13}$$

which in the limit $t \to \pm\infty$ goes to the speed of light, i.e. $\dot{x}(t) = |V| \to 1$. Using Eqs. (4.12) and (3.1)-(3.7), the ray-tracing functions in null coordinates and proper time as well as the transcendental inversion are defined as,

$$p(u) = \frac{u}{1 + \kappa u}, \qquad f(v) = \frac{v}{1 - \kappa v}, \tag{4.14}$$

$$t(x) = -\sqrt{x^2 - \frac{2x}{\kappa}}, \tag{4.15}$$

where $u > -\frac{1}{\kappa}$ and $v < \frac{1}{\kappa}$. Using Eqs. (4.12)-(4.15) and (3.23)-(3.27), the corresponding acceleration is,

$$\alpha = -\kappa, \tag{4.16}$$

i.e. it is constant over all times. It is worth noting that the minus sign in Eq. (4.16) indicates that there is one branch of the mirror that moves to the left.

UA: Energy

Using Eqs. (4.12)-(4.15) and (3.41)-(3.44), the expectation value of the uniform acceleration mirror energy flux is zero,

$$F = 0, \tag{4.17}$$

even though particles are produced. This is confirmed and investigated by numerous authors, see e.g. [19, 20, 21, 22]. For completeness, the trivial plot of the UA mirror energy flux is presented in Fig. (4.6).

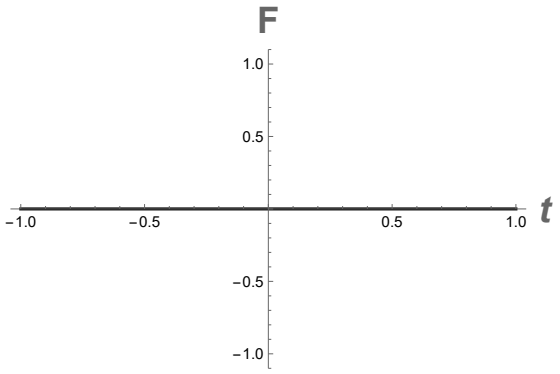

Figure 4.6: Uniformly accelerated mirror energy flux.

Such mirrors lead to the vanishing flux, correspondingly, the energy can not be evaluated.

UA: Particles

Using Eqs. (4.14a) and (3.89), the beta Bogolubov coefficient for the uniformly accelerated mirror is [3],

$$\beta_{\omega\omega'} = \frac{i}{\pi\kappa} e^{\frac{i(\omega-\omega')}{\kappa}} K_1\left(\frac{2\sqrt{\omega\omega'}}{\kappa}\right), \tag{4.18}$$

where $K_n(y)$ is the modified Bessel function of the second kind with the order n. Taking complex conjugate squaring of Eq. (4.18) yields,

$$|\beta_{\omega\omega'}|^2 = \frac{1}{\pi^2\kappa^2} K_1^2\left(\frac{2\sqrt{\omega\omega'}}{\kappa}\right). \tag{4.19}$$

Using Eqs. (4.19) and (3.94), the numerical result for the UA mirror particle spectrum is demonstrated in Fig. (4.7).

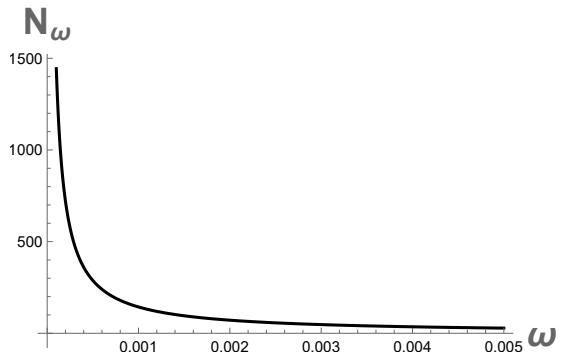

Figure 4.7: Uniformly accelerated mirror particle spectrum.

The particle spectrum of the UA mirror obeys Bessel function distribution and is infra-red divergent, i.e. there is infinite particle production.

UA: Entropy

Using Eqs. (4.13) and (3.101), the entanglement entropy of the uniformly accelerated mirror simply is,

$$S(t) = \frac{1}{6} \tanh^{-1} \left[\frac{\kappa t}{\sqrt{\kappa^2 t^2 + 1}} \right] . \tag{4.20}$$

The graphical illustration of Eq. (4.20) is given in Fig. (4.8).

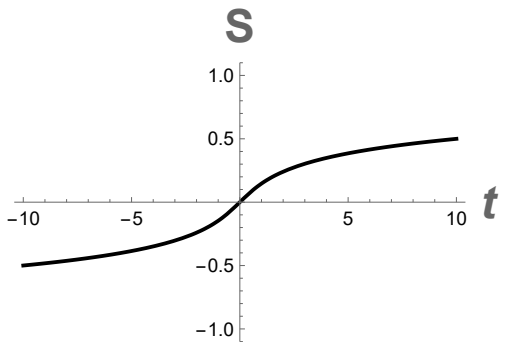

Figure 4.8: Uniformly accelerated mirror entropy.

The entropy diverges logarithmically in the $t \to \pm\infty$ limits, i.e. in both past and future times. This means that unitarity is not preserved.

4.1.3 Carlitz-Willey

CW: Dynamics

The Carlitz-Willey, or the eternally thermal, mirror is described by the following trajectory [15, 23],

$$x(t) = -t - \frac{1}{\kappa} W(e^{-2\kappa t}), \tag{4.21}$$

where W is a product log or Lambert function. The dynamics of the CW mirror trajectory is depicted in Fig. (4.9). The trajectory moves with the speed of light at

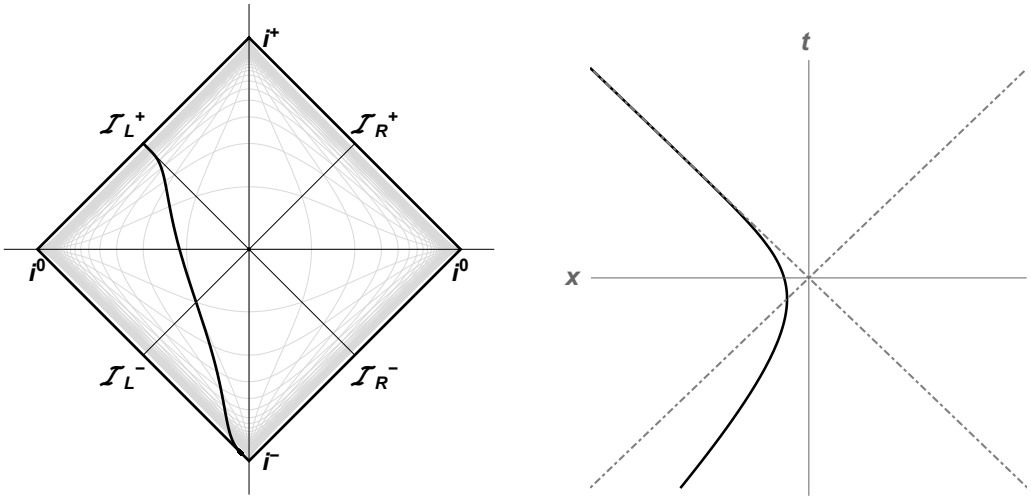

Figure 4.9: (a) Penrose and (b) Spacetime diagrams for the Carlitz-Willey mirror trajectory.

$v_H = 0$ horizon. The derivative of the trajectory with respect to time gives its velocity,

$$\dot{x}(t) = -1 + \frac{2W(e^{-2\kappa t})}{1 + W(e^{-2\kappa t})}, \tag{4.22}$$

which in the limits $t \to \pm\infty$ goes to the speed of light, i.e. $\dot{x}(t) = |V| \to 1$. Using Eqs. (4.21) and (3.1)-(3.7), the ray-tracing functions in null coordinates and proper time as well as the transcendental inversion are defined as,

$$p(u) = -\frac{1}{\kappa} e^{-\kappa u}, \tag{4.23}$$

$$f(v) = -\frac{1}{\kappa} \ln(-\kappa v), \tag{4.24}$$

$$t(x) = -x + \frac{1}{\kappa} W\left(-e^{2\kappa x}\right), \tag{4.25}$$

where $x < -\frac{1}{2\kappa}$. Using Eqs. (4.21)-(4.25) and (3.23)-(3.27), the corresponding proper accelerations are,

$$\alpha(u) = -\frac{\kappa}{2} e^{\kappa u/2}, \qquad \alpha(v) = -\frac{1}{2}\sqrt{\frac{\kappa}{|v|}}, \qquad \alpha(\tau) = \frac{1}{\tau}, \tag{4.26}$$

where $\alpha(\tau)$ is scale invariant, i.e. it does not depend on κ as long as the horizon is at $v_H = 0$.

CW: Energy

Using Eqs. (4.21)-(4.25) and (3.41)-(3.44), the expectation value of the Carlitz-Willey mirror energy flux is constant,

$$F = \frac{\kappa^2}{48\pi}. \tag{4.27}$$

For completeness, the trivial plot of the CW mirror energy flux is presented in Fig. (4.10).

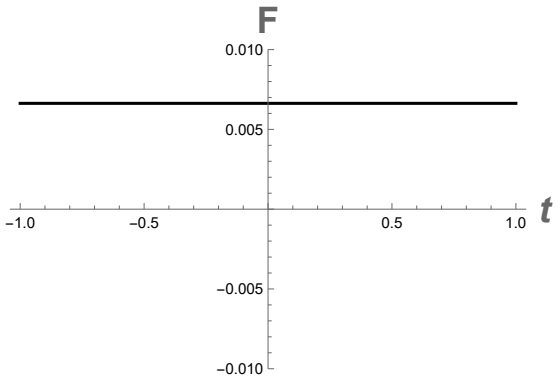

Figure 4.10: Carlitz-Willey mirror energy flux.

The CW trajectory motion creates non-zero constant energy flux that is thermal for all-times. For further discussion see also [18, 19, 32]. The constant form of the eternal thermal flux can also be verified in terms of rapidity and proper time as given in [36]. The integration of the flux using Eqs. (3.75)-(3.78) gives divergent integral, meaning that the total energy emission is infinite.

CW: Particles

The beta Bogolubov coefficient for the Carlitz-Willey mirror is [15, 23, 27],

$$\beta_{\omega\omega'} = -\frac{1}{2\pi\kappa}\sqrt{\frac{\omega}{\omega'}}e^{-\pi\omega/2\kappa}\left(\frac{\omega'}{\kappa}\right)^{-i\omega/\kappa}\Gamma\left[\frac{i\omega}{\kappa}\right]. \tag{4.28}$$

The complex conjugate squaring of the beta coefficient yields,

$$|\beta_{\omega\omega'}|^2 = \frac{1}{2\pi\kappa\omega'}\frac{1}{e^{2\pi\omega/\kappa}-1}. \tag{4.29}$$

Using Eqs. (4.29) and (3.94), the numerical result for the CW mirror particle spectrum is demonstrated in Fig. (4.11).

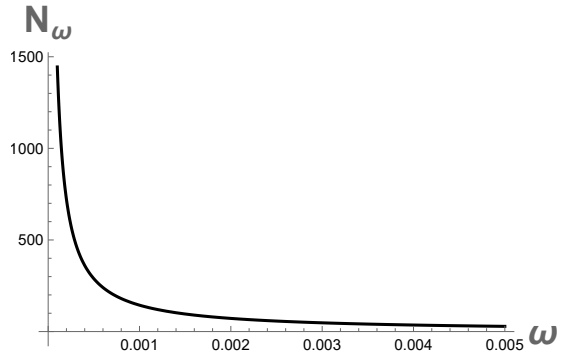

Figure 4.11: Carlitz-Willey mirror particle spectrum.

The particle spectrum of the CW mirror is divergent and obeys one dimensional Planck distribution at all times.

CW: Entropy

Using Eqs. (4.22) and (3.101), the entanglement entropy of the Carlitz-Willey mirror simply is,

$$S(t) = -\frac{1}{6}\tanh^{-1}\left[\frac{W\left(e^{-2\kappa t}\right)-1}{W\left(e^{-2\kappa t}\right)+1}\right]. \tag{4.30}$$

The graphical illustration of Eq. (4.30) is given in Fig. (4.12).

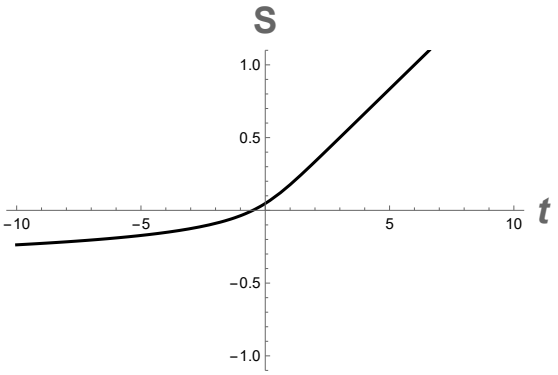

Figure 4.12: Carlitz-Willey mirror entropy.

The entropy increases monotonically, diverging in the $t \to \infty$ limit, i.e. unitarity is not preserved.

Let us now consider the corresponding entropy in terms of u coordinate. Using Eqs. (4.23a), (3.15) and (3.99), it is

$$S_{EE}(u) = \frac{\kappa u}{12} = \frac{\pi T u}{6}, \tag{4.31}$$

where we did the substitution using the relation $T = \kappa/2\pi$. Expressing $F = \kappa^2/48\pi$ in terms of T gives $F = \pi T^2/12$. We can get the thermodynamic entropy density as in [58],

$$\overline{S}_T = \frac{\partial F}{\partial T} = \frac{\pi T}{6}. \tag{4.32}$$

Finding entropy density, $\overline{S}_{EE}$,

$$\overline{S}_{EE} \equiv \frac{S_{EE}}{u} = \frac{\pi T}{6}, \tag{4.33}$$

we come up with an important result that,

$$\overline{S}_{EE} = \overline{S}_T, \tag{4.34}$$

i.e. the CW mirror is the only mirror whose entropy has one-to-one correspondence with the thermodynamic entropy.

4.1.4 Schwarzschild

Sch: Dynamics

The trajectory of the moving mirror in black hole collapse, or the Schwarzschild black hole analog mirror, is as follows [57, 25, 26, 28, 27, 29, 37, 8],

$$x(t) = v_H - t - \frac{W(2e^{2\kappa(v_H - t)})}{2\kappa}, \tag{4.35}$$

where v_H is the black hole event horizon location, W is a product log or Lambert function. The dynamics of the Sch mirror trajectory is depicted in Fig. (4.13).

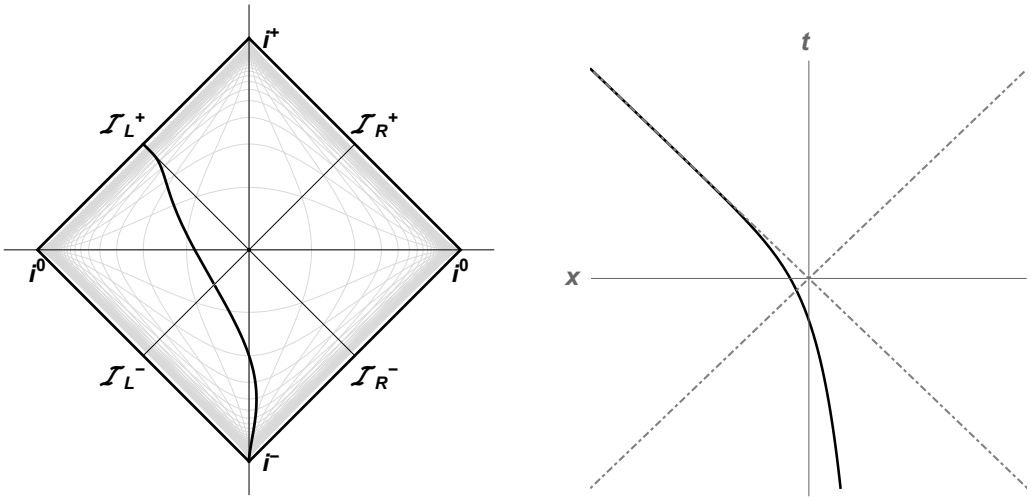

Figure 4.13: (a) Penrose and (b) Spacetime diagrams for the Schwarzschild mirror trajectory, with $v_H = 0$.

The trajectory starts with asymptotically static behavior and approaches the speed of light at $v_H = 0$ horizon. This can be verified mathematically by finding the mirror velocity as,

$$\dot{x}(t) = -\frac{1}{1 + W(2e^{2\kappa(v_H - t)})}, \tag{4.36}$$

which in the limit $t \to \infty$ goes to the speed of light, i.e. $\dot{x}(t) = |V| \to 1$, and $\dot{x}(t) = |V| \to 0$ in the $t \to -\infty$ limit. Using Eqs. (4.35) and (3.1)-(3.7), the ray-tracing functions in null coordinates and the transcendental inversion are defined as,

$$p(u) = v_H - \frac{1}{\kappa} W(e^{-\kappa(u - v_H)}), \qquad f(v) = v - \frac{1}{\kappa} \ln[\kappa(v_H - v)], \tag{4.37}$$

$$t(x) = v_H - x - \frac{1}{\kappa} e^{2\kappa x}, \tag{4.38}$$

The simplest form of the corresponding proper acceleration is found in terms of x space coordinate using Eqs. (4.38) and (3.24) as,

$$\alpha(x) = \frac{\kappa}{2e^{\kappa x}(1 + e^{2\kappa x})^{3/2}}, \tag{4.39}$$

which in the limit $x \to -\infty$ goes to $\alpha(x) \to \infty$, i.e. the trajectory accelerates infinitely into the far future.

Sch: Energy

Using Eqs. (4.35) and (3.42), the expectation value of the Schwarzschild mirror energy flux is [29],

$$F(t) = \frac{\kappa^2}{48\pi} \frac{[1 + 2W(2e^{2\kappa(v_H - t)})]}{[1 + \frac{1}{2}W(2e^{2\kappa(v_H - t)})]^4}. \tag{4.40}$$

The graphical illustration of Eq. (4.40) is demonstrated in Fig. (4.14).

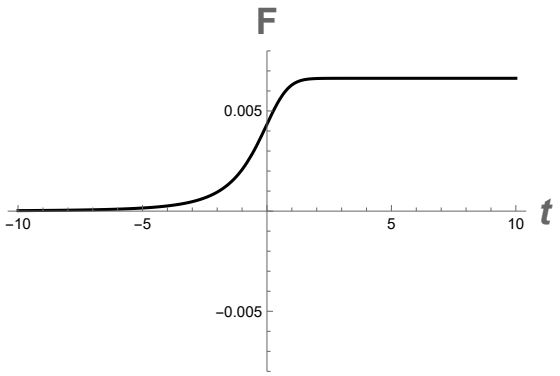

Figure 4.14: Schwarzschild mirror energy flux, with $v_H = 0$.

The flux is monotonic in the positive direction of t and becomes constant at late times, i.e. it has a monotonic approach to thermality. Notably, the simplest form of the flux is given in terms of x coordinate as,

$$F(x) = \frac{\kappa^2}{48\pi} \frac{(1 + 4e^{2\kappa x})}{(1 + e^{2\kappa x})^4}. \tag{4.41}$$

This is an interesting result which tells us that the flux $F(x)$ does not depend on the black hole horizon.

The integration of the flux using Eqs. (3.75)-(3.78) gives divergent integral, meaning that the total energy emission is infinite.

Sch: Particles

The beta Bogolubov coefficient for the Schwarzschild mirror is [28],

$$\beta_{\omega\omega'} = \frac{\sqrt{\omega\omega'}}{2\pi\kappa\omega_p} e^{-\pi\omega/2\kappa} \left(\frac{\omega_p}{\kappa}\right)^{-\frac{i\omega}{\kappa}} \Gamma\left[\frac{i\omega}{\kappa}\right], \tag{4.42}$$

where $w_p \equiv \omega + \omega'$. The complex conjugation of the beta coefficient yields,

$$|\beta_{\omega\omega'}|^2 = \frac{\omega'}{2\pi\kappa(\omega+\omega')^2} \frac{1}{e^{2\pi\omega/\kappa} - 1}. \tag{4.43}$$

In the $\omega' \gg \omega$ limit (late times), Eq. (4.43) reduces to,

$$|\beta_{\omega\omega'}|^2 = \frac{1}{2\pi\kappa\omega'} \frac{1}{e^{2\pi\omega/\kappa} - 1}. \tag{4.44}$$

Using Eqs. (4.43) and (3.94), the numerical result for the Sch mirror particle spectrum is demonstrated in Fig. (4.15).

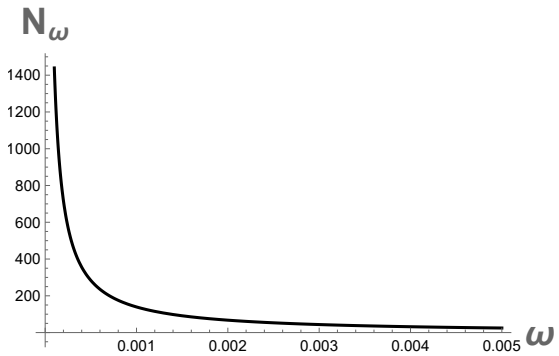

Figure 4.15: Schwarzschild mirror particle spectrum.

The particle spectrum of the Schwarzschild mirror is divergent and obeys Planck distribution at late times.

Sch: Entropy

Using Eqs. (4.36) and (3.101), the entanglement entropy of the Schwarzschild mirror simply is,

$$S(t) = \frac{1}{6}\coth^{-1}\left[1 + W(2e^{2\kappa(v_H - t)})\right]. \tag{4.45}$$

The graphical illustration of Eq. (4.45) is given in Fig. (4.16).

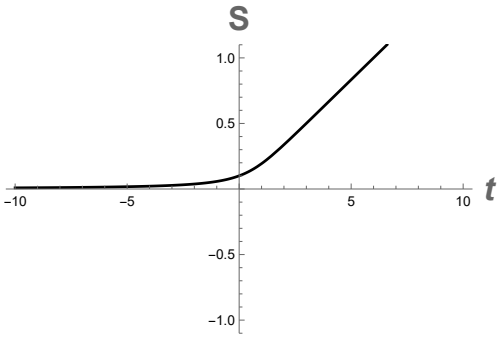

Figure 4.16: Scwarzschild mirror entropy, with $v_H = 0$.

Similar to the Carlitz-Willey mirror case, the entropy increases monotonically at early times, diverging in the limit $t \to \infty$, i.e. unitarity is not preserved.

4.2 Static

There are 5 beta-known asymptotically static moving mirror models:

- Walker-Davies
- Arctx
- Self-dual
- Good-Linder
- Scwarzschild-Planck

The static mirrors are undoubtedly the most physical in the moving mirror solutions since they solve the problems associated with the Hawking radiation. Namely, the static mirrors have total particle and energy emission that are finite, and unitarity is preserved. There are no null horizons, and mirrors move with a velocity less than the speed of light, becoming asymptotically static in the past and future. Such mirrors motion serves as a direct analogy of a black hole with unitary evolution and complete evaporation.

The Scwarzschild-Planck mirror is unusual in the sense that it represents the modification of the usual Schwarzschild mirror by adding another quantum length scale, Planck length, which is considered to be beyond the event horizon location. The particle production is quasi-thermal with finite evaporation and no remnant.

Throughout the thesis, κ is a positively defined quantity within a mirror model that has a unit of acceleration in natural units, i.e. $\hbar = c = 1$. The graphs are plotted with $\kappa = 1$ since its value does not affect the general physical properties of the system.

4.2.1 Walker-Davies

WD: Dynamics

This is the first introduced moving mirror model that gives finite total energy and particle emission, with solved beta coefficient. So, the trajectory reads as [11],

$$t(x) = -x \pm \frac{\pi}{\kappa}\left[\exp\left(-\frac{(1+\xi)x\kappa}{\pi\xi}\right) - 1\right]^{1/2}, \tag{4.46}$$

for $t > 0$ and $t < 0$ respectively. Here ξ is the maximum speed of the mirror with a range $0 < \xi < 1$. The dynamics of the WD mirror trajectory is depicted in Fig. (4.17). The trajectory starts motion with acceleration from the past decelerating at $t = 0$, then

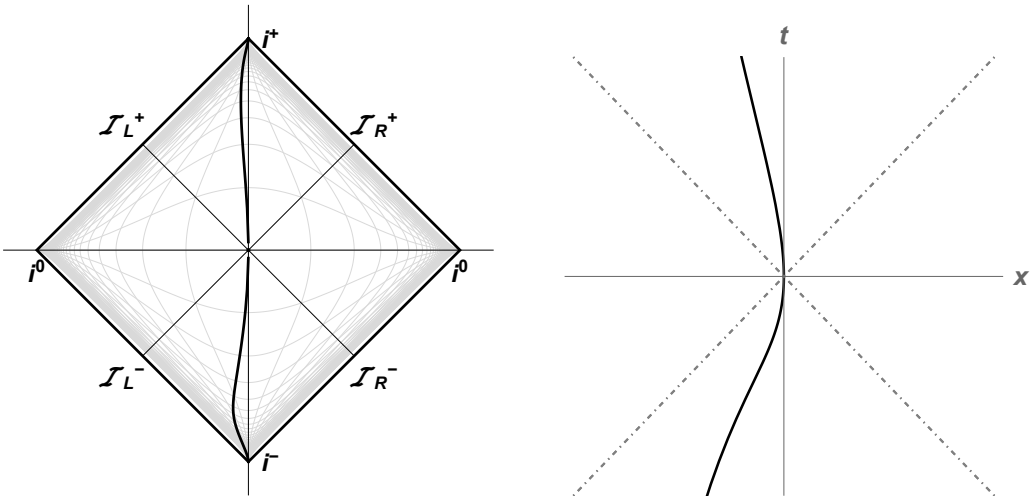

Figure 4.17: (a) Penrose and (b) Spacetime diagrams for the Walker-Davies mirror trajectory, with $\xi = \frac{1}{2}$.

again accelerating from the left and receding as approaching time-like future infinity, $t = \infty$ (see also [23, 57]). The asymptotic static behavior of the trajectory at $t \to \pm\infty$ limits can be also verified mathematically by finding the mirror velocity using Eqs. (4.46) and (3.3) as,

$$\dot{x}(t) = [t'(x)]^{-1} = -\frac{\sqrt{e^{-2Bx} - 1}}{\sqrt{e^{-2Bx} - 1} + ABe^{-2Bx}}, \tag{4.47}$$

which in the $x \to 0$ limit goes to zero, i.e. $\dot{x}(t) \equiv V \to 0$, and $A \equiv \frac{\pi}{\kappa}$, $B \equiv \frac{2\pi\xi}{(1+\xi)\kappa}$. The ray-tracing function in v null coordinate is defined as,

$$f(v) = v + \frac{2\pi\xi}{\kappa(1+\xi)} \ln\left(1 + \frac{\kappa^2 v^2}{\pi^2}\right), \tag{4.48}$$

whereas the trajectories in other coordinates are intractable. Using Eq. (4.48) and (3.26), the corresponding proper acceleration is,

$$\alpha(v) = \frac{B(v^2 - A^2)}{\sqrt{A^2 + v^2}\,(A^2 + v^2 + 2Bv)^{3/2}}, \tag{4.49}$$

which in the $v \to \pm\infty$ limits goes to 0.

WD: Energy

Using Eqs. (4.48) and (3.44), the expectation value of the Walker-Davies mirror energy flux is found to be,

$$F(v) = \frac{1}{12\pi} \frac{B\left[(B-2v)v^4 + 2A^2v^2(2v-3B) - 3A^4(B-2v)\right]}{\left[A^2 + v(v-2B)\right]^4}. \tag{4.50}$$

The graphical illustration of Eq. (4.50) is demonstrated in Fig. (4.18).

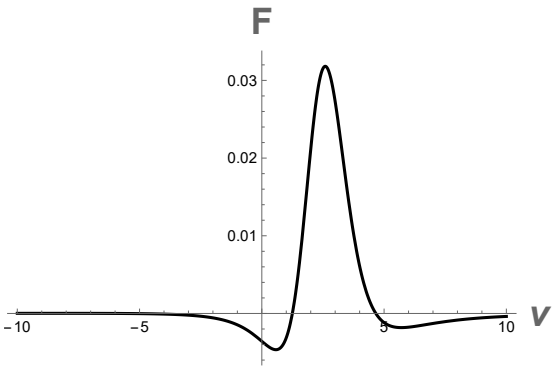

Figure 4.18: Walker-Davies mirror energy flux, with $\xi = \frac{1}{2}$.

From Fig. (4.18) one can see that the flux is not divergent, reaching a high peak at late times and having negative values at some points in time. Using Eqs. (4.50) and (3.76), the total emitted energy is finite and confirmed to be the same as the one found by Walker and Davies,

$$E = \frac{\kappa(1+\xi)\xi^2}{12\pi\left[(1+\xi)^2 - 4\xi^2\right]^{3/2}}. \tag{4.51}$$

Here the energy is found by reparametrization of coefficients (A, B) in terms of (κ, ξ). For more details on this mirror flux and energy see [11, 23].

WD: Particles

Using Eqs. (4.48) and (3.90), the beta Bogolubov coefficient for the Walker-Davies mirror is found to be,

$$\beta_{\omega\omega'} = \frac{1}{\sqrt{\pi}}\sqrt{\frac{\omega'}{\omega}}A^{\frac{1}{2}+iB\omega}\left(\frac{2}{\omega+\omega'}\right)^{\frac{1}{2}-iB\omega}\frac{K_a\left[A(\omega+\omega')\right]}{\Gamma\left[iB\omega\right]}, \tag{4.52}$$

where $K_a(y)$ is the second kind modified Bessel function with the order $a \equiv \frac{1}{2} - iB\omega$. The complex conjugate squaring of Eq. (4.52) yields [11],

$$|\beta_{\omega\omega'}|^2 = \frac{2AB}{\pi^2}\left(\frac{\omega'}{\omega'+\omega}\right)\sinh(\pi\omega B)|K_q[A(\omega'+\omega)]|^2. \tag{4.53}$$

Using Eqs. (4.53) and (3.94), the numerical result for the WD mirror particle spectrum is demonstrated in Fig. (4.19).

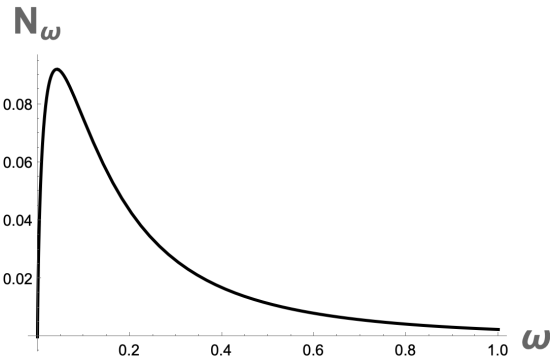

Figure 4.19: Walker-Davies mirror particle spectrum, with $\xi = \frac{1}{2}$.

The Walker-Davies mirror particle spectrum obeys Bessel function distribution, and there is no divergence in the spectrum, i.e. the particle production is finite. Consequently, the total particle count, found via Eqs. (4.53) and (3.97), results in the numerical value 0.027 when the maximum speed is $\xi = \frac{1}{2}$.

The numerical result for the mirror energy found via the beta Bogolubov coefficient using Eq. (3.95) is consistent with the energy result found via the flux, Eq. (4.51).

WD: Entropy

Using Eqs. (4.48) and (3.100), the entanglement entropy of the Walker-Davies mirror simply is,

$$S(v) = \frac{1}{12} \ln \left[1 + \frac{4\kappa\pi\xi v}{(1+\xi)(\pi^2 + \kappa^2 v^2)} \right]. \tag{4.54}$$

The graphical illustration of Eq. (4.54) is given in Fig. (4.20).

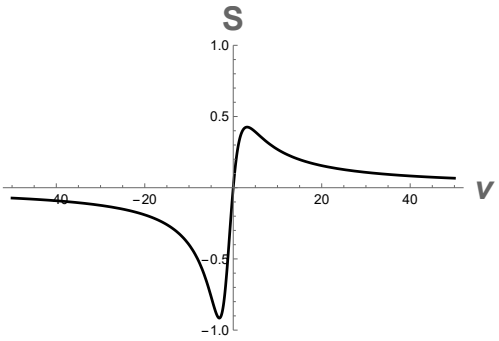

Figure 4.20: Walker-Davies mirror entropy, with $\xi = \frac{1}{2}$.

Overall, the entropy is not divergent, being positive at future time and negative at past time. Also, the graph is normalised by a factor of 10 for better illustration of the monotonic (asymptotic) approach to zero value at $v \to \pm\infty$ limits.

4.2.2 Arctx

ARCTX: Dynamics

This is the second introduced asymptotically static mirror model with the $x(t)$ trajectory [23],

$$x(t) = -\frac{1}{\kappa}\tan^{-1}(e^{\kappa t}), \tag{4.55}$$

whose dynamics is depicted in Fig. (4.21).

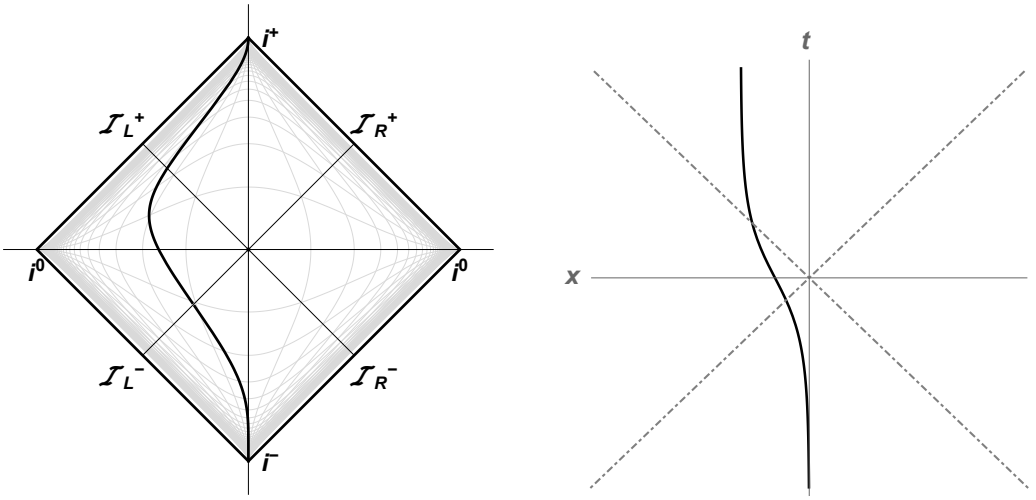

Figure 4.21: (a) Penrose and (b) Spacetime diagrams for the Arctx mirror trajectory.

The trajectory is seen to be asymptotically static at far past and far future. This can be verified mathematically by finding the mirror velocity as,

$$\dot{x}(t) = -\frac{e^{\kappa t}}{1+e^{2\kappa t}}, \tag{4.56}$$

which in the limits $t \to \pm\infty$ goes to zero, i.e. $\dot{x}(t) \equiv V \to 0$. The corresponding proper acceleration is,

$$\alpha(t) = \frac{4\kappa\,\mathrm{sech}(\kappa t)\tanh(\kappa t)}{[4-\mathrm{sech}(\kappa t)]^{3/2}}, \tag{4.57}$$

which in the limit $t \to \pm\infty$ is 0. The transcendental inversion of Eq. (4.55) is,

$$t(x) = \frac{1}{\kappa}\ln[-\tan(\kappa x)], \tag{4.58}$$

whereas the ray-tracing functions in null coordinates are not tractable.

ARCTX: Energy

The energy flux is easily solved [23],

$$F(t) = \frac{\kappa^2 \cosh(\kappa t)\left[\cosh(4\kappa t) - 2\cosh(2\kappa t) - 5\right]}{3\pi\left[1 - 2\cosh(\kappa t)\right]^2\left[1 + 2\cosh(\kappa t)\right]^4}, \tag{4.59}$$

and the graphical illustration of Eq. (4.59) is demonstrated in Fig. (4.22).

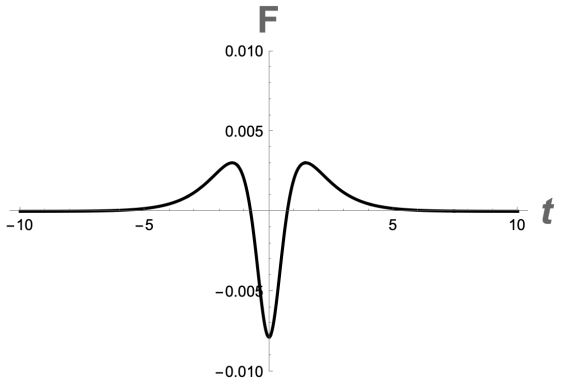

Figure 4.22: Arctx mirror energy flux.

The flux is symmetric with respect to time reaching a minimum at the origin, $t = 0$. The energy emission is finite and has the following form,

$$E = \frac{\kappa}{2592\pi}\left(13\sqrt{3}\pi - 36\right). \tag{4.60}$$

This result is consistent with the numerical verification of the energy found by using the beta Bogolubov coefficient.

ARCTX: Particles

The analytically found beta Bogolubov coefficient of the Arctx mirror is [23],

$$\beta_{\omega\omega'} = g_0[g_1\Gamma(-m)\Gamma(-q) - g_2\Gamma(m)\Gamma(q)]. \tag{4.61}$$

Here

$$q \equiv \frac{i}{\kappa}(\omega' + \omega), \qquad m \equiv \frac{1}{2\kappa}(\omega' - \omega), \tag{4.62}$$

$$g_0 \equiv ie^{\frac{i\pi q}{2}} \frac{\sqrt{4m^2 + q^2}}{2\pi\kappa} \frac{\sin(\pi m)}{\sin[\pi(m+q)]}, \tag{4.63}$$

$$g_1 \equiv {}_2F_{1R}(1-m, 1-q, 1-m-q, -1)e^{-i\pi(m+q)}, \tag{4.64}$$

$$g_2 \equiv {}_2F_{1R}(1+m, 1+q, 1+m+q, -1), \tag{4.65}$$

where ${}_2F_{1R}$ are regularized hypergeometric functions. The complex conjugate squaring of Eq. (4.61) is found to be,

$$\begin{aligned} |\beta_{\omega\omega'}|^2 = &- \frac{\omega\omega'}{\kappa^4\pi^2} \csc\left[\pi(m+q)\right]^2 \sin(\pi m)^2 \\ &\left[g_3\Gamma(-m)\Gamma(q) - g_4\Gamma(-m)\Gamma(-q)\right]\left[g_1\Gamma(-m)\Gamma(-q) - g_2\Gamma(m)\Gamma(q)\right], \end{aligned} \tag{4.66}$$

where

$$g_3 \equiv {}_2F_{1R}[1-m, 1+q, 1-m+q, -1]e^{i\pi(m-q)}, \tag{4.67}$$

$$g_4 \equiv {}_2F_{1R}[1+m, 1-q, 1+m-q, -1]. \tag{4.68}$$

The numerical result for the Arctx mirror particle spectrum is demonstrated in Fig. (4.23).

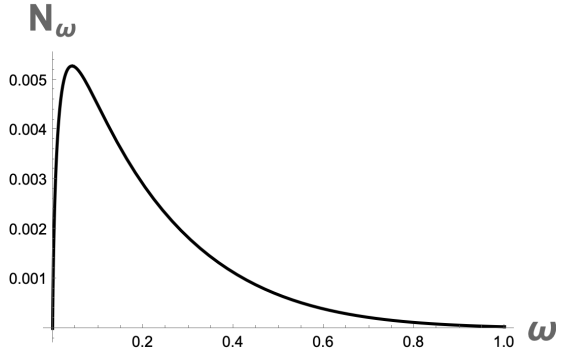

Figure 4.23: Arctx mirror particle spectrum.

The spectrum of the Arctx mirror obeys hypergeometric function distribution and is not divergent, i.e. the particle production is finite. Consequently, the total particle count, found via Eqs. (4.66) and (3.97), results in the numerical value 0.0067.

ARCTX: Entropy

The entanglement entropy of the Arctx mirror simply is,

$$S(t) = \frac{1}{6} \coth^{-1} \left[2 \cosh(\kappa t) \right] . \tag{4.69}$$

The graphical illustration of Eq. (4.69) is given in Fig. (4.24).

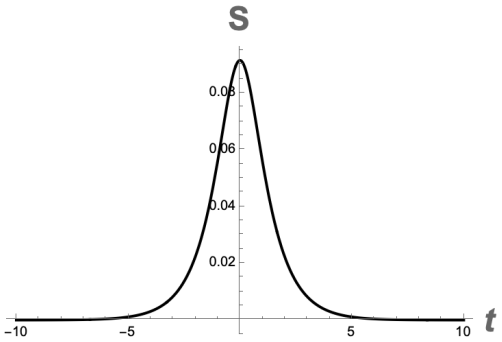

Figure 4.24: Arctx mirror entropy.

The figure demonstrates that the entropy is symmetric with respect to time, reaching a maximum at the origin, $t = 0$. Also, the entropy does not diverge asymptotically, meaning that the unitarity is preserved.

4.2.3 Self-dual

SD: Dynamics

The self-dual mirror trajectory reads as [32],

$$x(t) = -\frac{\xi}{\kappa} \ln\left(1 + \kappa^2 t^2\right), \tag{4.70}$$

where ξ is the maximum speed of the mirror with a range $0 < \xi < 1$. The dynamics of Eq. (4.70) is depicted in Fig. (4.25).

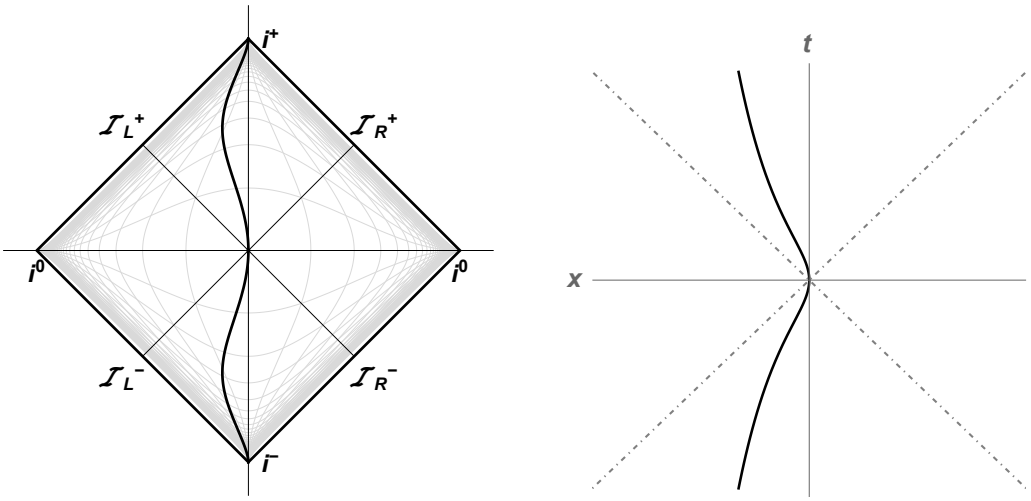

Figure 4.25: a) Penrose and b) Spacetime diagrams for the Self-dual mirror trajectory, with $\xi = \frac{1}{2}$.

The trajectory is symmetric with respect to time, and is static at far past and far future. This can be verified mathematically by finding the mirror velocity as,

$$\dot{x}(t) = -\frac{2\xi\kappa t}{1 + \kappa^2 t^2}, \tag{4.71}$$

which in the $t \to \pm\infty$ limits goes to zero, i.e. $\dot{x}(t) \equiv V \to 0$. The corresponding proper acceleration is found to be,

$$\alpha(t) = -\frac{2\xi\kappa\left(1 - \kappa^4 t^4\right)}{\left[\left(1 + \kappa^2 t^2\right)^2 - 4\kappa^2 t^2 \xi^2\right]^{3/2}}, \tag{4.72}$$

which in the $t \to \pm\infty$ limits goes to 0. The transcendental inversion of Eq. (4.70) is,

$$t(x) = \pm\frac{1}{\kappa}\sqrt{e^{-\frac{\kappa x}{\xi}} - 1}, \tag{4.73}$$

where "$\pm$" signs correspond to the upper and lower parts of the trajectory. The ray-tracing functions in null coordinates are not tractable.

SD: Energy

The expectation value of the self-dual mirror energy flux is [32],

$$F(t)=\frac{\kappa^3\xi t\left(\kappa^2t^2+1\right)\left[2\xi^2\left(\kappa^4t^4+3\right)+\left(\kappa^2t^2-3\right)\left(\kappa^2t^2+1\right)^2\right]}{3\pi\left[\kappa t\left(\kappa t-2\xi\right)+1\right]^2\left[\kappa t\left(2\xi+\kappa t\right)+1\right]^4}. \tag{4.74}$$

The graphical illustration of Eq. (4.74) is demonstrated in Fig. (4.26).

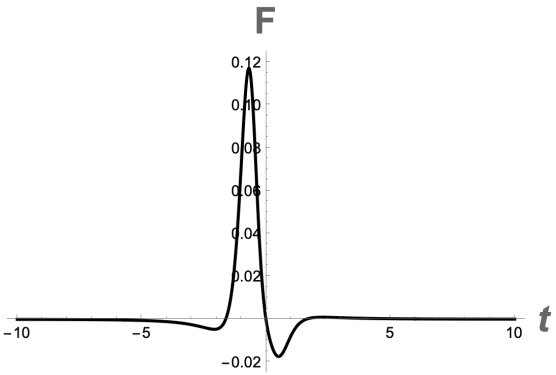

Figure 4.26: Self-dual mirror energy flux, with $\xi=\frac{1}{2}$.

The flux has considerably large positive value at early time and small negative value at late time. The symmetric behavior of the mirror with respect to time results in the same energy on both the left and right sides of the mirror,

$$E=E_R=E_L=\frac{\kappa}{48\gamma}(\gamma^2-1)(\gamma^2+3). \tag{4.75}$$

where $\gamma\equiv 1/\sqrt{1-\xi^2}$. According to Eq. (4.75), if the maximum speed of the mirror is zero, then the energy emission becomes 0. Eq. (4.75) is consistent with the numerical verification of the energy found by using the beta Bogolubov coefficient.

SD: Particles

The beta Bogolubov coefficient of the self-dual mirror is found to be,

$$\beta_{\omega\omega'} = \frac{2^r\sqrt{\omega\omega'}\left(\frac{\kappa}{\omega_p}\right)^q}{\kappa\sqrt{\pi}\omega_n}\frac{K_q\left(\frac{\omega_p}{\kappa}\right)}{\Gamma\left[\frac{i\omega_n\xi}{\kappa}\right]}, \tag{4.76}$$

where $\omega_p \equiv \omega + \omega'$, $\omega_n \equiv \omega - \omega'$, and $K_n(y)$ is the modified Bessel function of the second kind, and

$$r = \frac{3}{2} - \frac{i\xi\omega_n}{\kappa}, \qquad q = \frac{1}{2} - \frac{i\xi\omega_n}{\kappa}. \tag{4.77}$$

The complex conjugate squaring of the beta Bogolubov coefficient yields [32],

$$|\beta_{\omega\omega'}|^2 = \frac{8\xi\omega\omega'}{\kappa^2\pi^2\omega_n\omega_p}\sinh\left(\frac{\pi\xi\omega_n}{\kappa}\right)\left|K_q\left(\frac{\omega_p}{\kappa}\right)\right|^2. \tag{4.78}$$

The numerical result for the SD mirror particle spectrum is demonstrated in Fig. (4.27).

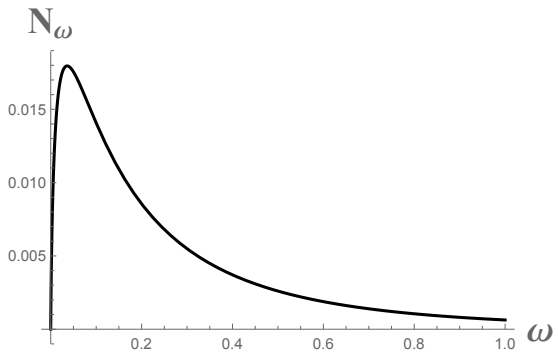

Figure 4.27: Self-dual mirror particle spectrum, with $\xi = \frac{1}{2}$.

The spectrum obeys Bessel function distribution and is not divergent, i.e. the particle production is finite. Consequently, the particle count found using Eq. (3.97) results in the numerical value 0.047 when the maximum speed is $\xi = \frac{1}{2}$.

SD: Entropy

The entanglement entropy of the self-dual mirror simply is,

$$S(t) = \frac{1}{6} \tanh^{-1} \left[\frac{2\xi\kappa t}{1+\kappa^2 t^2} \right]. \tag{4.79}$$

The graphical illustration of Eq. (4.79) is given in Fig. (4.28).

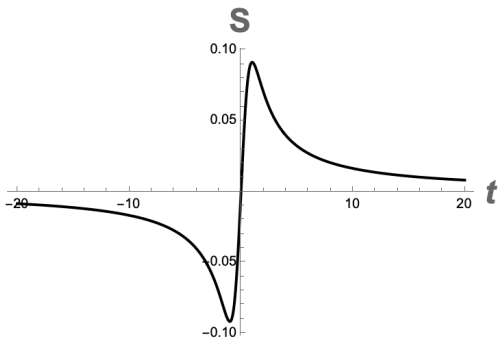

Figure 4.28: Self-dual mirror entropy, with $\xi = \frac{1}{2}$.

Similar to the Walker-Davies mirror entropy, Fig. (4.20), the self-dual mirror entropy is negative at early time and positive at late time. Also, it is not divergent in the limits $t \to \pm\infty$ and has an asymmetric behaviour in time.

It has been investigated recently that the self-dual mirror can be treated as an electron, so the corresponding mirror Larmor power is found and other interesting features on this duality are studied in [66].

4.2.4 Good-Linder

GL: Dynamics

An asymptotically static mirror with time-asymmetry is defined as [33],

$$x(t) = -\frac{\xi}{\kappa} \ln\left(\kappa t + \sqrt{\kappa^2 t^2 + 1}\right), \tag{4.80}$$

where ξ is the maximum speed of the mirror with a range $0 < \xi < 1$. The dynamics of Eq. (4.80) is depicted in Fig. (4.29).

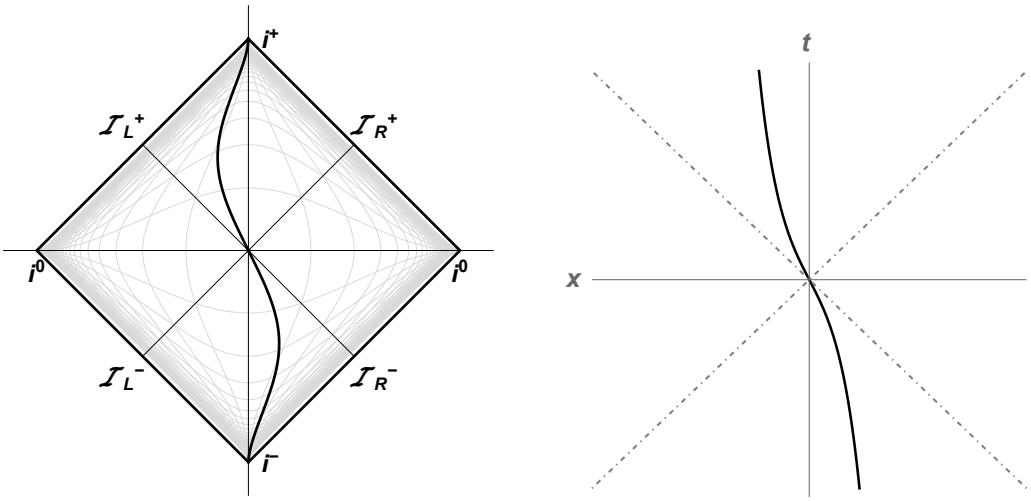

Figure 4.29: a) Penrose and b) Spacetime diagrams for the Good-Linder mirror trajectory, with $\xi = \frac{1}{2}$.

The trajectory is seen to be asymmetric in time, being asymptotically static at far past and far future, which is verified by finding the mirror velocity as,

$$\dot{x}(t) = -\frac{\xi}{\sqrt{\kappa^2 t^2 + 1}}, \tag{4.81}$$

which in the $t \to \pm\infty$ limits goes to 0, i.e. $\dot{x}(t) \equiv V \to 0$. The corresponding proper acceleration is,

$$\alpha(t) = \frac{\kappa^2 \xi t}{\left(\kappa^2 t^2 + 1 - \xi^2\right)^{3/2}}, \tag{4.82}$$

which in the $t \to \pm\infty$ limits goes to 0. The transcendental inversion of Eq. (4.80) is,

$$t(x) = -\frac{1}{\kappa} \sinh\left(\frac{\kappa x}{\xi}\right), \tag{4.83}$$

whereas the ray-tracing functions in null coordinates are not tractable.

GL: Energy

The expectation value of the energy flux is [33],

$$F(t) = \frac{\kappa^2}{12\pi} \frac{\xi\sqrt{\kappa^2 t^2+1}\,(\xi^2+2\kappa^2 t^2-1)}{\left(\xi-\sqrt{\kappa^2 t^2+1}\right)^2\left(\xi+\sqrt{\kappa^2 t^2+1}\right)^4}. \tag{4.84}$$

The graphical illustration of Eq. (4.84) is demonstrated in Fig. (4.30).

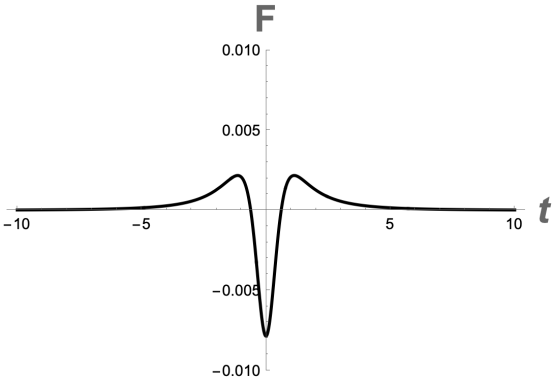

Figure 4.30: Good-Linder mirror energy flux, with $\xi = \frac{1}{2}$.

The flux is symmetric with respect to time reaching a minimum at the origin, $t = 0$. The right side energy emission of the mirror is finite,

$$E_R = \frac{\kappa}{96\pi}\frac{\gamma^2}{\xi^2}\left[\gamma(6-8\xi^2)\sin^{-1}\xi + \pi\gamma\xi^4 + 4\xi^3 - 6\xi\right]. \tag{4.85}$$

whereas the total energy, which is the sum of right and left sides, has a simple form as,

$$E_T = E_R + E_L = \frac{\kappa\gamma^3\xi^2}{48}. \tag{4.86}$$

Here $\gamma \equiv 1/\sqrt{1-\xi^2}$ is the Lorentz factor. According to Eq. (4.86), there is no energy emission at $\xi \to 0$; the total energy is non-negative at $0 < \xi < 1$; the energy is divergent at $\xi \to 1$. In fact, Eq. (4.86) is the energy for the light from an electron that moves along the Good-Linder mirror trajectory (see [66] for more details).

GL: Particles

The beta Bogolubov coefficient of the Good-Linder mirror is [33],

$$\beta_{\omega\omega'} = -\frac{2\xi\sqrt{\omega\omega'}}{\pi\omega_p} e^{-\frac{\pi\xi\omega_n}{2}} K_q(\omega_p). \tag{4.87}$$

Here $\omega_p \equiv \omega + \omega'$, $\omega_n \equiv \omega - \omega'$, $q \equiv -i\xi\omega_n$, $K_q(y)$ is the second kind modified Bessel function, and $\kappa = 1$ for convenience. The complex conjugate squaring of Eq. (4.87) yields,

$$|\beta_{\omega\omega'}|^2 = \frac{4\xi^2\omega\omega'}{\pi^2\omega_p^2} e^{-\pi\xi\omega_n} |K_{i\xi\omega_n}(\omega_p)|^2. \tag{4.88}$$

The numerical result for the GL mirror particle spectrum is demonstrated in Fig. (4.31).

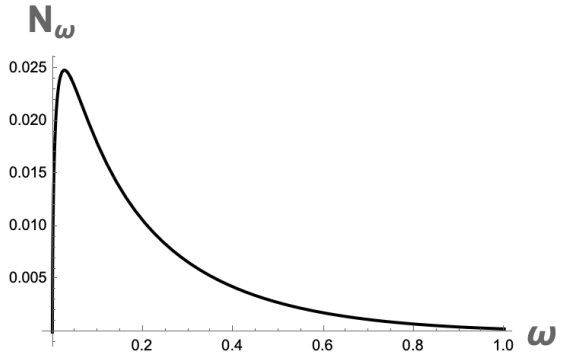

Figure 4.31: Good-Linder mirror particle spectrum, with $\xi = \frac{1}{2}$.

The particle spectrum of the Good-Linder mirror obeys Bessel function distribution and is not divergent, i.e. the particle production is finite. As a result, the particle count found using Eq. (3.97) results in the numerical value 0.0109 when the maximum speed is $\xi = \frac{1}{2}$.

The numerical result for the mirror energy found via the beta Bogolubov coefficient using Eq. (3.95) is consistent with the energy result found via the flux, Eq. (4.85).

GL: Entropy

The entanglement entropy of the Good-Linder mirror simply is,

$$S(t) = \frac{1}{6} \tanh^{-1} \left(\frac{\xi}{\sqrt{\kappa^2 t^2 + 1}} \right). \tag{4.89}$$

The graphical illustration of Eq. (4.89) is given in Fig. (4.32).

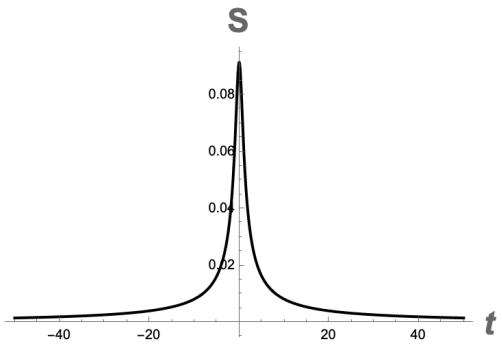

Figure 4.32: Good-Linder mirror entropy, with $\xi = \frac{1}{2}$.

The GL mirror entropy has a similar behavior as the Arctx mirror case: the entropy is symmetric with respect to time, reaching a maximum at the origin, $t = 0$. Also, the entropy does not diverge asymptotically, meaning that the unitarity is preserved. Moreover, the entropy decreases as the time increases, i.e. $S \sim \frac{1}{|t|}$ as determined in [33].

4.2.5 Schwarzschild-Planck

SP: Dynamics

The trajectories of the Schwarzschild-Planck mirror, or quantum pure black hole collapse mirror, that have asymptotically static behavior with additional length scale, are [47, 48, 49],

$$f(v) = v - \frac{1}{\kappa}\sinh^{-1}|gv|, \tag{4.90}$$

$$t(x) = -x - \frac{\sinh(2\kappa x)}{g}. \tag{4.91}$$

Here $g = 1/(2l_p)$, and $l_p = \sqrt{\hbar G/c^3}$ is the Planck length, whose introduction indicates the presence of both quantum and gravity counterparts in the model. The ray-tracing functions in (u, t) coordinates are intractable. The dynamics of the Schwarzschild-Planck mirror is depicted in Fig. (4.33).

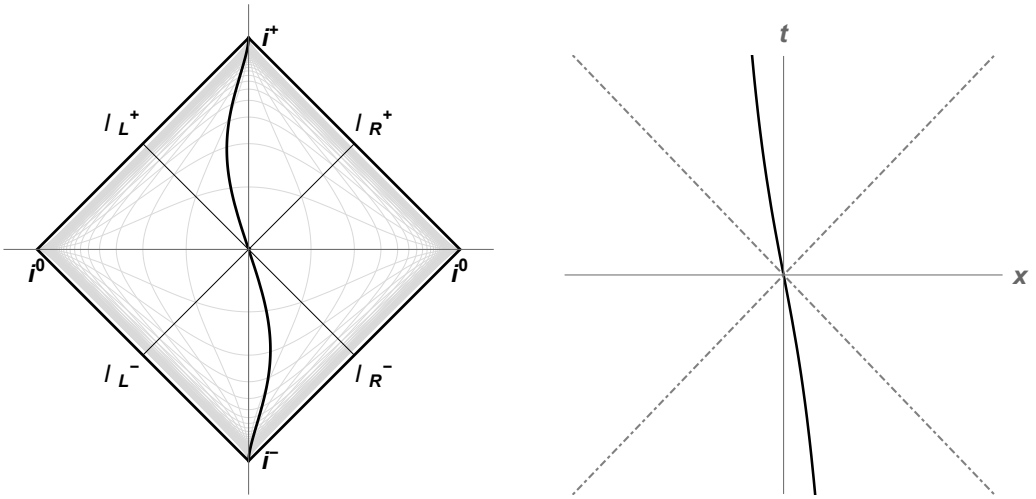

Figure 4.33: (a) Penrose and (b) Spacetime diagrams for the Schwarzschild-Planck mirror, with $g = \frac{1}{2}$.

Similar to the Good-Linder mirror behavior, the Schwarzschild-Planck mirror trajectory is asymmetric in time. The velocity of the mirror is,

$$\dot{x}(t) \equiv [t(x)]^{-1} = -\frac{g}{g + 2\kappa\cosh(2\kappa x)}, \tag{4.92}$$

which in the $x \to \pm\infty$ limits goes to 0, i.e. $\dot{x}(t) \equiv V \to 0$, whereas in the $x \to 0$ limit, the velocity has its maximum value, $V_{max} = -\frac{g}{g+2\kappa}$. The corresponding proper acceleration is,

$$\alpha(v) = -\frac{g^3\sqrt{\kappa}v}{2\left(1+g^2v^2\right)^{3/4}\left(\kappa\sqrt{1+g^2v^2} - g\right)^{3/2}}, \tag{4.93}$$

which in the $v \to \pm\infty$ limits goes to 0.

SP: Energy

The flux in terms of null coordinate v is,

$$F(v)=\frac{g^3\kappa^2}{48\pi}\frac{\left[2\kappa\sqrt{1+g^2v^2}\,(1-2g^2v^2)-g\,(2-g^2v^2)\right]}{(1+g^2v^2)\left(g-\kappa\sqrt{1+g^2v^2}\right)^4}, \tag{4.94}$$

whose plot is given in Fig. (4.34).

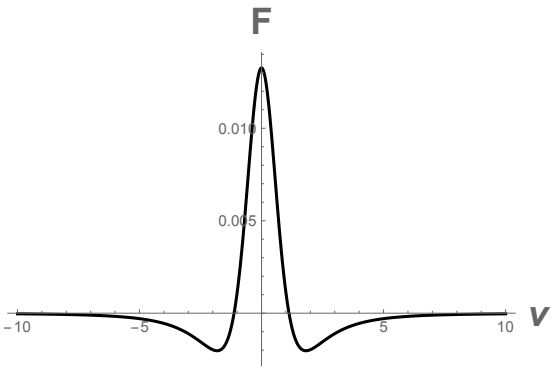

Figure 4.34: Schwarzschild-Planck mirror energy flux, with $g=\frac{1}{2}$.

The flux is symmetric, having negative values on both sides and a peak at the origin, $v=0$. The thermal behavior of the flux occurs when $g\gg\kappa$ [47, 48]. The corresponding energy emission is finite,

$$E=\frac{\kappa}{96\pi}\left[\frac{10g^2-12\kappa^2}{g^2-\kappa^2}+\frac{6\pi\kappa}{g}-\frac{2g^4-9g^2\kappa^2+6\kappa^4}{g\left(\kappa^2-g^2\right)^{3/2}}\left(\pi+2\tan^{-1}\frac{g}{\sqrt{\kappa^2-g^2}}\right)\right]. \tag{4.95}$$

Eq. (4.95) is consistent with the numerical verification of the energy found by using the beta Bogolubov coefficient.

It has been investigated recently that the Schwarzschild-Planck mirror can be treated as an electron, so the corresponding energy for both sides of the mirror as well as the Larmor power are found, and other interesting features on this duality are studied in [67].

SP: Particles

The beta Bogolubov coefficient of the Schwarzschild-Planck mirror is [47],

$$\beta_{\omega\omega'} = -\frac{\sqrt{\omega\omega'}}{\pi\kappa\omega_p} e^{-\frac{\pi\omega}{2\kappa}} K_q\left(\frac{\omega_p}{g}\right), \tag{4.96}$$

where $\omega_p \equiv \omega + \omega'$, $q = \frac{i\omega}{\kappa}$, and $K_q(y)$ is the modified Bessel function of the second kind. The complex conjugate square of Eq. (4.96) yields,

$$|\beta_{\omega\omega'}|^2 = \frac{\omega\omega'}{\pi^2\kappa^2\omega_p} e^{-\frac{\pi\omega}{\kappa}} \left| K_{\frac{i\omega}{\kappa}}\left(\frac{\omega_p}{g}\right)\right|^2. \tag{4.97}$$

The thermal character of the particle spectrum is obtained when $\omega' \gg \omega$ and $g \gg \kappa$, then Eq. (4.97) reduces to,

$$|\beta_{\omega\omega'}|^2 \approx \frac{1}{\pi\omega'} \frac{1}{e^{2\pi\omega} - 1}. \tag{4.98}$$

The numerical result for the SP mirror particle spectrum is demonstrated in Fig. (4.35).

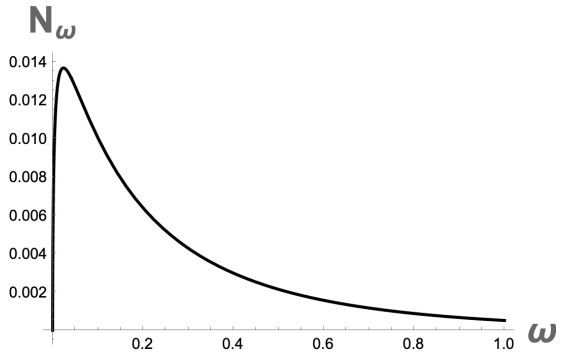

Figure 4.35: Schwarzschild-Planck mirror particle spectrum, with $g = \frac{1}{2}$.

The particle spectrum of the Schwarzschild-Planck mirror obeys Bessel function distribution and is not divergent, i.e. the particle production is finite. As a result, the particle count for the mirror, found as in Eq. (3.97), results in the numerical value 0.0041 when $g = \frac{1}{2}$.

SP: Entropy

The mirror entanglement entropy in terms of v coordinate simply is,

$$S(v) = \frac{1}{12} \ln \left(1 - \frac{g}{\kappa \sqrt{1 + g^2 v^2}} \right). \tag{4.99}$$

The graphical illustration of Eq. (4.99) is given in Fig. (4.36).

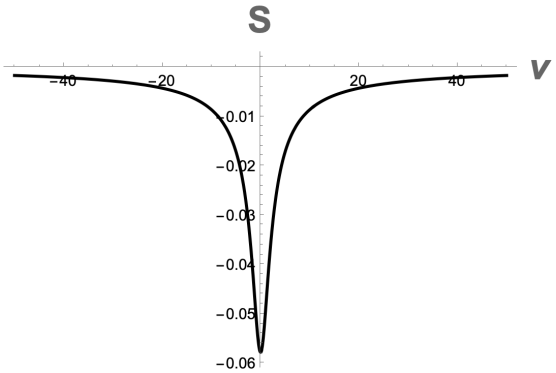

Figure 4.36: Schwarzschild-Planck mirror entropy, with $g = \frac{1}{2}$.

Overall, the total entropy is negative, being symmetric with respect to advanced time and having a minimum value at the origin, $v = 0$. Also, it is not divergent in the limits $v \to \pm\infty$, meaning that the unitarity is preserved.

4.3 Null

There are 3 beta-known asymptotically null moving mirror models:

- Logex
- Evans
- Dual-Temperature

The null mirrors travel with the speed of light at some point in their dynamics, emitting corresponding thermal radiation. As a result, the total particle count and energy emission is infinite.

The Logex mirror has non-monotonic energy flux with a pulse of hyper-thermal radiation before reaching thermal equilibrium at late times.

The Evans mirror stands out because it does not have null horizon; however, still approaches the speed of light asymptotically.

The Dual-temperature mirror is unique in the sense that it emits radiation at two different temperatures, corresponding to thermal equilibrium and non-thermal transition states, respectively.

Throughout the thesis, κ is a positively defined quantity within a mirror model that has a unit of acceleration in natural units, i.e. $\hbar = c = 1$. The graphs are plotted with $\kappa = 1$ since its value does not affect the general physical properties of the system.

4.3.1 Logex

Logex: Dynamics

Another moving mirror model that mimics black hole evaporation process is described by the following trajectory [57],

$$x(t) = -\frac{1}{2\kappa}\ln\Big(e^{2\kappa t}+1\Big), \tag{4.100}$$

where the horizon is located at $v = 0$. The dynamics of the Logex mirror is depicted in Fig. (4.37).

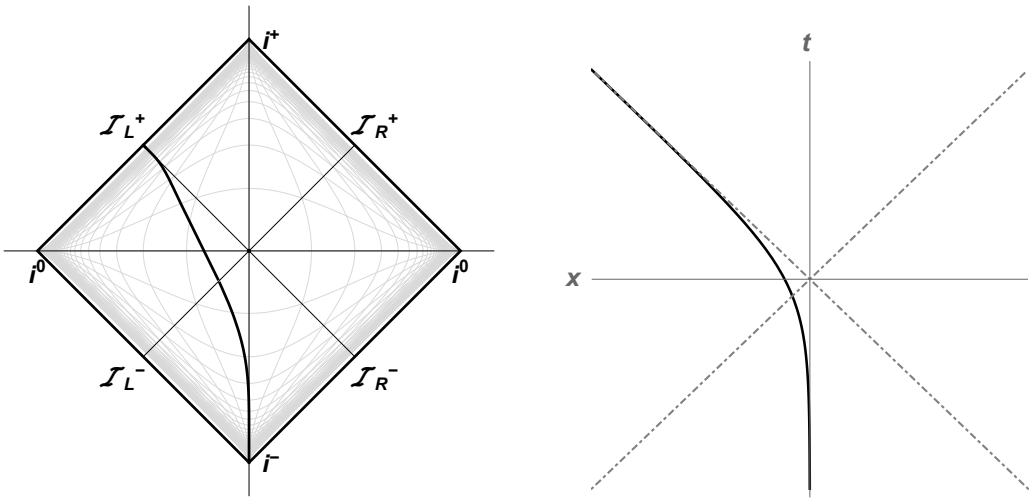

Figure 4.37: a) Penrose and b) Spacetime diagrams for the Logex mirror trajectory.

The trajectory starts asymptotically static, then attains the speed of light and goes to infinite acceleration in the far future. These can be verified mathematically by finding the mirror velocity and the corresponding proper acceleration as,

$$\dot{x}(t) = -\frac{e^{2\kappa t}}{1+e^{2\kappa t}}, \tag{4.101}$$

and

$$\alpha(t) = -\frac{2\kappa e^{2\kappa t}(1+e^{2\kappa t})}{(1+2e^{2\kappa t})^{3/2}}, \tag{4.102}$$

which in the $t \to \infty$ limit go to $\dot{x}(t) \equiv |V| \to 1$ and $|\alpha(t)| \to \infty$, respectively. The ray-tracing functions in null coordinates and the transcendental inversion of Eq. (4.100) are defined as,

$$p(u) = \frac{1}{\kappa}\text{csch}^{-1}(2e^{\kappa u}). \tag{4.103}$$

$$f(v) = v - \frac{1}{\kappa}\ln\Big(1-e^{2\kappa v}\Big), \tag{4.104}$$

$$t(x) = \frac{1}{2\kappa}\ln\Big(e^{-2\kappa x}-1\Big). \tag{4.105}$$

So, all ray-tracing functions in both spacetime and null coordinates are tractable.

Logex: Energy

The expectation value of the Logex mirror energy flux is,

$$F(t) = \frac{\kappa^2}{3\pi} \frac{e^{2\kappa t}\left(1+e^{2\kappa t}\right)\left(1+e^{2\kappa t}+e^{4\kappa t}\right)}{\left(1+2e^{2\kappa t}\right)^4}, \tag{4.106}$$

whose plot is given in Fig. (4.38).

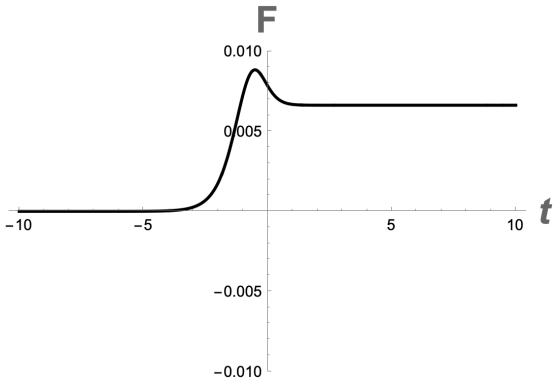

Figure 4.38: Logex mirror energy flux.

The flux has a positive hyper-thermal radiation before reaching thermal equilibrium at late times.

Logex: Particles

The beta Bogolubov coefficient of the Logex mirror is [57]:

$$\beta_{\omega\omega'} = \frac{\sqrt{\omega\omega'}}{2\pi\kappa\omega_n} B\left[\frac{i\omega}{\kappa}, -\frac{i\omega_p}{2\kappa}\right], \tag{4.107}$$

where $\omega_p \equiv \omega + \omega'$, $\omega_n \equiv \omega - \omega'$, and $B(a, b)$ is the Euler integral of the first kind, or beta function. The complex conjugate squaring of Eq. (4.107) is,

$$|\beta_{\omega\omega'}|^2 = \frac{\omega\omega'}{4\pi^2\kappa^2\omega_n^2} \left|B\left[-\frac{i\omega}{\kappa}, \frac{i\omega_p}{2\kappa}\right]\right|^2. \tag{4.108}$$

The numerical result for the Logex mirror particle spectrum is demonstrated in Fig. (4.39).

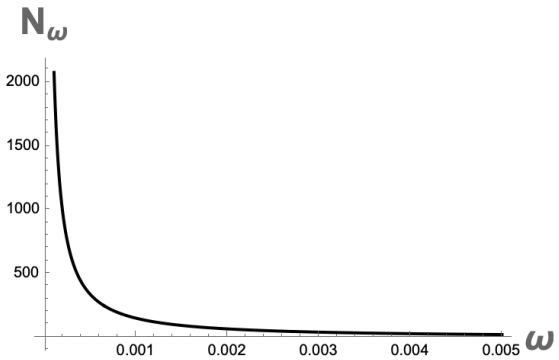

Figure 4.39: Logex mirror particle spectrum.

It can be seen from the figure that the spectrum of the Logex mirror is divergent and obeys beta function distribution. In a high frequency regime, $\omega' \gg \omega$, Eq. (4.108) reduces to,

$$|\beta_{\omega\omega'}|^2 \approx \frac{1}{2\pi\kappa\omega'} \frac{1}{e^{2\pi\omega/\kappa} - 1}, \tag{4.109}$$

i.e. the spectrum obeys Planck distribution at late times.

Logex: Entropy

The entanglement entropy of the Logex mirror is,

$$S(t) = \frac{1}{6} \tanh^{-1}\left(\frac{e^{2\kappa t}}{1+e^{2\kappa t}}\right), \tag{4.110}$$

the graphical illustration of which is demonstrated in Fig. (4.40).

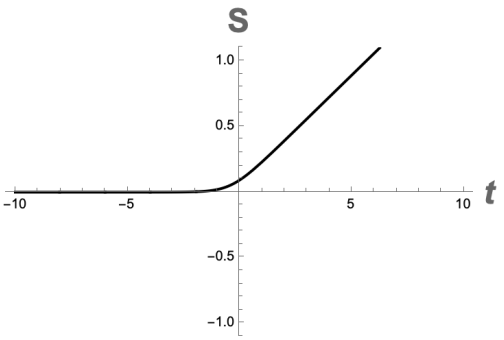

Figure 4.40: Logex mirror entropy.

Similar to the Schwarzschild mirror case, the Logex mirror entropy also increases monotonically over time, diverging linearly in the $t \to \infty$ limit. The drifting case of the Logex mirror is investigated in further section, Sec. (4.8.4).

4.3.2 Evans

Evans: Dynamics

Constructed by Evans in [23], the modified Carlitz-Willey mirror trajectory is,

$$x(t) = -\frac{1-\sigma}{1+\sigma}t - \frac{1}{\kappa}W\left(\frac{e^{-\frac{2\kappa t}{1+\sigma}}}{1+\sigma}\right), \tag{4.111}$$

where $0 \leq \sigma \leq 1$. If $\sigma = 0$, then this trajectory reduces to the Carlitz-Willey mirror trajectory, Eq. (4.21). So, the trajectory starts asymptotically inertial and goes to

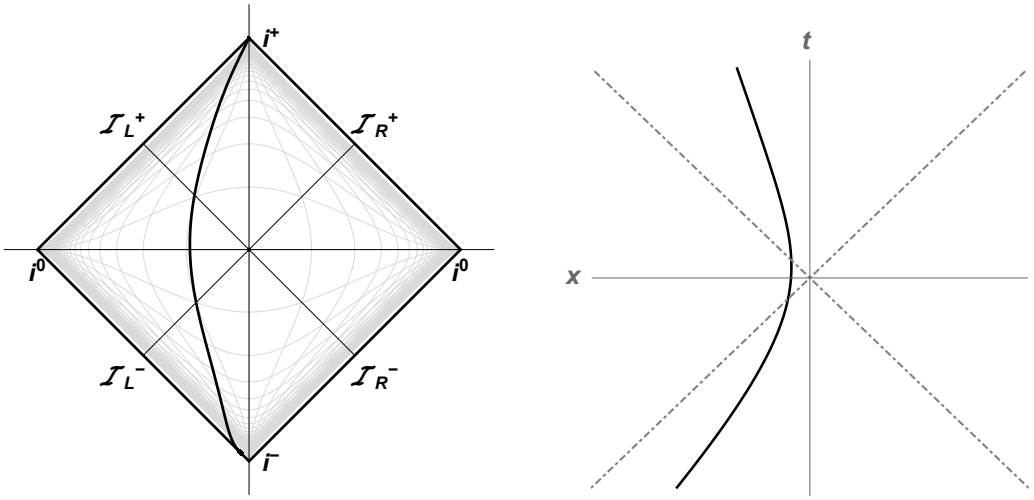

Figure 4.41: a) Penrose and b) Spacetime diagrams for the Evans mirror trajectory, with $\sigma = \frac{1}{2}$.

future time infinity, Fig. (4.41). The ray-tracing functions in null coordinates and the transcendental inversion of Eq. (4.111) are,

$$p(u) = \sigma u - \frac{1}{\kappa}e^{-\kappa u}, \qquad f(v) = \frac{v}{\sigma} + \frac{1}{\kappa}W\left(\frac{e^{-\frac{\kappa v}{\sigma}}}{\sigma}\right), \tag{4.112}$$

$$t(x) = -\frac{1+\sigma}{1-\sigma}x + \frac{1}{\kappa}W\left(\frac{e^{\frac{2\kappa x}{\sigma-1}}}{\sigma-1}\right). \tag{4.113}$$

Noting that the trajectories in null coordinates look much simpler than the trajectories in spacetime coordinates, it is more practical to find the velocity of the mirror using Eqs. (3.20) and (3.22),

$$V = \frac{e^{-\kappa u} + \sigma - 1}{e^{-\kappa u} + \sigma + 1}. \tag{4.114}$$

So, the Evans mirror starts at the speed of light in past times and ends at the speed $V_{max} < c$ in future times. Interesting to note that $\frac{dp}{du}|_{u\to\infty} = \sigma$, which, in turn, is equal to Eq. (3.20). Therefore, $\sigma = e^{2\eta}$ has the meaning of the mirror speed at late times in null coordinates. The corresponding proper acceleration is,

$$\alpha(u) = -\frac{\kappa e^{-\kappa u}}{2\left(\sigma + e^{-\kappa u}\right)^{3/2}}, \tag{4.115}$$

which in the $u \to \infty$ limit goes to 0.

Evans: Energy

The simplest form of the Evans mirror energy flux is given in u coordinate [23],

$$F(u) = \frac{\kappa^2}{48\pi} \frac{1 - 2\sigma e^{\kappa u}}{(1 + \sigma e^{\kappa u})^2}, \tag{4.116}$$

whose plot is shown in Fig. (4.42).

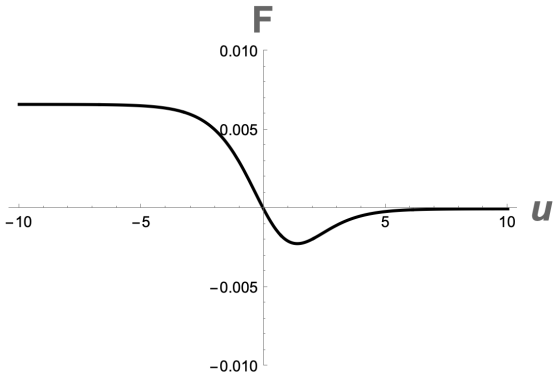

Figure 4.42: Evans mirror energy flux, with $\sigma = \frac{1}{2}$.

The energy flux is unusual with thermal radiation at early time and negative value at late time before vanishing in the $u \to \infty$ limit.

Evans: Particles

The beta Bogolubov coefficient of the Evans mirror is [23],

$$\beta_{\omega\omega'} = -\frac{1}{2\pi\kappa}\sqrt{\frac{\omega}{\omega'}}e^{\frac{-\pi(\omega+\sigma\omega')}{2\kappa}}\left(\frac{\omega'}{\kappa}\right)^{\frac{-i(\omega+\sigma\omega')}{\kappa}}\Gamma\left[\frac{i(\omega+\sigma\omega')}{\kappa}\right]. \tag{4.117}$$

The complex conjugate squaring of Eq. (4.117) yields,

$$|\beta_{\omega\omega'}|^2 = \frac{\omega}{2\pi\kappa\omega'\left(\omega+\sigma\omega'\right)}\frac{1}{e^{\frac{2\pi(\omega+\sigma\omega')}{\kappa}}-1}. \tag{4.118}$$

The numerical result for the Evans mirror particle spectrum is demonstrated in Fig. (4.43).

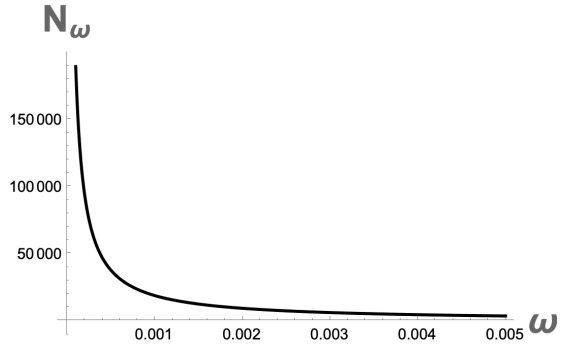

Figure 4.43: Evans mirror particle spectrum, with $\sigma = \frac{1}{2}$.

The spectrum obeys Gamma function distribution and is infra-red divergent.

Evans: Entropy

The entanglement entropy of the Evans mirror simply is,

$$S(u) = -\frac{1}{12}\ln\Big(\sigma + e^{-\kappa u}\Big), \tag{4.119}$$

the graphical illustration of which is demonstrated in Fig. (4.44).

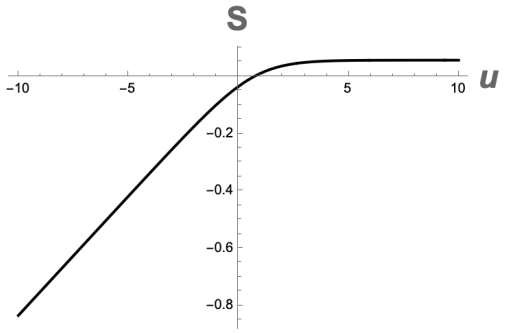

Figure 4.44: Evans mirror entropy, with $\sigma = \frac{1}{2}$.

Unusually, the entropy is shown to be constant at late times. However, it is divergent in the opposite direction, i.e. at early times.

4.3.3 Dual-Temperature

DT: Dynamics

The Dual-temperature mirror trajectory is given as [51],

$$f(v) = -\frac{1}{\kappa}\ln\left[\kappa v(\kappa v - 1)\right], \tag{4.120}$$

whose dynamics is depicted in Fig. (4.45). The trajectory starts asymptotically inertial

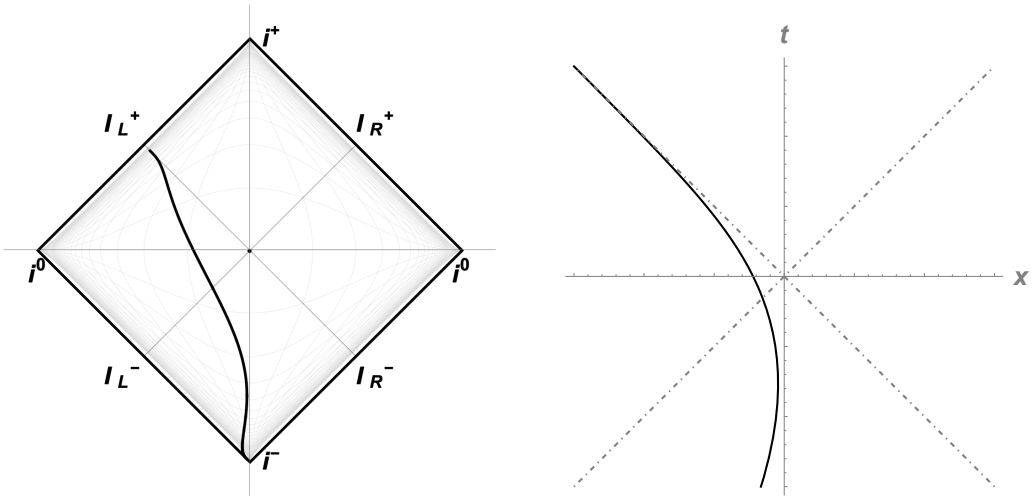

Figure 4.45: a) Penrose and b) Spacetime diagrams for the Dual-temperature mirror trajectory.

and ends at the speed of light with infinite acceleration as approaches the event horizon located at $v_H = 0$. The ray-tracing function in terms of retarded time u is found to be,

$$p(u) = \frac{1}{2\kappa}\left(1 - \sqrt{1 + 4e^{-\kappa u}}\right), \tag{4.121}$$

whereas the trajectories in spacetime coordinates are not tractable. Using Eqs. (3.20) and (3.22), the mirror velocity is,

$$V(v) = -\tanh\left[\frac{1}{2}\ln\left(\frac{1-2\kappa v}{\kappa v(\kappa v - 1)}\right)\right], \tag{4.122}$$

which in the limits $v \to (-\infty, 0)$ goes to the speed of light, i.e. $|V| \to 1$. The corresponding proper accelerations after expanding to leading order terms at $v \to -\infty$ and $v \to v_H = 0$, respectively, are:

$$\alpha_{past}(v) = -\frac{1}{2\sqrt{2}}\sqrt{-\frac{\kappa}{v}}, \tag{4.123}$$

and

$$\alpha_{horizon}(v) = -\frac{1}{2}\sqrt{-\frac{\kappa}{v}}. \tag{4.124}$$

Apparently, the relation between these accelerations is $\alpha_{past} = \frac{\alpha_{horizon}}{\sqrt{2}}$, which indicates that radiation occurring near horizon is hotter than the radiation occurring at early times, i.e. $T_{past} < T_{horizon}$.

DT: Energy

The energy flux as a function of retarded time u is,

$$F(u) = \frac{\kappa^2 \left(4 + 8e^{\kappa u} + e^{2\kappa u}\right)}{48\pi \left(4 + e^{\kappa u}\right)^2}, \tag{4.125}$$

which, to leading order terms at $u \to (-\infty, \infty)$, reduces to [51],

$$F_{past} = \frac{\kappa^2}{192\pi}, \qquad F_{horizon} = \frac{\kappa^2}{48\pi}. \tag{4.126}$$

The graphical illustration of Eq. (4.125) is demonstrated in Fig. (4.46).

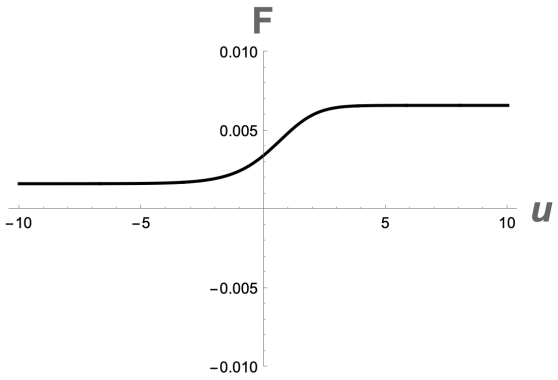

Figure 4.46: Dual-temperature mirror energy flux.

The general flux asymptotically increases over time. However, the flux has constant thermal behavior at the past and near horizon. So, the dual-temperature mirror flux is similar to the Schwarzschild mirror flux at late times, Sec. (4.1.4).

DT: Particles

The associated beta Bogolubov coefficient of the dual-temperature mirror is,

$$\beta_{\omega\omega'} = \frac{\sqrt{\omega\omega'}}{2\sqrt{\pi}} \left(-\frac{i\omega'}{\kappa}\right)^{-\frac{1}{2}-\frac{i\omega}{\kappa}} e^{-\frac{i\omega'}{2\kappa}} \operatorname{csch}\left(\frac{\pi\omega}{\kappa}\right) \frac{K_a\left[-\frac{i\omega'}{2\kappa}\right]}{\Gamma\left[1-\frac{i\omega}{\kappa}\right]}, \tag{4.127}$$

where $a \equiv \frac{1}{2} + \frac{i\omega}{\kappa}$. The complex conjugate square of Eq. (4.127) yields [51],

$$|\beta_{\omega\omega'}|^2 = \frac{1}{2\pi^2\kappa^2} \frac{\left|K_a\left[\frac{i\omega'}{2\kappa}\right]\right|^2}{e^{2\pi\omega/\kappa}-1}. \tag{4.128}$$

The numerical result for the DT mirror particle spectrum is demonstrated in Fig. (4.47).

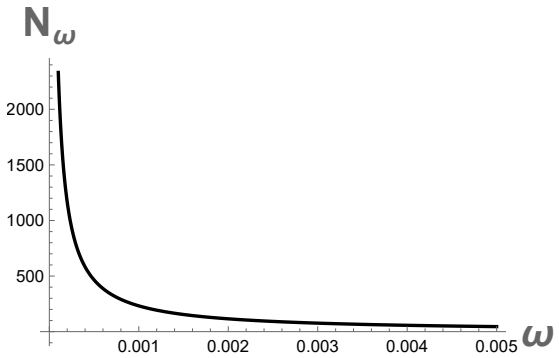

Figure 4.47: Dual-temperature mirror particle spectrum.

The spectrum is infra-red divergent, i.e. the particle production is infinite. For past ($\omega' \ll \omega$) and future ($\omega' \gg \omega$) times separately, to leading order terms, the spectrum becomes,

$$N^{past}_{\omega\omega'} = \frac{1}{\pi\kappa\omega'} \frac{1}{e^{4\pi\omega/\kappa}-1}, \tag{4.129}$$

$$N^{horizon}_{\omega\omega'} = \frac{1}{2\pi\kappa\omega'} \frac{1}{e^{2\pi\omega/\kappa}-1}. \tag{4.130}$$

So, the spectrum obeys Planck distribution at future times.

DT: Entropy

The mirror entanglement entropy simply is,

$$S(u) = -\frac{1}{12} \ln \left| \frac{e^{-\kappa u}}{\sqrt{1 + 4e^{-\kappa u}}} \right|, \tag{4.131}$$

the graphical illustration of which is shown in Fig. (4.48).

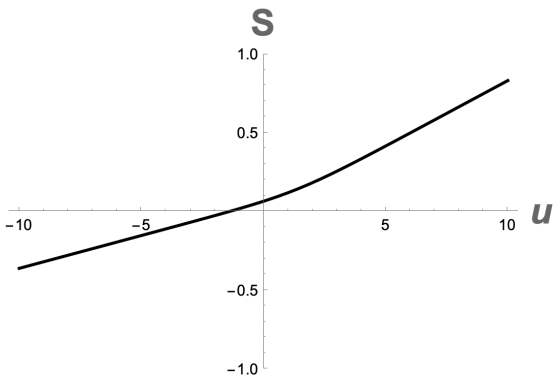

Figure 4.48: Dual-temperature mirror entropy.

The entropy increases logarithmically over time diverging linearly in the $u \to \pm\infty$ limits.

4.4 Black Hole Null

There are 4 beta-known black hole analog moving mirrors, excluding the Schwarzschild mirror model:

- CGHS
- Reissner-Nordström
- Kerr
- Taub-NUT

Here black hole models are approximated by (1+1)-dimensional moving mirrors, except the CGHS and Taub-NUT cases, which are themselves simplified (1+1)D black hole toy models.

Black hole null mirrors have qualitatively similar dynamics: trajectories start asymptotically static and go to infinite acceleration in the far future. All these mirrors have an event horizon. The energy fluxes have monotonic approach to thermality, with infinite energy emission and infinite particle production. Moreover, all the mirrors obey Planck distribution at late times.

The CGHS and Taub-NUT mirrors are one parameter systems, while the Reissner-Nordström (RN) and Kerr models have two parameters that complicate the calculations of some quantities of interest, i.e. not all ray-tracing functions are tractable. In the Kerr solution, the surface gravity is defined via the Schwarzschild surface gravity and black hole spring constant.

Throughout the thesis, κ is a positively defined quantity within a mirror model that has a unit of acceleration in natural units, i.e. $\hbar = c = 1$. The graphs are plotted with $\kappa = 1$ since its value does not affect the general physical properties of the system.

4.4.1 CGHS

CGHS: Dynamics

The CGHS black hole analog moving mirror trajectory is described as [57, 61, 36],

$$z(t) = -\frac{1}{\kappa}\sinh^{-1}\left(\frac{e^{\kappa(t-v_H)}}{2}\right), \tag{4.132}$$

where the exact mirror event horizon location is found to be [44],

$$v_H = \frac{1}{\Lambda}\ln\left(\frac{\Lambda}{M}\right). \tag{4.133}$$

The dynamics of Eq. (4.132) is depicted in Fig. (4.49). The trajectory starts

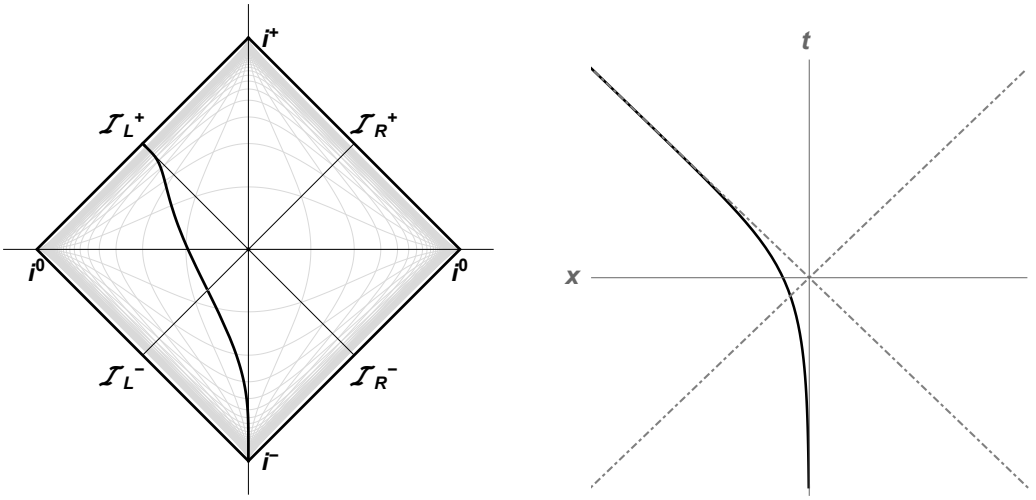

Figure 4.49: a) Penrose and b) Spacetime diagrams for the CGHS mirror trajectory, with $v_H = 0$.

asymptotically static and goes to null future infinity. The ray-tracing functions in other coordinates are,

$$p(u) = u - \frac{1}{\kappa}\ln\left[1 + e^{\kappa(u-v_H)}\right], \tag{4.134}$$

$$f(v) = v - \frac{1}{\kappa}\ln\left[1 - e^{\kappa(v-v_H)}\right], \tag{4.135}$$

$$t(x) = v_H + \frac{1}{\kappa}\ln[-2\sinh(\kappa x)]. \tag{4.136}$$

The mirror velocity is,

$$\dot{z}(t) = -\frac{e^{\kappa(t-v_H)}}{\sqrt{4 + e^{2\kappa(t-v_H)}}}, \tag{4.137}$$

which in the $t \to \infty$ limit goes to the speed of light, i.e. $\dot{z}(t) \equiv |V| \to 1$. The corresponding proper acceleration is,

$$\alpha(t) = -\frac{\kappa}{2}e^{\kappa(t-v_H)}, \tag{4.138}$$

which in the $t \to \infty$ limit goes to $\alpha(t) \to -\infty$, i.e. the trajectory accelerates infinitely into the far future.

CGHS: Energy

The energy flux of the CGHS mirror in terms of u retarded time simply is,

$$F(u) = \frac{\kappa^2}{48\pi} \frac{e^{\kappa u}(e^{\kappa u} + 2e^{\kappa v_H})}{(e^{\kappa u} + e^{\kappa v_H})^2}, \tag{4.139}$$

whose graphical illustration is given in Fig. (4.50).

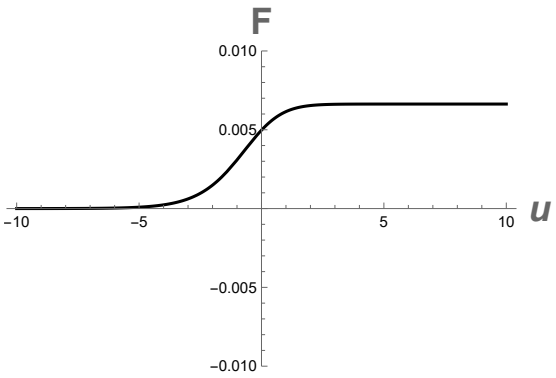

Figure 4.50: CGHS mirror energy flux, with $v_H = 0$.

The flux is as expected: it has monotonic approach to equilibrium in the future, i.e. there is constant thermal emission at late times. In terms of space coordinate x, the energy flux is,

$$F(x) = \frac{\kappa^2}{48\pi} \left(1 - e^{4\kappa x}\right). \tag{4.140}$$

Similar to the Schwarzschild mirror case, Eq. (4.41), the CGHS mirror flux as a function of x coordinate is also independent of the horizon location.

CGHS: Particles

First solved in [19], the beta Bogolubov coefficient of the CGHS mirror is [44],

$$\beta_{\omega\omega'} = \frac{1}{2\pi\kappa}\sqrt{\frac{\omega'}{\omega}}B\left[-\frac{i\omega_+}{\kappa}, 1+\frac{i\omega}{\kappa}\right], \tag{4.141}$$

where $B(a,b) = \frac{\Gamma(a)\Gamma(b)}{\Gamma(a+b)}$ is the Euler integral of the first kind, and $\omega_+ \equiv \omega + \omega'$. The complex conjugate squaring of Eq. (4.141) yields,

$$|\beta_{\omega\omega'}|^2 = \frac{1}{4\pi^2\kappa^2}\frac{\omega'}{\omega}\left|B\left[\frac{i\omega_+}{\kappa}, 1-\frac{i\omega}{\kappa}\right]\right|^2. \tag{4.142}$$

In high frequency regime, $\omega' \gg \omega$, Eq. (4.142) reduces to,

$$|\beta_{\omega\omega'}|^2 \approx \frac{1}{2\pi\kappa\omega'}\frac{1}{e^{2\pi\omega/\kappa}-1}. \tag{4.143}$$

Using (4.142), the numerical result for the CGHS particle spectrum is demonstrated in Fig. (4.51).

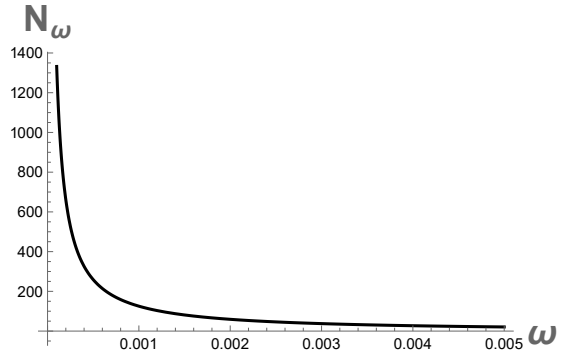

Figure 4.51: CGHS mirror particle spectrum.

The CGHS particle spectrum is divergent, and obeys Planck distribution at late times.

CGHS: Entropy

The entanglement entropy of the CGHS mirror simply is,

$$S(t) = \frac{1}{6}\tanh^{-1}\left(\frac{e^{\kappa(t-v_H)}}{\sqrt{4+e^{2\kappa(t-v_H)}}}\right), \tag{4.144}$$

the graphical illustration of which is demonstrated in Fig. (4.52).

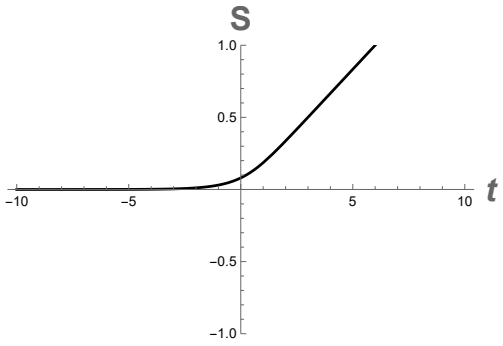

Figure 4.52: CGHS mirror entropy, with $v_H = 0$.

It can be noted that the CGHS mirror entropy has similar behaviour as in the Schwarzschild mirror case, Fig. (4.16): the entropy increases monotonically over time, diverging in the $t \to \infty$ limit.

The drifting cousin of the CGHS mirror is investigated in Sec. (4.8.2). Also, the CGHS mirror Larmor power and radiation reaction force are studied in [44]. As a result, it was found that the Larmor power and self-force for the mirror describe quantum radiation.

4.4.2 Reissner-Nordström

RN: Dynamics

The Reissner-Nordström mirror trajectory is identified as [39],

$$f(v) = v - \frac{1}{\kappa_+}\ln\left|\frac{v}{2r_+}\right| - \frac{1}{\kappa_-}\ln\left|\frac{2r_- - 2r_+ + v}{2r_-}\right|. \tag{4.145}$$

Here $r_\pm$ are the RN black hole outer $\&$ inner horizons, and $\kappa_\pm$ are the surface gravities defined as,

$$r_\pm = \frac{1}{2}\left(r_s \pm \sqrt{r_s^2 - 4r_q^2}\right), \qquad \kappa_\pm = \frac{r_\pm - r_\mp}{2r_\pm^2}, \tag{4.146}$$

where $r_s = 2M$ is the Schwarzschild black hole horizon, $r_q = Q$ is a charge, and the event horizon is located at $v_H \equiv -2\left(M + \sqrt{M^2 - Q^2}\right)$. It is easy to verify that in the limit $Q \to 0$, i.e. when the black hole is not charged, Eq. (4.145) reduces to the Schwarzschild mirror trajectory, Eq. (4.37). The RN mirror trajectory has qualitatively

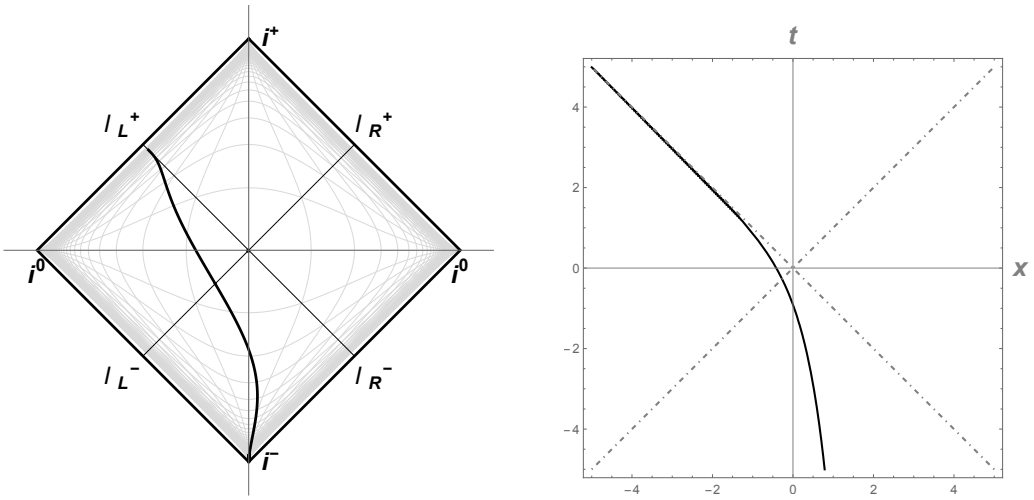

Figure 4.53: a) Penrose and b) Spacetime diagrams for the Reissner-Nordström mirror trajectory, with $M = \frac{1}{4}$ and $Q = \frac{\sqrt{3}}{8}$.

similar dynamics as the Schwarzschild mirror trajectory, i.e. it starts asymptotically static and goes to infinite acceleration in the far future, Fig. (4.13). It is worth to note that the value of the charge hardly affects the mirror dynamics. Using Eqs. (3.20) and (3.22), the mirror velocity is,

$$V = \frac{\kappa_-(2r_+ - 2r_- - v) - \kappa_+ v}{\kappa_+ v + \kappa_-(2r_+ - 2r_- - v)(2\kappa_+ v - 1)}, \tag{4.147}$$

which in the $v \to v_H = 0$ limit goes to the speed of light, i.e. $|V| \to 1$. Using Eq. (3.26), the corresponding proper acceleration to leading order in v is,

$$\alpha(v) = -\frac{\kappa_+}{\sqrt{-4\kappa_+ v}} + \mathcal{O}(v), \tag{4.148}$$

which diverges in the limit $v \to v_H = 0$. More interesting aspects of the RN mirror can be found in [38].

RN: Energy

The expression for the Reissner-Nordström mirror energy flux is found to be lengthy. However, to leading order in v near $v \to 0^-$, it is constant,

$$F(v) = \frac{\kappa_+^2}{48\pi} + \mathcal{O}(v^2). \tag{4.149}$$

The graphical illustration of the full expression for the RN mirror energy flux is demonstrated in Fig. (4.54).

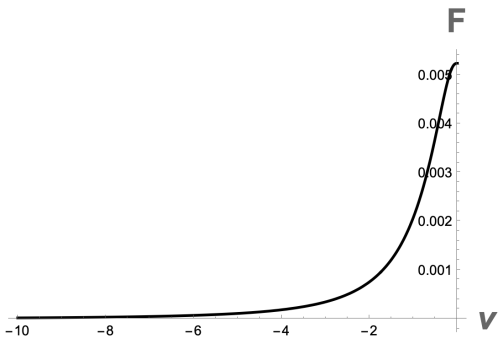

Figure 4.54: Reissner-Nordström mirror energy flux, with $M = \frac{1}{4}$ and $Q = \frac{\sqrt{3}}{8}$.

Similar to the Schwarzschild and CGHS cases, the RN mirror flux has a monotonic approach to thermality. The significant difference in the flux behavior occurs at high charge limit when $Q^2 \to M^2$, which corresponds to the extremal RN mirror model.

RN: Particles

The beta Bogolubov coefficient of the Reissner-Nordström mirror is [39],

$$\beta_{\omega\omega'} = \frac{1}{2\omega_p}\sqrt{\frac{\omega'}{\omega}}\,\mathrm{csch}\left(\frac{\pi\omega}{\kappa}\right)\overline{A}. \tag{4.150}$$

Here $\omega_p \equiv \omega + \omega'$, and

$$a \equiv \frac{i\omega}{\kappa_+}, \quad b \equiv \frac{i\omega}{\kappa}, \quad c \equiv -\frac{i\omega_p}{\overline{\kappa}}, \quad d \equiv -\frac{i\omega}{\kappa_-},$$

$$\overline{A} \equiv x(A - bB) + y(C - cD),$$

$$x \equiv -\frac{\Gamma(a)}{\Gamma(d)}\left(\frac{r_-}{r_+}\right)^d\left(\frac{1}{2\overline{\kappa}r_+}\right)^b, \qquad y \equiv \left(\frac{r_-}{r_+}\right)^a\left(\frac{1}{-2i\omega_p r_-}\right)^b,$$

$$A \equiv {}_1\tilde{F}_1(a;b;c), \qquad B \equiv {}_1\tilde{F}_1(a;1+b;c),$$

$$C \equiv {}_1\tilde{F}_1(1+d;-b;c), \qquad D \equiv {}_1\tilde{F}_1(1+d;1-b;c),$$

where $\kappa = 1/4M$, $\overline{\kappa}^{-1} = 2(r_+ - r_-) = 4\sqrt{M^2 - Q^2}$, ${}_1\tilde{F}_1(m;n;l)$ is the regularized confluent hypergeometric function, and $\Gamma[n]$ is the Gamma function. The complex conjugation of Eq. (4.150) yields,

$$|\beta_{\omega\omega'}|^2 = \frac{1}{2\pi\kappa_+}\frac{\omega'}{\omega_p^2}\frac{e^{-\pi\omega/\kappa_-}}{e^{2\pi\omega/\kappa_+} - 1}|U|^2, \tag{4.151}$$

where $U \equiv U\left(\frac{i\omega}{\kappa_-}, \frac{i\omega}{\kappa}, \frac{i\omega_p}{\overline{\kappa}}\right)$ is the second kind confluent hypergeometric Kummer function. The numerical result for the RN mirror particle spectrum is demonstrated in Fig. (4.55).

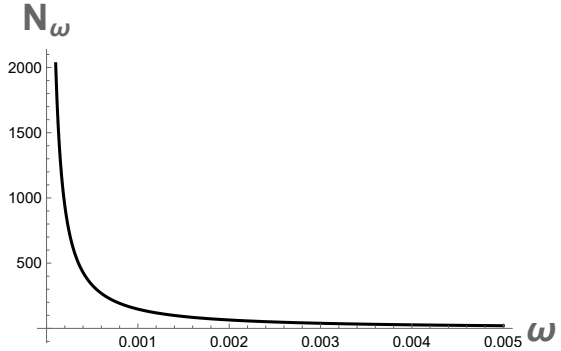

Figure 4.55: Reissner-Nordström mirror particle spectrum, with $M = \frac{1}{4}$ and $Q = \frac{\sqrt{3}}{8}$.

The spectrum obeys Kummer function distribution and is infra-red divergent. In high frequency limit, $\omega' \gg \omega$, Eq. (4.151) reduces to,

$$|\beta_{\omega\omega'}|^2 \approx \frac{1}{2\pi\kappa_+\omega'}\frac{1}{e^{2\pi\omega/\kappa_+} - 1}, \tag{4.152}$$

i.e. the RN mirror particle spectrum obeys Planck distribution at late times.

RN: entropy

The entanglement entropy of the Reissner-Nordström mirror simply is,

$$S(v) = \frac{1}{12} \ln \left[\frac{D-1}{D} - \frac{1}{\kappa_+ v} \right], \tag{4.153}$$

where $D \equiv \kappa_- (2r_- - 2r_+ + v)$. The graphical illustration of Eq. (4.153) is given in Fig. (4.56).

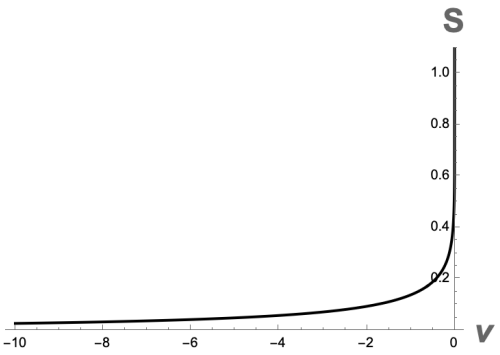

Figure 4.56: Reissner-Nordström mirror entropy, with $M = \frac{1}{4}$ and $Q = \frac{\sqrt{3}}{8}$.

The RN mirror entropy has qualitatively similar behavior as the Schwarzschild and CGHS mirrors' entropy. So, it increases monotonically at early times, diverging at horizon, $v = v_H = 0$.

4.4.3 Kerr

Kerr: dynamics

The Kerr mirror trajectory is identified as [40],

$$f(v) = v - \frac{1}{2g}\frac{1+\beta}{\beta}\ln|gv| + \frac{1}{2g}\frac{1-\beta}{\beta}\ln|gv-\beta|, \tag{4.154}$$

where $g = 1/(4M)$ is the Schwarzschild surface gravity, $\beta = \sqrt{1-a^2/M^2}$ and a is mass-normalised angular momentum. Even though the Kerr black hole has two horizons, there is only one surface gravity defined as $\kappa = g - k$, where $k \equiv g\frac{1-\beta}{1+\beta}$ is a black hole spring constant. The dynamics of Eq. (4.154) is depicted in Fig. (4.57).

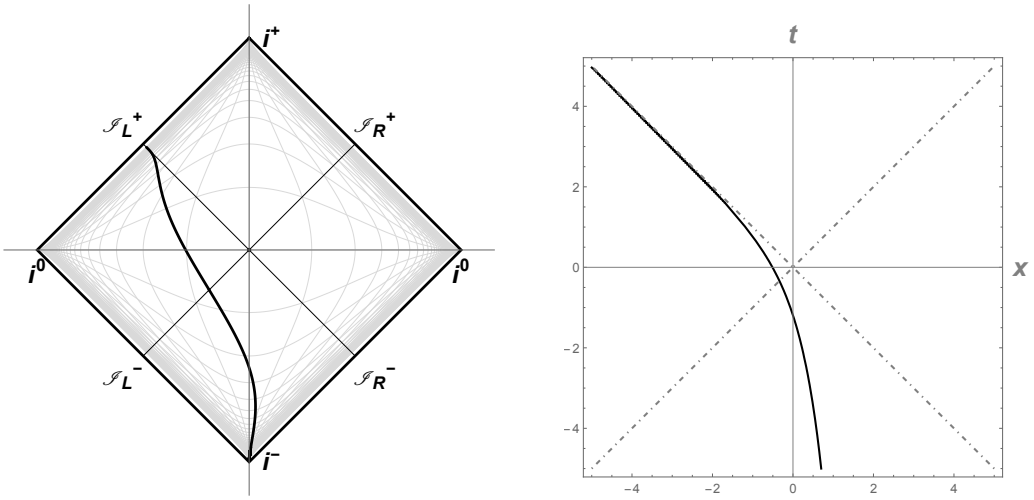

Figure 4.57: a) Penrose and b) Spacetime diagrams for the Kerr mirror trajectory, with $M = \frac{1}{4}$ and $a = \frac{\sqrt{3}}{8}$.

The Kerr mirror trajectory has qualitatively similar dynamics as the Schwarzschild mirror trajectory, i.e. it starts asymptotically static and goes to infinite acceleration in the far future. When $\beta = 1$, then Eq. (4.154) reduces to the Schwarzschild mirror case, Eq. (4.37). Using Eqs. (3.20) and (3.22), the mirror velocity is,

$$V = -\frac{1+b-2gv}{1+b-4bgv+2gv(2gv-1)}, \tag{4.155}$$

which in the limit $v \to v_H = 0$ goes to the speed of light, i.e. $|V| \to 1$. Using Eq. (3.26), the corresponding proper acceleration to leading order term in v is,

$$\alpha(v) = -\frac{\kappa}{\sqrt{-4\kappa v}} + \mathcal{O}(v), \tag{4.156}$$

which diverges in the limit $v \to v_H = 0$. Due to the complex form of the Kerr mirror trajectory, Eq. (4.154), not all ray-tracing functions are transcendentally invertible.

Kerr: energy

The expression for the Kerr mirror energy flux is cumbersome; however, to leading order in v near $v \to 0^-$, it is constant,

$$F(v) = \frac{\kappa^2}{48\pi} + \mathcal{O}(v^2). \tag{4.157}$$

The graphical illustration of the Kerr mirror energy flux is demonstrated in Fig. (4.58).

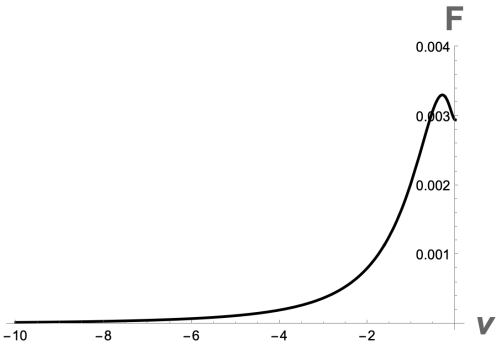

Figure 4.58: Kerr mirror energy flux, with $M = \frac{1}{4}$ and $a = \frac{\sqrt{3}}{8}$.

Similar to the Schwarzschild, CGHS and RN cases, the Kerr mirror flux has a monotonic approach to thermality. The difference is that the Kerr mirror first increases monotonically, then decreases slightly before diverging at horizon, $v = v_H = 0$.

Kerr: particles

The Kerr mirror beta Bogolubov coefficient is [40],

$$\beta_{\omega\omega'} = \frac{1}{2\omega_p}\sqrt{\frac{\omega'}{\omega}}\,\mathrm{csch}\left(\frac{\pi\omega}{g}\right)\tilde{A}, \tag{4.158}$$

where $\omega_p \equiv \omega + \omega'$, and

$$\tilde{A} \equiv q(xA + yBC),$$

$$q \equiv (-\beta)^a(-g)^c\left(\frac{g}{\beta}\right)^{-c}, \qquad x \equiv i(-i\omega_p)^{p-1}, \qquad y \equiv -\frac{i\beta}{g},$$

$$A \equiv {}_1F_1(a;b;d), \qquad B \equiv \frac{\Gamma[1+c]}{\Gamma[a]}, \qquad C \equiv {}_1F_1(1+c;2-b;d),$$

$$a \equiv \frac{i(1-\beta)\omega}{2\beta g}, \quad b \equiv -\frac{i\omega}{g}, \quad c \equiv \frac{i(1+\beta)\omega}{2\beta g}, \quad d \equiv -\frac{i\beta\omega_p}{g}.$$

Here ${}_1F_1(m;n;l)$ is the Kummer confluent hypergeometric function of the first kind, and $\Gamma[n]$ is the Gamma function. The complex conjugate square of Eq. (4.158) yields,

$$|\beta_{\omega\omega'}|^2 = \frac{1}{2\pi\kappa}\frac{\omega'}{\omega_p^2}\frac{e^{\frac{\pi\omega}{\kappa}\frac{1-\beta}{1+\beta}}}{e^{\frac{2\pi\omega}{\kappa}}-1}|U|^2, \tag{4.159}$$

where

$$U \equiv U\left(\frac{i\omega}{\kappa}\frac{1-\beta}{1+\beta}, -\frac{i\omega}{g}, -\frac{i\beta\omega_p}{g}\right)$$

is the second kind confluent hypergeometric Kummer function. The numerical result for the Kerr mirror particle spectrum is demonstrated in Fig. (4.59).

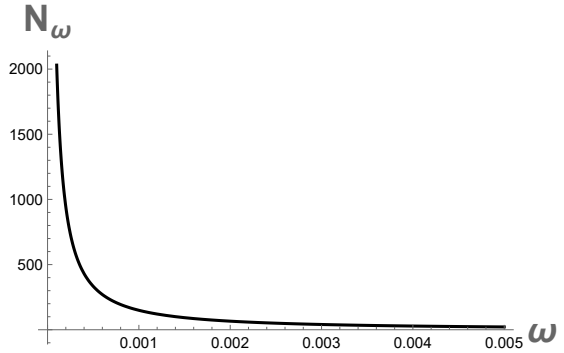

Figure 4.59: Kerr mirror particle spectrum, with $M = \frac{1}{4}$ and $a = \frac{\sqrt{3}}{8}$.

The spectrum obeys Kummer function distribution and is infra-red divergent, i.e. the particle production is infinite. In high frequency regime, $\omega' \gg \omega$, Eq. (4.159) reduces to,

$$|\beta_{\omega\omega'}|^2 \approx \frac{1}{2\pi\kappa\omega'}\frac{1}{e^{2\pi\omega/\kappa}-1}, \tag{4.160}$$

i.e. the Kerr mirror particle spectrum obeys Planck distribution at late times.

Kerr: entropy

The Kerr mirror entanglement entropy simply is,

$$S(v) = \frac{1}{12} \ln \left[1 - \frac{1+\beta}{2\beta g v} + \frac{1-\beta}{2\beta(gv-\beta)} \right]. \tag{4.161}$$

The graphical illustration of Eq. (4.161) is given in Fig. (4.60).

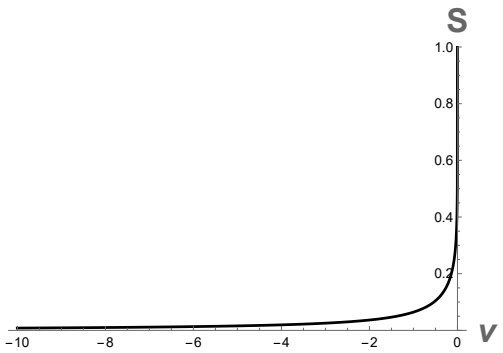

Figure 4.60: Kerr mirror entropy, with $M = \frac{1}{4}$ and $a = \frac{\sqrt{3}}{8}$.

The Kerr mirror entropy has qualitatively similar behavior as the Schwarzschild, CGHS, and RN mirrors' entropy. So, it increases monotonically at early times, diverging at horizon, $v = v_H = 0$.

4.4.4 Taub-NUT

Taub-NUT: dynamics

The generalisation of the Schwarzschild mirror with the additional NUT parameter, l, the Taub-NUT mirror trajectory reads as [68, 69, 43],

$$f(v) = v - \frac{1}{\kappa_+}\ln|\kappa_s v| - \frac{1}{\kappa_-}\ln|\kappa_s(v-4\psi)|, \tag{4.162}$$

where $\kappa_\pm = \frac{1}{2}\left(M \pm \sqrt{M^2+l^2}\right)^{-1}$ are the surface gravities at the inner and outer horizons, $\kappa_s = 1/4M$ is the Schwarzschild surface gravity, and $\psi = \sqrt{M^2+l^2}$. The dynamics of Eq. (4.162) is depicted in Fig. (4.61).

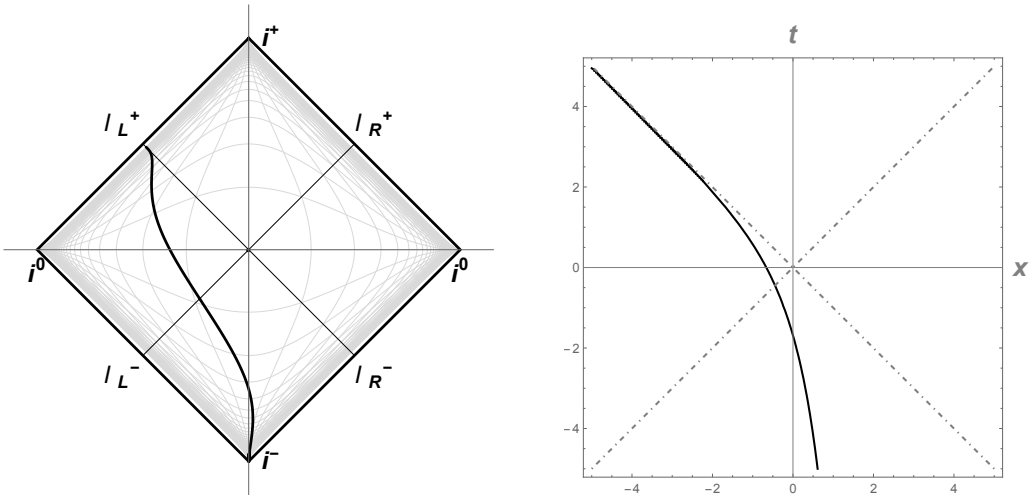

Figure 4.61: a) Penrose and b) Spacetime diagrams for the Taub-NUT mirror trajectory, with $M = \frac{1}{4}$ and $l = \frac{1}{2}$.

The Taub-NUT mirror trajectory has qualitatively similar dynamics as the Schwarzschild, CGHS, RN and Kerr mirrors' trajectory, i.e. it starts asymptotically static and goes to infinite acceleration in the far future. Using Eqs. (3.20) and (3.22), the mirror velocity is,

$$V = -\frac{\kappa_+ v + \kappa_-(v-4\psi)}{\kappa_+ v + \kappa_-(v-4\psi)(1-2\kappa_+ v)}, \tag{4.163}$$

which in the limit $v \to v_H = 0$ goes to the speed of light, i.e. $|V| \to 1$. Using Eq. (3.26), the corresponding proper acceleration to leading order in v is,

$$\alpha(v) = -\frac{\kappa_+}{\sqrt{-4\kappa_+ v}} + \mathcal{O}(v), \tag{4.164}$$

which diverges in the limit $v \to v_H = 0$. Due to the complex form of the Taub-NUT mirror trajectory, Eq. (4.162), not all ray-tracing functions are transcendentally invertible. The extension of the Taub-NUT mirror in the presence of charge and angular momentum as well as its extremal case is investigated in [43].

Taub-NUT: energy

The expression for the Taub-NUT mirror energy flux is found to be lengthy. However, to leading order in v near $v \to 0^-$, it is constant [43],

$$F(v) = \frac{\kappa_+^2}{48\pi} + \mathcal{O}(v^2). \tag{4.165}$$

The graphical illustration of Eq. (4.165) is demonstrated in Fig. (4.62).

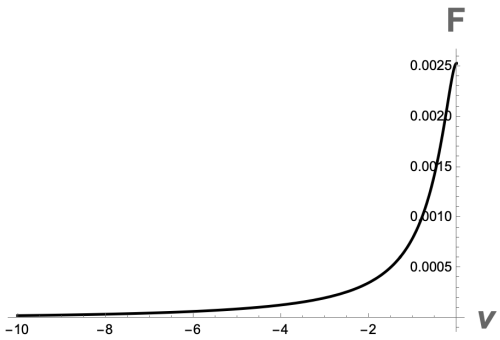

Figure 4.62: Taub-NUT mirror energy flux, with $M = \frac{1}{4}$ and $l = \frac{1}{2}$.

Similar to the Schwarzschild, CGHS, and RN mirrors, the Taub-NUT mirror flux has a monotonic approach to thermality.

Taub-NUT: particles

The Taub-NUT mirror beta Bogolubov coefficient is obtained to be,

$$\beta_{\omega\omega'} = \frac{1}{2\pi}\sqrt{\frac{\omega'}{\omega}}(-\kappa_s)^a(-\kappa_s\psi)^b\left[4^d\psi^{1+a}AB + \psi^{-b}(-i\omega_p)^{-d}CD\right]. \tag{4.166}$$

Here $\omega_p \equiv \omega + \omega'$, and

$$a \equiv \frac{i\omega}{\kappa_+}, \qquad b \equiv \frac{i\omega}{\kappa_-}, \qquad d \equiv 1 + a + b,$$

$$A \equiv {}_1F_1[1+a; 2+a+b; -4i\omega_p\psi], \qquad B \equiv \frac{\Gamma[1+a]\Gamma[-1-a-b]}{\Gamma[-b]},$$

$$C \equiv \Gamma[1+a+b], \qquad D \equiv {}_1F_1[-b; -a-b; -4i\omega_p\psi],$$

where ${}_1F_1[m; n; l]$ is the Kummer confluent hypergeometric function, and $\Gamma[n]$ is the Gamma function. The complex conjugate square of Eq. (4.166) is [43],

$$|\beta_{\omega\omega'}|^2 = \frac{1}{2\pi\kappa_+}\frac{\omega'}{\omega_p^2}\frac{e^{-\pi\omega/\kappa_-}}{e^{2\pi\omega/\kappa_+} - 1}|U|^2, \tag{4.167}$$

where $U \equiv U\left(\frac{i\omega}{\kappa_-}, \frac{i\omega}{\kappa_s}, \frac{i\omega_p}{\overline{\kappa}}\right)$ is the second kind confluent hypergeometric Kummer function, and $\overline{\kappa} \equiv (4\sqrt{M^2 + l^2})^{-1}$. The numerical result for the Taub-NUT mirror particle spectrum is demonstrated in Fig. (4.63).

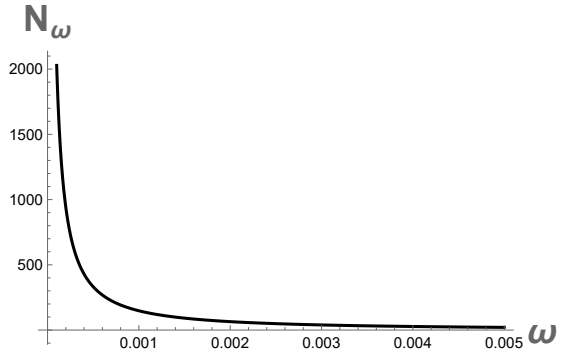

Figure 4.63: Taub-NUT mirror particle spectrum, with $M = \frac{1}{4}$ and $l = \frac{1}{2}$.

The spectrum obeys Kummer function distribution and is infra-red divergent, i.e. the particle production is infinite. Qualitatively, the Taub-NUT mirror spectrum is similar to the Schwarzschild, CGHS, RN and Kerr mirrors' spectra. In high frequency limit, $\omega' \gg \omega$, Eq. (4.167) reduces to,

$$|\beta_{\omega\omega'}|^2 \approx \frac{1}{2\pi\kappa_+\omega'}\frac{1}{e^{2\pi\omega/\kappa_+ - 1}}, \tag{4.168}$$

i.e. the Taub-NUT mirror particle spectrum obeys Planck distribution at late times.

Taub-NUT: entropy

The Taub-NUT mirror entanglement entropy simply is,

$$S(v) = \frac{1}{12} \ln \left(\frac{D-1}{D} - \frac{1}{\kappa_+ v} \right), \tag{4.169}$$

where $D = \kappa_-(v - 4\psi)$. The graphical illustration of Eq. (4.169) is given in Fig. (4.64).

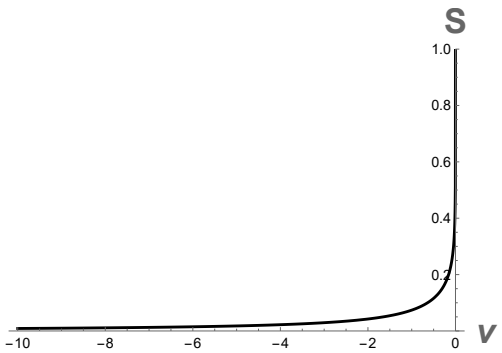

Figure 4.64: Taub-NUT mirror entropy, with $M = \frac{1}{4}$ and $l = \frac{1}{2}$.

The Taub-NUT mirror entropy has qualitatively similar behavior as the Schwarzschild, CGHS, RN and Kerr mirrors' entropy. So, it increases monotonically at early times, diverging at horizon, $v = v_H = 0$.

4.5 Extremal Null

There are 3 beta-known extremal black hole analog moving mirror models:

- Extremal Reissner-Nordström
- Extremal Kerr
- Extremal Kerr-Newman

All extremal null mirrors have qualitatively similar dynamics: trajectories start motion inertial at rest, then approach uniform acceleration in the asymptotic future. All three mirrors emit finite energy with no negative energy flux; however, the mirrors suffer from infinite soft particles production.

The prime feature of the extremal Reissner-Nordström (ERN) and extremal Kerr (EK) mirrors is that they have zero and vanishing surface gravities, respectively. Extremal Kerr-Newman (EKN) mirror is a two parameter (a, Q) model, that generalizes ERN and EK mirror models.

Throughout the thesis, κ is a positively defined quantity within a mirror model that has a unit of acceleration in natural units, i.e. $\hbar = c = 1$. The graphs are plotted with $\kappa = 1$ since its value does not affect the general physical properties of the system.

4.5.1 Extremal Reissner-Nordström

ERN: dynamics

The equivalence of the ERN black hole with the analog mirror model was first identified in the work [62], with the main emphasize on the late time dynamics. This subsection is mainly followed by the work [41], where all times scenario of the associated moving mirror, including both the early and late times, is studied comprehensively. The extremal limit of the Reissner-Nordström black hole is reached when $|Q| = M$. So, the extremal Reissner-Nordström mirror trajectory is identified as,

$$f(v) = v + \frac{1}{\kappa^2(v_H - v)} - \frac{2}{\kappa}\ln\left[\kappa(v_H - v)\right], \tag{4.170}$$

where $\kappa \equiv 1/(2M)$. In spacetime coordinate, this trajectory is expressed as,

$$t(x) = v_H - \frac{1}{2\kappa W\left(\frac{e^{-\kappa x}}{2}\right)} - x. \tag{4.171}$$

The dynamics of the ERN mirror trajectory is depicted in Fig. (4.65). The ERN

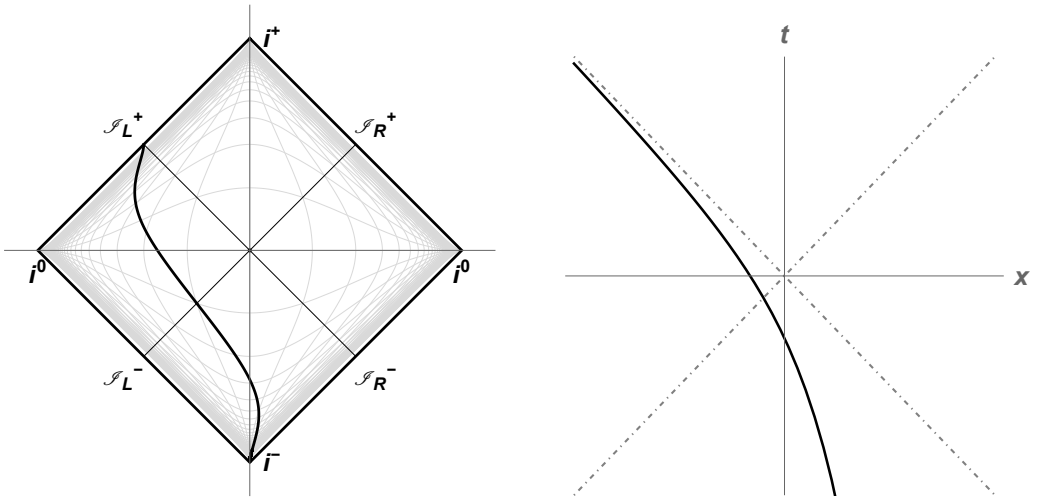

Figure 4.65: (a) Penrose and (b) Spacetime diagrams for the extremal Reissner-Nordström mirror trajectory, with $v_H = 0$.

mirror trajectory starts asymptotically static, finishing with the uniform acceleration as approaches the horizon. The latter can be seen from the corresponding proper acceleration,

$$\alpha(v) = -\frac{\kappa}{\left[\kappa(v_H - v) + 1\right]^2}, \tag{4.172}$$

where

$$\lim_{v \to v_H} \alpha = -\kappa, \tag{4.173}$$

i.e. the mirror becomes uniformly accelerated at late times. The mirror velocity is,

$$V = -\tanh\left[\frac{1}{2}\ln\left[\frac{(1 + \kappa(v_H - v))^2}{\kappa^2(v_H - v)^2}\right]\right], \tag{4.174}$$

which in the limit $v \to v_H = 0$ goes to the speed of light, i.e. $|V| \to 1$.

ERN: energy

The expectation value of the extremal Reissner-Nordström mirror energy flux is [41],

$$F(v) = \frac{\kappa^2}{6\pi} \frac{[\kappa(v_H - v)]^3}{[1 + \kappa(v_H - v)]^6}, \tag{4.175}$$

whose plot is shown in Fig. (4.66). So, the flux is positive over time, first, increasing at

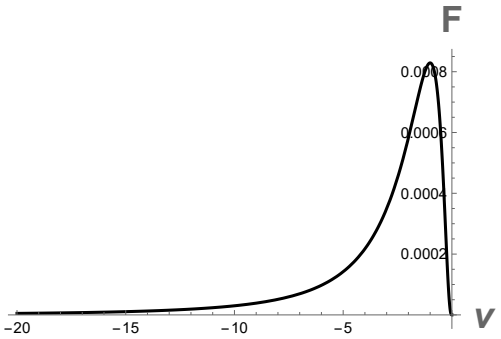

Figure 4.66: Extremal Reissner-Nordström mirror energy flux, with $v_H = 0$.

early times then decreasing as approaches the horizon. The flux in terms of x spacetime coordinate is,

$$F(x) = \frac{4\kappa^2}{3\pi} \frac{W\left[\frac{e^{-\kappa x}}{2}\right]^3}{\left[2W\left(\frac{e^{-\kappa x}}{2}\right) + 1\right]^6}, \tag{4.176}$$

that is independent of the event horizon location as for the other black hole analog mirrors. The flux as a function of null coordinate u happens to be symmetric with respect to the retarded time. The details on this note can be found in [41]. The above fluxes result in finite total energy emission,

$$E = \frac{\kappa}{36\pi}. \tag{4.177}$$

This result is consistent with the numerical verification of the energy found via the beta Bogolubov coefficient, Eq. (3.95).

ERN: particles

The associated mirror beta Bogolubov coefficient is [41],

$$\beta_{\omega\omega'} = -\frac{ie^{-\frac{\pi\omega}{\kappa}}}{\pi\kappa}\sqrt{\frac{\omega'}{\omega_p}}\left(\frac{\omega}{\omega_p}\right)^{\frac{i\omega}{\kappa}} K_a\left(\frac{2}{\kappa}\sqrt{\omega\omega_p}\right), \tag{4.178}$$

where $\omega_p \equiv \omega + \omega'$, $a \equiv 1 + \frac{2i\omega}{\kappa}$, and $K_a(n)$ is the modified Bessel function of the second kind. The complex conjugate square of Eq. (4.178) yields,

$$|\beta_{\omega\omega'}|^2 = \frac{e^{-\frac{2\pi\omega}{\kappa}}}{\pi^2\kappa^2}\frac{\omega'}{\omega_p}\left|K_a\left(\frac{2}{\kappa}\sqrt{\omega\omega_p}\right)\right|^2. \tag{4.179}$$

The numerical result for the ERN mirror particle spectrum is demonstrated in Fig. (4.67).

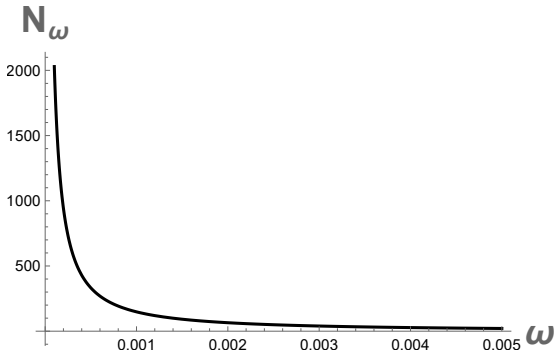

Figure 4.67: Extremal Reissner-Nordström mirror particle spectrum, with $v_H = 0$.

The ERN mirror particle spectrum has qualitatively the same behavior as the other black hole null mirrors' spectra, i.e. the spectrum is infra-red divergent; however, with infinite soft particle production.

ERN: entropy

The extremal Reissner-Nordström mirror entanglement entropy simply is,

$$S(v) = \frac{1}{12} \ln \left[\frac{(1 + \kappa(v_H - v))^2}{\kappa^2 (v_H - v)^2} \right]. \tag{4.180}$$

The graphical illustration of Eq. (4.180) is demonstrated in Fig. (4.68).

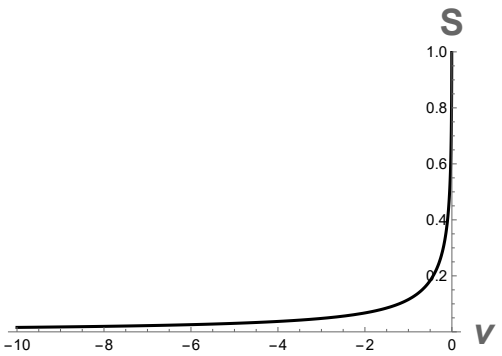

Figure 4.68: Extremal Reissner-Nordström mirror entropy, with $v_H = 0$.

The ERN mirror entropy has qualitatively similar behavior as the other black hole analog mirrors' entropy: it increases monotonically at early times, diverging at horizon, $v = v_H = 0$.

4.5.2 Extremal Kerr

EK: dynamics

The extremal Kerr black hole analog moving mirror model was first studied in [63], and was further developed in [40]. So, the associated mirror trajectory reads as,

$$f(v) = v + \frac{1}{\sqrt{2}\mathcal{A}} - \frac{1}{\mathcal{A}^2 v} - \frac{\sqrt{2}}{\mathcal{A}} \ln\left(-\frac{\mathcal{A}v}{\sqrt{2}}\right), \tag{4.181}$$

where $\mathcal{A} \equiv \frac{1}{2\sqrt{2}M}$, and the horizon is located at $v_H = 0$. The dynamical behaviour of the EK mirror trajectory is illustrated in Fig. (4.69).

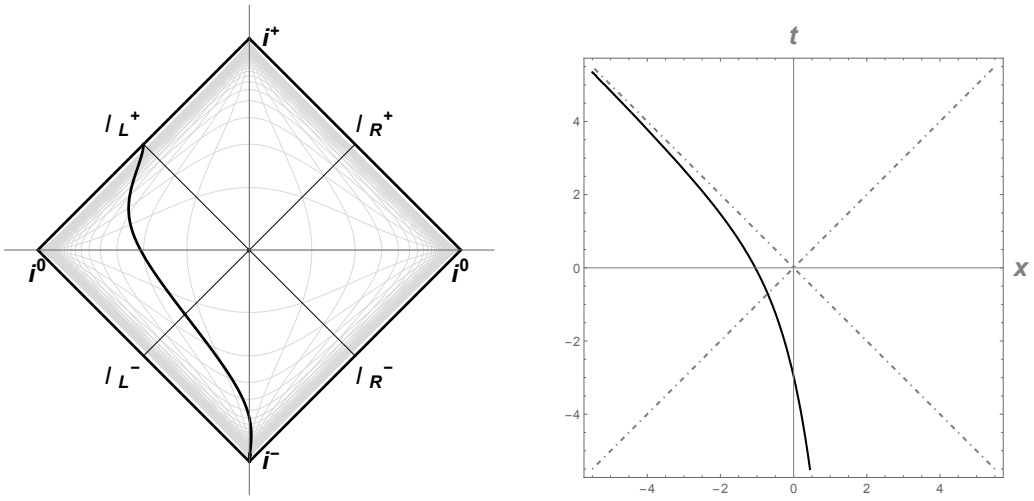

Figure 4.69: (a) Penrose and (b) Spacetime diagrams for the extremal Kerr mirror trajectory, with $\mathcal{A} = 1$.

The dynamics of the EK mirror is similar to the ERN mirror: trajectory starts asymptotically static, then finishing with uniform acceleration in the asymptotic future. The latter that can be seen from the corresponding proper acceleration,

$$\alpha(v) = \frac{\mathcal{A}\left[\sqrt{2} - \mathcal{A}v\right]}{\sqrt{2}\left[1 - \mathcal{A}v\left(\sqrt{2} - \mathcal{A}v\right)\right]^{3/2}}. \tag{4.182}$$

where

$$\lim_{v \to v_H} \alpha(v) = -\mathcal{A}, \tag{4.183}$$

i.e. the mirror moves with asymptotic uniform acceleration, as a result, the energy flux vanishes near horizon. The mirror velocity is,

$$V = -\frac{1 - \sqrt{2}\mathcal{A}v}{1 - \sqrt{2}\mathcal{A}v + 2\mathcal{A}^2 v^2}, \tag{4.184}$$

which in the limit $v \to v_H = 0$ goes to the speed of light, i.e. $|V| \to 1$.

EK: energy

The expectation value of the extremal Kerr mirror energy flux is,

$$F(v) = -\frac{\mathcal{A}^5 v^3 \left(2\sqrt{2} - 7\mathcal{A}v + 2\sqrt{2}\mathcal{A}^2 v^2\right)}{24\pi \left(1 - \sqrt{2}\mathcal{A}v + \mathcal{A}^2 v^2\right)^4}, \tag{4.185}$$

whose plot is shown in Fig. (4.70). The EK mirror flux has qualitatively similar

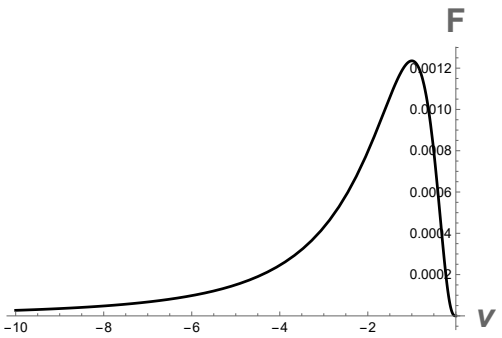

Figure 4.70: Extremal Kerr mirror energy flux, with $\mathcal{A} = 1$.

behaviour as the ERN mirror case: the flux is positive over time, first, increasing at early times then vanishing as approaches the horizon. The total emitted energy is finite [40],

$$E = \frac{\mathcal{A}}{48\pi}\frac{\pi - 1}{\sqrt{2}}. \tag{4.186}$$

This result is consistent with the one derived via the beta coefficient using Eq. (3.95).

EK: particles

The associated mirror beta Bogolubov coefficient is,

$$\beta_{\omega\omega'} = \frac{i}{\pi\mathcal{A}}\sqrt{\frac{\omega'}{\omega}}\left[2^{-\frac{i\omega}{\sqrt{2}\mathcal{A}}}e^{-\frac{(i+\pi)\omega}{\sqrt{2}\mathcal{A}}}\left(\frac{\omega}{\omega_p}\right)^{\frac{1}{2}+\frac{i\omega}{\sqrt{2}\mathcal{A}}}\right]K_a\left(\frac{2}{\mathcal{A}}\sqrt{\omega\omega_p}\right). \tag{4.187}$$

Here $\omega_p \equiv \omega + \omega'$, $a \equiv 1 + \frac{i\omega\sqrt{2}}{\mathcal{A}}$, and $K_a(n)$ is the modified Bessel function of the second kind. The complex conjugate squaring of Eq. (4.187) yields [40],

$$|\beta_{\omega\omega'}|^2 = \frac{e^{-\sqrt{2}\pi\omega/\mathcal{A}}\omega'}{\pi^2\mathcal{A}^2\omega_p}\left|K_a\left(\frac{2}{\mathcal{A}}\sqrt{\omega\omega_p}\right)\right|^2. \tag{4.188}$$

The numerical result for the EK mirror particle spectrum is demonstrated in Fig. (4.71).

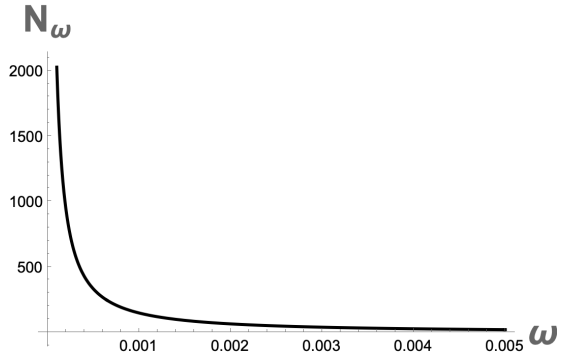

Figure 4.71: Extremal Kerr mirror particle spectrum, with $\mathcal{A} = 1$.

The EK mirror particle spectrum has qualitatively the same behavior as the ERN mirror case: i.e. the spectrum is infra-red divergent with infinite soft particle production.

EK: entropy

The extremal Kerr mirror entanglement entropy simply is,

$$S(v) = \frac{1}{12} \ln \left(1 + \frac{1}{\mathcal{A}^2 v^2} - \frac{\sqrt{2}}{\mathcal{A} v} \right), \tag{4.189}$$

whose graphical illustration is given in Fig. (4.72).

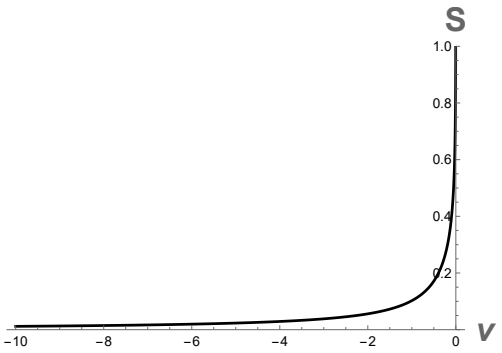

Figure 4.72: Extremal Kerr mirror entropy, with $\mathcal{A} = 1$.

The EK mirror entropy has qualitatively similar behavior as the other black hole analog mirrors' entropy. So, it increases monotonically at early times diverging at horizon, $v = v_H = 0$.

4.5.3 Extremal Kerr-Newman

EKN: dynamics

Occurring in the $M^2 = a^2 + Q^2$ limit, the extremal Kerr-Newman black hole analog moving mirror trajectory reads as [42],

$$f(v) = v - \frac{1}{\mathcal{A}^2 v} - \frac{1}{\kappa} \ln |\kappa v|, \tag{4.190}$$

where $\kappa = \frac{1}{4M}$ is the Schwarzschild surface gravity, and $\mathcal{A} = \frac{1}{2\sqrt{2a^2+Q^2}}$. When $a = 0$, then Eq. (4.190) reduces to the ERN mirror trajectory, Eq. (4.170). When $Q = 0$, then Eq. (4.190) reduces to the EK mirror trajectory, Eq. (4.181). The EKN mirror dynamics is depicted in Fig. (4.73).

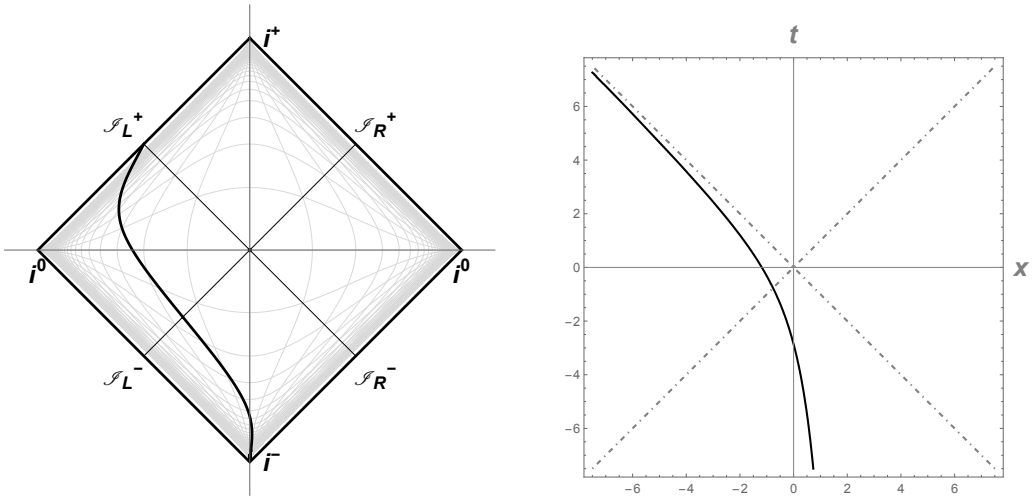

Figure 4.73: (a) Penrose and (b) Spacetime diagrams for the extremal Kerr-Newman mirror trajectory, with $a = \frac{1}{2}$ and $Q = \frac{1}{2}$.

The EKN mirror has qualitatively similar dynamics as the other extremal null mirrors: the trajectory starts asymptotically static, then finishing with uniform acceleration in the asymptotic future. The latter that can be seen from the corresponding proper acceleration,

$$\alpha(v) = \frac{\mathcal{A}\sqrt{\kappa}\,(\mathcal{A}^2 v - 2\kappa)}{2\,(\mathcal{A}^2 v^2 \kappa - \mathcal{A}^2 v + \kappa)^{3/2}}, \tag{4.191}$$

where

$$\lim_{v \to 0} \alpha(v) = -\mathcal{A}, \tag{4.192}$$

i.e. the mirror moves with uniform acceleration in the asymptotic future. The mirror velocity is,

$$V = \frac{\mathcal{A}^2 v - \kappa}{2\mathcal{A}^2 v^2 \kappa - \mathcal{A}^2 v + \kappa}, \tag{4.193}$$

which in the limit $v \to v_H = 0$ goes to the speed of light, i.e. $|V| \to 1$.

EKN: energy

The expectation value of the extremal Kerr-Newman mirror energy flux is [42],

$$F(v) = \frac{\kappa^2}{48\pi} \frac{\mathcal{A}^6 v^3 \left[\mathcal{A}^2 v(1-4\kappa v) + 4\kappa(3\kappa v - 1)\right]}{\left[\mathcal{A}^2 v(\kappa v - 1) + \kappa\right]^4}. \tag{4.194}$$

The graphical illustration of Eq. (4.194) is shown in Fig. (4.74).

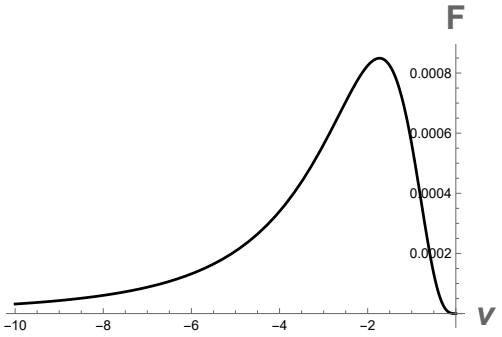

Figure 4.74: Extremal Kerr-Newman mirror energy flux, with $a = \frac{1}{2}$ and $Q = \frac{1}{2}$.

The EKN mirror flux has qualitatively similar behaviour as the other extremal null mirrors: the flux is positive over time, first, increasing at early times then vanishing as approaches the horizon. The total emitted energy is finite,

$$E = \frac{\kappa}{48\pi}\left[-\frac{1}{j^2} + \left(\frac{1}{j^3} + \frac{3}{j}\tanh^{-1} j\right)\right], \tag{4.195}$$

where $j \equiv \frac{a}{M}$ is a mass normalised angular momentum. Remembering that $M^2 = a^2 + Q^2$, Eq. (4.195) at certain limits reduces to the EK and ERN mirrors' energies, respectively,

$$\lim_{Q\to 0} E = E_{KN}, \qquad \lim_{a\to 0} E = E_{ERN}. \tag{4.196}$$

Eq. (4.195) is consistent with the energy result calculated using the beta coefficient, Eq. (3.95).

EKN: particles

The associated mirror beta Bogolubov coefficient is,

$$\beta_{\omega\omega'} = \frac{1}{\pi}\sqrt{\frac{\omega'}{\omega}}(-\kappa)^{\frac{i\omega}{\kappa}}\left(-\frac{i\mathcal{A}^2}{\omega}\right)^{-\frac{1}{2}-\frac{i\omega}{2\kappa}}(-i\omega_p)^{-\frac{1}{2}-\frac{i\omega}{2\kappa}}K_a\left[\frac{2}{\mathcal{A}}\sqrt{\omega\omega_p}\right] \tag{4.197}$$

where $\omega_p \equiv \omega + \omega'$, $a \equiv 1 + \frac{i\omega}{\kappa}$, and $K_a(n)$ is the modified Bessel function of the second kind. The complex conjugate squaring of Eq. (4.197) yields [42],

$$|\beta_{\omega\omega'}|^2 = \frac{e^{-\pi\omega/\kappa}\omega'}{\pi^2\mathcal{A}^2\omega_p}\left|K_a\left(\frac{2}{\mathcal{A}}\sqrt{\omega\omega_p}\right)\right|^2. \tag{4.198}$$

The numerical result for the EKN mirror particle spectrum is demonstrated in Fig. (4.75).

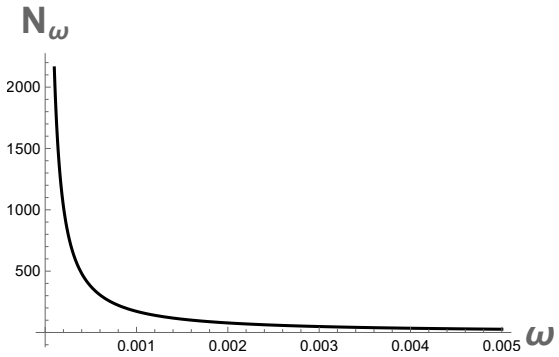

Figure 4.75: Extremal Kerr-Newman mirror particle spectrum, with $a = \frac{1}{2}$ and $Q = \frac{1}{2}$.

The EKN mirror particle spectrum has qualitatively the same behavior as the other extremal null mirrors, i.e. the spectrum is infra-red divergent with infinite soft particle production.

EKN: entropy

The extremal Kerr-Newman mirror entanglement entropy simply is,

$$S(v) = \frac{1}{12} \ln \left(1 + \frac{1}{\mathcal{A}^2 v^2} - \frac{1}{\kappa v} \right), \tag{4.199}$$

whose graphical illustration is given in Fig. (4.76).

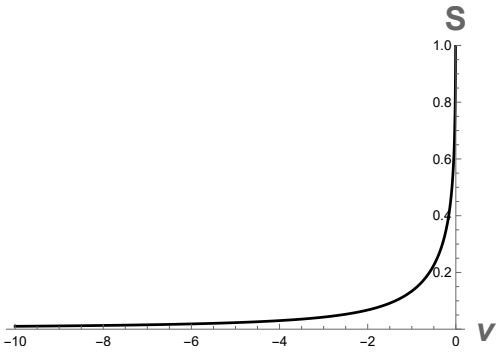

Figure 4.76: Extremal Kerr-Newman mirror entropy, with $a = \frac{1}{2}$ and $Q = \frac{1}{2}$.

The EKN mirror entropy has qualitatively similar behavior as the other black hole and extremal null mirrors' entropy. So, it increases monotonically at early times diverging at horizon, $v = v_H = 0$.

4.6 Cosmo Null

There are 3 beta-known cosmo null moving mirror models:

- de Sitter
- Anti de Sitter
- Schwarzschild de Sitter

All three solutions start and end motions with the speed of light, having thermal radiation emission and infinite particle production.

The de Sitter (dS) solution has two asymptotic null horizons, and the mirror goes to infinite acceleration at these horizons. The radiation is thermal and positive over all times. As a result, the radiation energy is infinite; however, the energy of particles is finite.

The Anti de Sitter (AdS) mirror is unique for several respects. It also has thermal radiation over time but with negative sign. The particle spectrum is obtained using the symmetry with the dS mirror case. Other significant results are found in the following corresponding section.

Schwarzschild de Sitter (SdS) model has three horizons: two physical and one unphysical, correspondingly, there are three surface gravities. The general energy flux has a monotonic increase, starting from cosmological horizon at early time to black hole horizon at late time. However, for the past and future time periods separately, the flux is thermal over time. Consequently, the total energy emission is infinite.

Throughout the thesis, κ is a positively defined quantity within a mirror model that has a unit of acceleration in natural units, i.e. $\hbar = c = 1$. The graphs are plotted with $\kappa = 1$ since its value does not affect the general physical properties of the system.

4.6.1 de Sitter

dS: dynamics

The moving mirror trajectory associated with the de Sitter space is [45],

$$f(v) = \frac{2}{\kappa} \tanh^{-1} \frac{\kappa v}{2}. \tag{4.200}$$

Here the analogy with the cosmological model is done through a correspondence condition $\kappa \equiv 1/L$, where $L^2 \equiv 1/\Lambda$, and Λ is the cosmological constant. The event horizon location is at $v_H = \pm\frac{2}{\kappa}$, i.e. the mirror posses double asymptotic null horizons. The ray-tracing function in retarded time is given as,

$$p(u) = \frac{2}{\kappa} \tanh \frac{\kappa u}{2}. \tag{4.201}$$

The dynamics of the dS mirror is depicted in Fig. (4.77). The trajectory is asymmetric

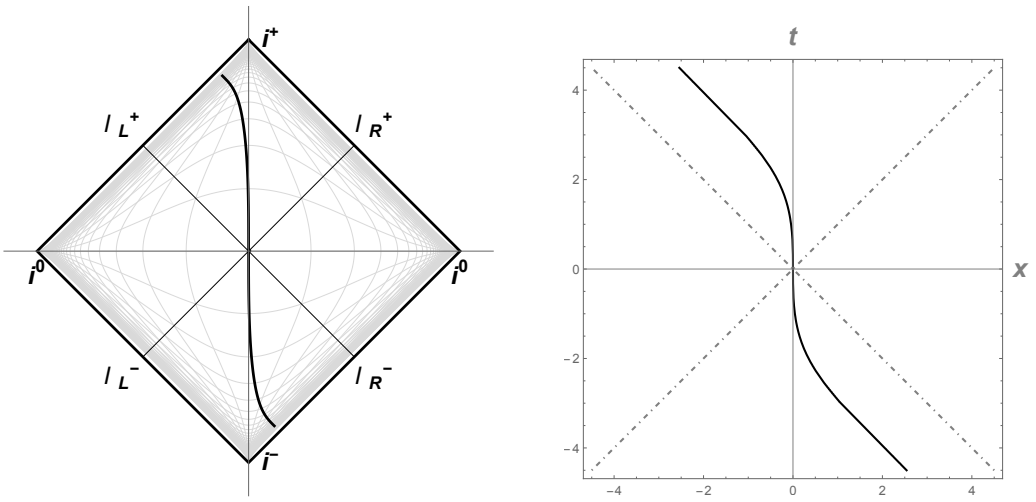

Figure 4.77: (a) Penrose and (b) Spacetime diagrams for the de Sitter mirror trajectory.

with respect to time, starting and ending its motion with infinite acceleration at double asymptotic null horizons. This is verified mathematically by finding the corresponding proper acceleration,

$$\alpha(v) = -\frac{1}{2} \frac{\kappa^2 v}{\sqrt{4 - \kappa^2 v^2}}, \tag{4.202}$$

where

$$\lim_{v \to v_H} \alpha(v) = \pm\infty. \tag{4.203}$$

The mirror velocity is,

$$V = \frac{\kappa^2 v^2}{\kappa^2 v^2 - 8}, \tag{4.204}$$

which in the $v \to v_H$ limit goes to the speed of light, i.e. $|V| \to 1$.

dS: energy

The expectation value of the de Sitter mirror energy flux is constant [45],

$$F = \frac{\kappa^2}{48\pi}, \tag{4.205}$$

i.e. is in thermal equilibrium over all times. For completeness, the trivial plot of the dS mirror energy flux is presented in Fig. (4.78).

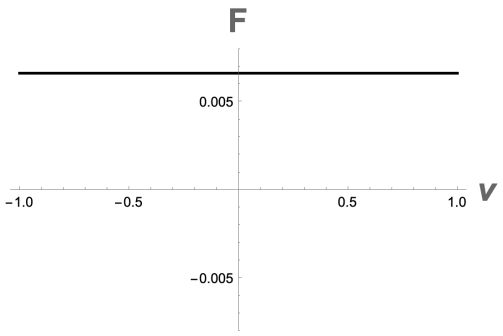

Figure 4.78: de Sitter mirror energy flux.

The dS mirror flux has similar behavior as the Carlitz-Willey mirror flux. The total energy, calculated using the flux, results in infinite value for the region bounded by the two horizons $v_H = \pm\frac{2}{\kappa}$. However, the numerical calculation of the energy via the beta coefficient using Eq. (3.95) gives finite answer. This is explained with the fact that, for the de Sitter mirror, the energy carried by the particles is finite whereas the energy of radiation is infinite.

dS: particles

The beta Bogolubov coefficient for the de Sitter mirror is [45],

$$\beta_{\omega\omega'} = \frac{2\sqrt{\omega\omega'}}{\kappa^2} e^{-2i\omega'/\kappa} \operatorname{csch}\left(\frac{\pi\omega}{\kappa}\right) {}_1F_1\left(1+\frac{i\omega}{\kappa}; 2; \frac{4i\omega'}{\kappa}\right). \tag{4.206}$$

Here ${}_1F_1\left(m; n; q\right)$ is the Kummer function of the first kind or confluent hypergeometric function. The complex conjugate squaring of the beta coefficient yields,

$$|\beta_{\omega\omega'}|^2 = \frac{4\omega\omega'}{\kappa^4} \operatorname{csch}^2\left(\frac{\pi\omega}{\kappa}\right) \left|{}_1F_1\left(1-\frac{i\omega}{\kappa}; 2; -\frac{4i\omega'}{\kappa}\right)\right|^2. \tag{4.207}$$

The numerical result for the dS mirror particle spectrum is demonstrated in Fig. (4.79).

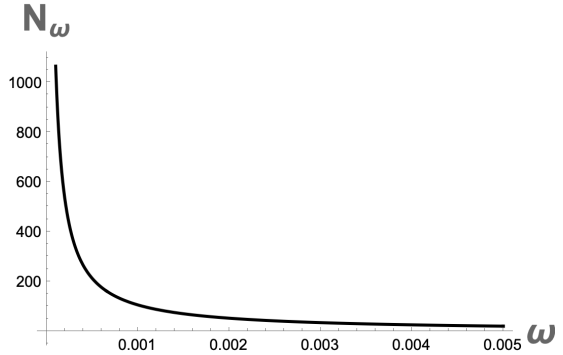

Figure 4.79: de Sitter mirror particle spectrum.

The dS mirror spectrum is infra-red divergent and obeys hypergeometric function distribution. It is not straightforward to see that the spectrum can also be written as a Planck distribution,

$$N_\omega = \frac{\delta(\omega-\omega_2)}{e^{2\pi\omega/\kappa}-1}, \tag{4.208}$$

the detailed calculation of which is given in [45].

dS: entropy

The dS mirror entanglement entropy simply is,

$$S(v) = -\frac{1}{12}\ln\left(1 - \frac{\kappa^2 v^2}{4}\right), \tag{4.209}$$

the graphical illustration of which is given in Fig. (4.80).

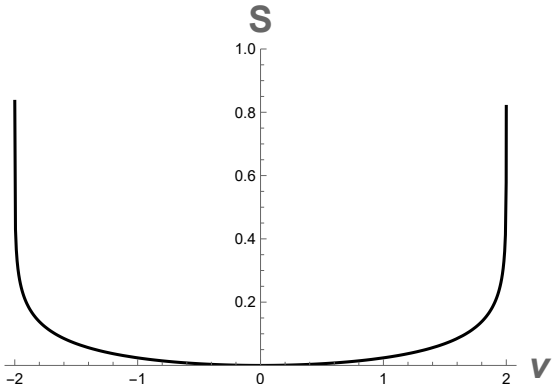

Figure 4.80: de Sitter mirror entropy.

The entropy has a symmetric monotonic increase with respect to the coordinate origin, diverging at the horizons, $v_H = \pm\frac{2}{\kappa}$.

4.6.2 Anti de Sitter

AdS: dynamics

The Anti de Sitter spacetime analog moving mirror trajectory is identified as [45],

$$f(v) = \frac{2}{\kappa} \tan^{-1} \frac{\kappa v}{2}. \tag{4.210}$$

The ray-tracing function in retarded time is,

$$p(u) = \frac{2}{\kappa} \tan \frac{\kappa u}{2}, \tag{4.211}$$

where the horizons are located at $u_H = \pm\pi/\kappa$. The dynamics of the AdS mirror is depicted in Fig. (4.81).

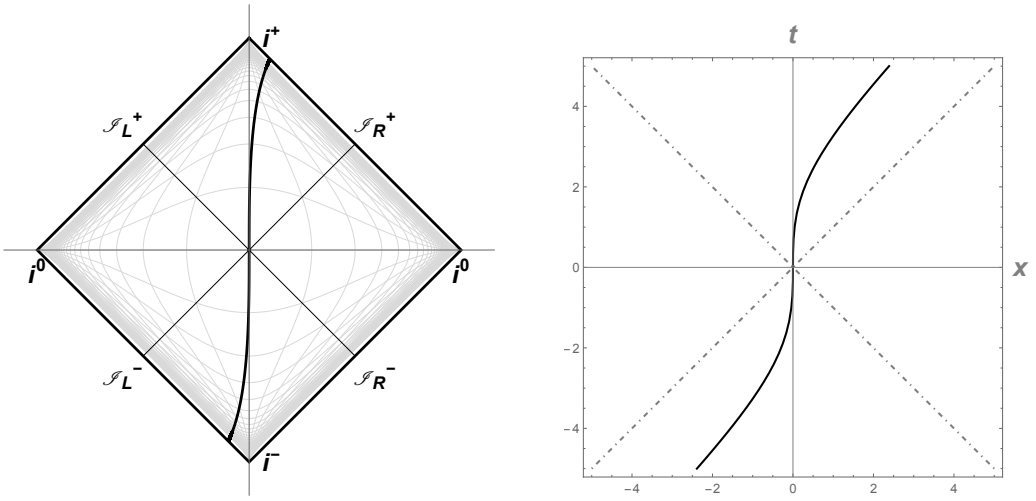

Figure 4.81: (a) Penrose and (b) Spacetime diagrams for the Anti de Sitter mirror trajectory.

The trajectory moves in the opposite direction with respect to the dS mirror trajectory with horizons in retarded time. The mirror velocity in u coordinate is,

$$V = \tanh\left[\frac{1}{2} \ln\left[\sec\left(\frac{\kappa u}{2}\right)\right]\right], \tag{4.212}$$

which in the $u \to u_H$ limit goes to the speed of light, i.e. $V \to 1$. The corresponding proper acceleration is,

$$\alpha(u) = \frac{\kappa}{2} \sin\left(\frac{\kappa u}{2}\right), \tag{4.213}$$

where

$$\lim_{u \to \pm u_H} \alpha(u) = \pm\frac{\kappa}{2}, \tag{4.214}$$

i.e. the mirror becomes asymptotically uniformly accelerated as approaches the horizons.

AdS: energy

The expectation value of the Anti de Sitter mirror energy flux is constant but negative over all times [45],

$$F = -\frac{\kappa^2}{48\pi}, \tag{4.215}$$

which is the opposite of the dS mirror flux. For completeness, the trivial plot of the AdS mirror energy flux is presented in Fig. (4.82).

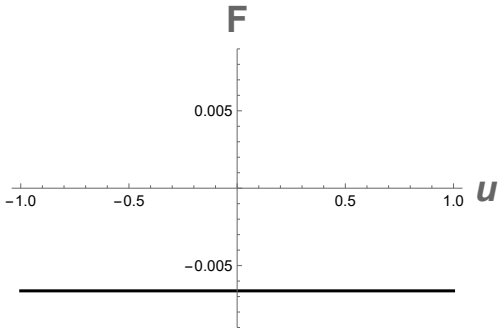

Figure 4.82: Anti de Sitter mirror energy flux.

The flux is thermal and negative over all times resulting in negative total energy,

$$E = -\frac{\kappa}{24}. \tag{4.216}$$

So, the radiation energy by the Anti de Sitter mirror is finite.

AdS: particles

The AdS mirror beta Bogolubov coefficient is found by the symmetry $\beta^{AdS}_{\omega\omega'} = -\beta^{dS}_{\omega\omega'}$ [45],

$$\beta_{\omega\omega'} = -\frac{2\sqrt{\omega\omega'}}{\kappa^2} e^{-2i\omega'/\kappa} \operatorname{csch}\left(\frac{\pi\omega}{\kappa}\right) {}_1F_1\left(1 + \frac{i\omega}{\kappa}; 2; \frac{4i\omega'}{\kappa}\right). \tag{4.217}$$

Here ${}_1F_1\left(m; n; q\right)$ is the Kummer confluent hypergeometric function of the first kind. The complex conjugate square of the beta coefficient yields,

$$|\beta_{\omega\omega'}|^2 = \frac{4\omega\omega'}{\kappa^4} \operatorname{csch}^2\left(\frac{\pi\omega}{\kappa}\right) \left|{}_1F_1\left(1 - \frac{i\omega}{\kappa}; 2; -\frac{4i\omega'}{\kappa}\right)\right|^2. \tag{4.218}$$

The numerical result for the AdS mirror particle spectrum is demonstrated in Fig. (4.83).

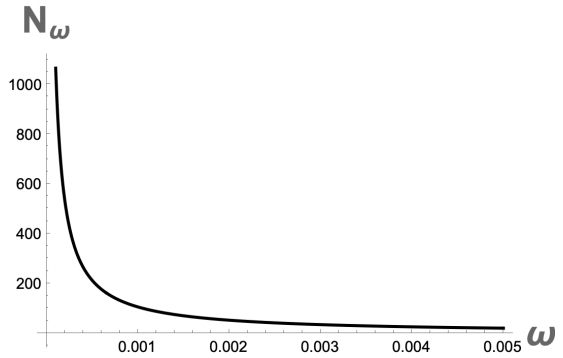

Figure 4.83: Anti de Sitter mirror particle spectrum.

The AdS mirror particle spectrum is identical to the de Sitter mirror case, i.e. the spectrum is divergent, and can also be written as a Planck distribution,

$$N_\omega = \frac{\delta(\omega - \omega_2)}{e^{2\pi\omega/\kappa} - 1}, \tag{4.219}$$

the detailed calculation of which is given in [45].

AdS: entropy

The mirror entanglement entropy simply is,

$$S(v) = -\frac{1}{12}\ln\left(1+\frac{\kappa^2 v^2}{4}\right), \tag{4.220}$$

whose graphical illustration is given in Fig. (4.84).

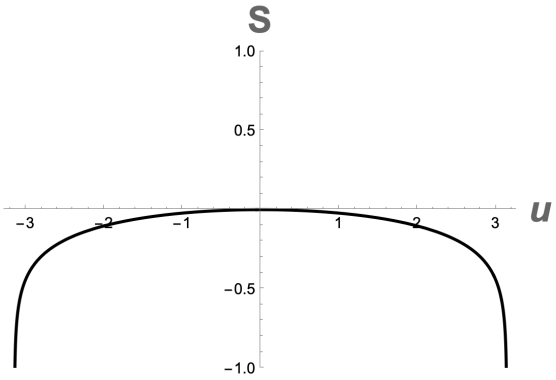

Figure 4.84: Anti de Sitter mirror entropy.

The entropy is negative over all times being symmetric with respect to the coordinate origin, and diverging at horizons, $u \to u_H = \pm\frac{\pi}{\kappa}$.

4.6.3 Schwarzschild de Sitter

SdS: dynamics

This subsection is based on the SdS cosmological model analog moving mirror solution studied in [46]. So, the SdS mirror trajectory is identified as,

$$f(v) = -\frac{1}{\kappa_B}\ln\left[\tilde{\kappa}_B(v_B - v)\right] + \frac{1}{\kappa_C}\ln\left[\tilde{\kappa}_C(v - v_C)\right] - \frac{1}{\kappa_0}\ln\left[\tilde{\kappa}_0(v + v_B + v_C)\right]. \tag{4.221}$$

Here κ_B and κ_C are acceleration parameters in future (black hole) and past (cosmological) times, respectively, whereas κ_0 has no physical meaning,

$$\kappa_B = \frac{(r_C - r_B)(r_B - r_0)}{2L^2 r_B}, \qquad \kappa_C = \frac{(r_C - r_B)(r_C - r_0)}{2L^2 r_C}, \qquad \kappa_0 = -\frac{\kappa_B \kappa_C}{\kappa_C - \kappa_B},$$

where $r_0 = -(r_B + r_C)$, and

$$r_B = \frac{2L}{\sqrt{3}}\sin\left[\frac{\pi}{6} - \frac{1}{3}\cos^{-1}\left(\frac{3\sqrt{3}M}{L}\right)\right], \qquad r_C = \frac{2L}{\sqrt{3}}\sin\left[\frac{\pi}{6} + \frac{1}{3}\cos^{-1}\left(\frac{3\sqrt{3}M}{L}\right)\right].$$

Also, $L = 1/\Lambda$, $\tilde{\kappa}_B \equiv \frac{1}{2r_B}$, $\tilde{\kappa}_C \equiv \frac{1}{2r_C}$, and $\tilde{\kappa}_0 \equiv \frac{1}{2r_0}$. The mirror event horizon locations are defined as $v_B = -2r_B$ and $v_C = -2r_C$. In certain limits, Eq. (4.221) reduces to the Schwarzschild and de Sitter mirrors separately. In order to calculate the beta coefficient,

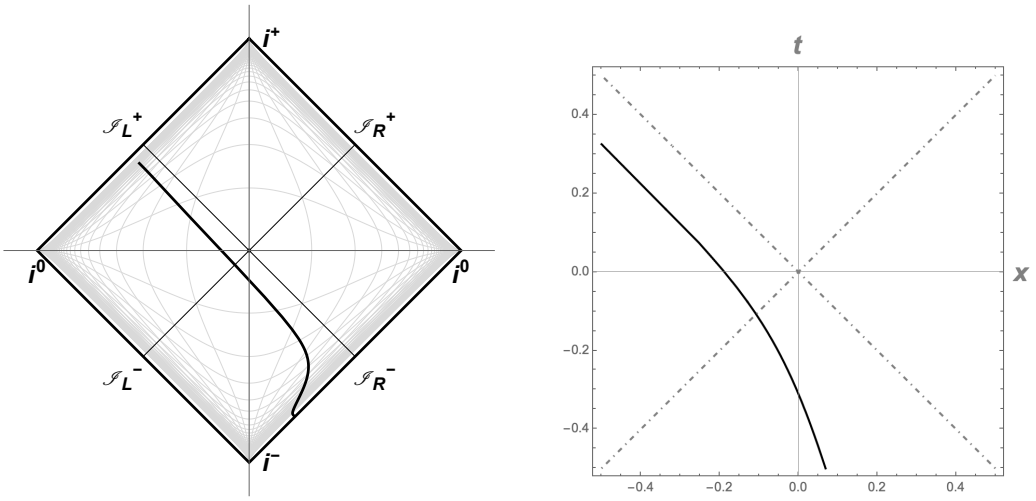

Figure 4.85: (a) Penrose and (b) Spacetime diagrams for the Schwarzschild de Sitter mirror trajectory, with $M = \frac{1}{24}$ and $L = \frac{2}{3}$.

it is useful to find the approximated form of the trajectory, Eq. (4.221),

$$f(v) \approx -\frac{1}{\kappa_B}\ln\left[\tilde{\kappa}_B(v_B - v)\right] + \frac{1}{\kappa_C}\ln\left[\tilde{\kappa}_C(v - v_C)\right]. \tag{4.222}$$

Here the third term is omitted as it is effect is negligible, though it describes the intermediate time period (between past and future), whereas the first and second terms describe an early and late times particle production. So, the first two terms in Eq. (4.221) give rise to the most important physics when considering asymptotic approach method [2, 3].

SdS: energy

The SdS mirror energy flux is found to be lengthy; however, the graphical illustration for the general v is demonstrated in Fig. (4.86).

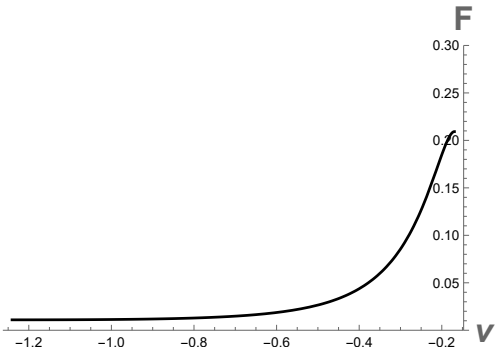

Figure 4.86: Schwarzschild de Sitter mirror energy flux, with $M = \frac{1}{24}$ and $L = \frac{2}{3}$.

The energy flux for general v has a monotonic increase starting from cosmological horizon at early time to black hole horizon at late time. Specifically, for the past and future time periods separately, the flux is thermal over time. In the $v \to v_C$ limit, i.e. near the cosmological event horizon location, the flux is,

$$F(v) = \frac{\kappa_C^2}{48\pi} + \mathcal{O}(v - v_C)^2. \tag{4.223}$$

In the $v \to v_B$ limit, i.e. near the black hole horizon location, the flux is,

$$F(v) = \frac{\kappa_B^2}{48\pi} + \mathcal{O}(v - v_B)^2. \tag{4.224}$$

This means that near the horizon positions the mirror has two different temperatures, that, in turn, results in two different Planck distributions [46].

SdS: particles

The SdS model's particle production and extension from black hole to cosmological horizon was first studied in 70's [64]. The corresponding spectrum is found to be thermal at early time and late time regimes separately. However, it is non-thermal when considering all times together [65]. Taking into account the reduced trajectory, Eq. (4.222), the SdS mirror beta Bogolubov coefficient is found as [46],

$$\beta_{\omega\omega'} = \frac{1}{2\pi}\sqrt{\frac{\omega'}{\omega}}\frac{(\tilde{\kappa}_B)^b(\tilde{\kappa}_C)^{-c}}{(\kappa')^{1+b-c}}e^{-i\omega' v_B}B\left(1+b,1-c\right){}_1F_1\left(1+b;2+b-c;a\right). \tag{4.225}$$

Here $B(m,n)$ is the beta function, ${}_1F_1(m;n;l)$ is the Kummer confluent hypergeometric function of the first kind, $\kappa' = 1/(v_B - v_C)$, and

$$a \equiv \frac{i\omega'}{\kappa'}, \quad b \equiv \frac{i\omega}{\kappa_B}, \quad c \equiv \frac{i\omega}{\kappa_C}. \tag{4.226}$$

The complex conjugate square of Eq. (4.225) yields,

$$|\beta_{\omega\omega'}|^2 = \frac{1}{4\pi^2\kappa'^2}\frac{\omega'}{\omega}\left|B\left(1-b,1+c\right)\right|^2\left|{}_1F_1(1-b;2-b+c;-a)\right|^2, \tag{4.227}$$

The numerical result for the SdS mirror particle spectrum is demonstrated in Fig. (4.87). So, the SdS mirror particle spectrum has qualitatively similar behavior as the

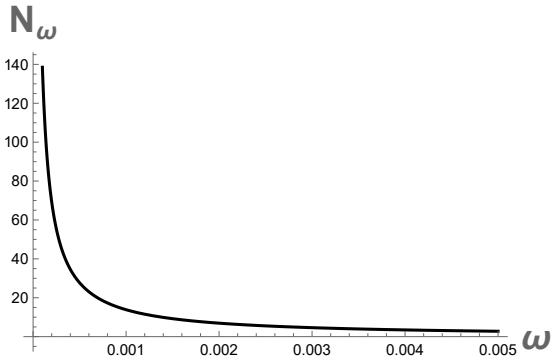

Figure 4.87: Schwarzschild de Sitter mirror particle spectrum, with $M = \frac{1}{24}$ and $L = \frac{2}{3}$.

Schwarzschild and de Sitter mirrors: the spectrum is divergent over all times, i.e. there is infinite particle production. For future ($\omega' \gg \omega$) and past ($\omega' \ll \omega$) times separately, the spectrum obeys Planck distribution, i.e. it is thermal,

$$N_B = \frac{1}{2\pi\kappa_B\omega'}\frac{1}{e^{2\pi\omega/\kappa_B}-1}, \tag{4.228}$$

$$N_C = \frac{1}{2\pi\kappa_B\omega'}\frac{1}{e^{2\pi\omega/\kappa_B}-1}. \tag{4.229}$$

Taking series of Eq. (4.227) to leading order in ω', where $\omega' \gg \omega$, gives,

$$N_{\omega\omega'} = N_B + N_C + N_{BC}, \tag{4.230}$$

where N_{BC} is the term that describes interaction between the Schwarzschild black hole and de Sitter spacetime horizons.

SdS: entropy

The SdS mirror entanglement entropy simply is,

$$S(v) = \frac{1}{12} \ln \left[\frac{1}{\kappa_B (v_B - v)} + \frac{1}{\kappa_C (v - v_C)} - \frac{1}{\kappa_0 (v + v_B + v_C)} \right], \tag{4.231}$$

whose graphical illustration is given in Fig. (4.88).

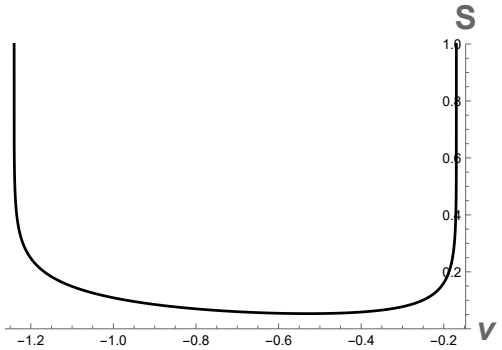

Figure 4.88: Schwarzschild de Sitter mirror entropy, with $M = \frac{1}{24}$ and $L = \frac{2}{3}$.

The entropy is positive over all times, diverging at the two horizons, i.e. when $v \to (v_B, v_C)$.

4.7 Inertial Null

There are 3 beta-known inertial null moving mirror models:

- Proex
- Inertial Horizon
- Light-Airy

All three mirrors travel with the speed of light at some point in their dynamics, having asymptotic zero acceleration at the start and the end of their motion. All three solutions have transcendentally invertible trajectories in both null and spacetime coordinates.

Proex and Light-Airy stand out in the sense that they have no null horizon, whereas Inertial Horizon has one.

All three solutions admit negative energy flux at some point, and have finite total energy emission with thermal radiation. However, all three mirror models suffer from soft infinite particle production.

Throughout the thesis, κ is a positively defined quantity within a mirror model that has a unit of acceleration in natural units, i.e. $\hbar = c = 1$. The graphs are plotted with $\kappa = 1$ since its value does not affect the general physical properties of the system.

4.7.1 Proex

Proex: Dynamics

This mirror is technically asymptotically inertial; however, it coasts at the speed of light, with the trajectory [23],

$$x(t) = -\frac{1}{\kappa} W\left(e^{\kappa t}\right). \tag{4.232}$$

The dynamics of Eq. (4.232) is depicted in Fig. (4.89). The trajectory starts

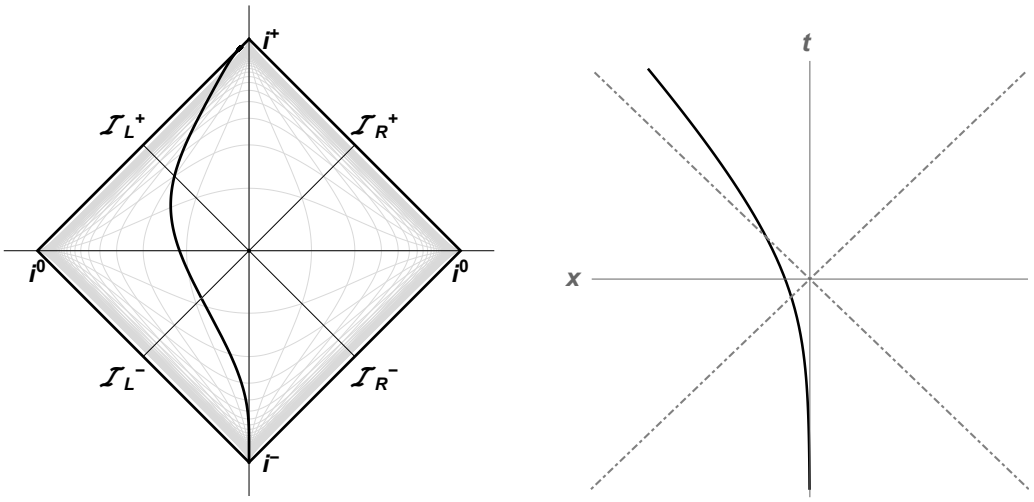

Figure 4.89: a) Penrose and b) Spacetime diagrams for the Proex mirror trajectory.

asymptotically static and goes to the timelike future infinity with the speed of light. This can be verified mathematically by finding the mirror velocity,

$$\dot{x}(t) = -\frac{W(e^{\kappa t})}{1 + W(e^{\kappa t})}, \tag{4.233}$$

which in the $t \to \infty$ limit goes to the speed of light, i.e. $\dot{x}(t) \equiv V \to 1$. However, the corresponding proper acceleration is,

$$\alpha(t) = -\frac{\kappa W(e^{\kappa t})}{[1 + 2W(e^{\kappa t})]^{3/2}}, \tag{4.234}$$

where

$$\lim_{t\to\infty} \alpha(t) = 0. \tag{4.235}$$

The trajectories in other coordinates are,

$$p(u) = u - \frac{1}{\kappa} W(2e^{\kappa u}), \qquad f(v) = v + \frac{2}{\kappa} e^{\kappa v}, \tag{4.236}$$

$$t(x) = -x + \frac{\ln(-\kappa x)}{\kappa}. \tag{4.237}$$

It is worth noting that the velocity of the mirror with respect to x space coordinate is simple, $\dot{x}(t) = [t(x)]^{-1} = \frac{\kappa x}{1-\kappa x}$, indicating that the Proex mirror calculations are simpler in x, or, equivalently, in v coordinates.

Proex: Energy

The expectation value of the Proex mirror energy flux is,

$$F(t) = -\frac{\kappa^2}{12\pi}\frac{\left[W\left(e^{\kappa t}\right)-1\right]W\left(e^{\kappa t}\right)}{\left[2W\left(e^{\kappa t}\right)+1\right]^4}, \tag{4.238}$$

the graphical illustration of which is demonstrated in Fig. (4.90).

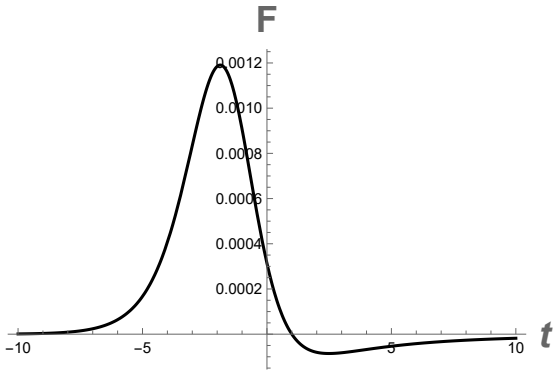

Figure 4.90: Proex mirror energy flux.

The flux has a considerable positive value at early time and a small negative value at late time. The total energy is finite [23],

$$E = \frac{\kappa}{96\pi}. \tag{4.239}$$

This result is consistent with the one derived via the beta coefficient using Eq. (3.95).

Proex: Particles

The beta Bogolubov coefficient of the Proex mirror is [23],

$$\beta_{\omega\omega'} = \frac{1}{4\pi\sqrt{\omega\omega'}}\left(\frac{2\omega'}{\kappa}\right)\left(\frac{2\omega}{\kappa}\right)^{\frac{i\omega_p}{\kappa}} e^{-\frac{\pi\omega_p}{2\kappa}}\Gamma\left[-\frac{i\omega_p}{\kappa}\right], \tag{4.240}$$

where $\omega_p \equiv \omega + \omega'$. The complex conjugate squaring of Eq. (4.240) yields,

$$|\beta_{\omega\omega'}|^2 = \frac{\omega'}{2\pi\kappa\omega\omega_p}\frac{1}{e^{\frac{2\pi\omega_p}{\kappa}}-1}. \tag{4.241}$$

When $\omega' \gg \omega$, the above expression reduces to the Planck spectrum,

$$|\beta_{\omega\omega'}|^2 = \frac{1}{2\pi\kappa\omega}\frac{1}{e^{2\pi\omega'/\kappa}-1}. \tag{4.242}$$

The numerical result for the Proex mirror particle spectrum is demonstrated in Fig. (4.91).

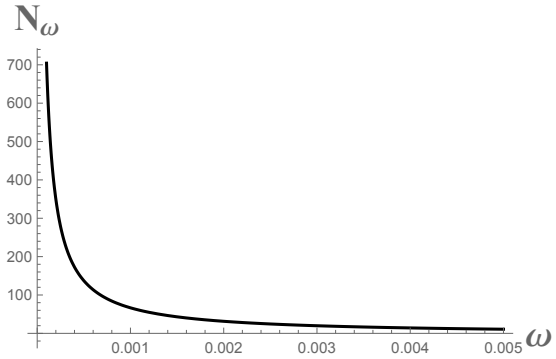

Figure 4.91: Proex mirror particle spectrum.

The spectrum is infra-red divergent and obeys Planck distribution at late times.

Proex: Entropy

The entanglement entropy of the Proex mirror is,

$$S(t) = \frac{1}{6}\tanh^{-1}\left[\frac{W(e^{\kappa t})}{1+W(e^{\kappa t})}\right], \tag{4.243}$$

whose graphical illustartion is shown in Fig. (4.92).

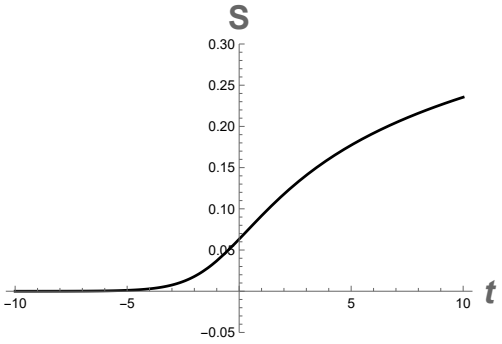

Figure 4.92: Proex mirror entropy.

The entropy increases at early-times, diverging in the $t \to \infty$ limit. The drifting cousin of the Proex mirror is investigated in Sec. (4.8.3).

4.7.2 Inertial Horizon

IH: Dynamics

The trajectory of the asymptotically inertial mirror with the formation of the horizon is given as [50],

$$f(v) = v + \frac{4\lambda^3}{v^2}, \tag{4.244}$$

where λ is a free parameter, and the horizon is located at $v_H = 0$. The dynamics of the mirror is depicted in Fig. (4.93). Similar to the black hole null mirrors, the IH mirror

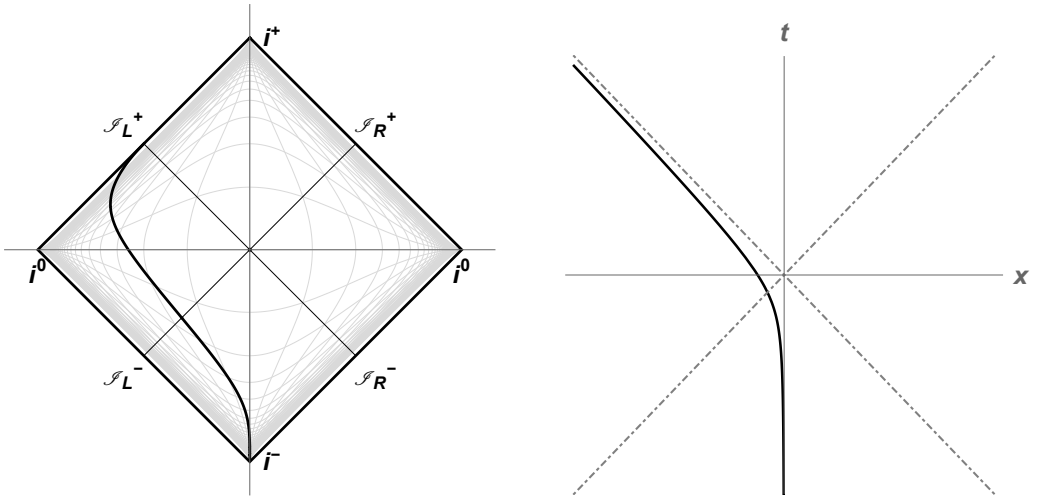

Figure 4.93: a) Penrose and b) Spacetime diagrams for the Inertial Horizon mirror trajectory, with $\lambda = 1$.

trajectory starts asymptotically static and travels with the speed of light as approaches the horizon. This is verified by finding the mirror velocity,

$$V(v) = -\tanh\left[\frac{1}{2}\ln\left(1 - \frac{8\lambda^3}{v^3}\right)\right], \tag{4.245}$$

which in the $v \to v_H = 0$ limit goes to the speed of light, i.e. $|V| \to 1$. The corresponding proper acceleration is,

$$\alpha(v) = -\frac{12\lambda^3}{v^4\left(1 - \frac{8\lambda^3}{v^3}\right)^{3/2}}, \tag{4.246}$$

which in the $v \to v_H = 0$ limit goes to 0. The maximum acceleration occurs at $v = -\lambda$. The trajectories in other coordinates are,

$$p(u) = \frac{1}{3}\left(u + \frac{u^2}{B} + B\right), \tag{4.247}$$

$$t(x) = -x - \sqrt{-\frac{2\lambda^3}{x}}, \qquad x(t) = \frac{(t-A)^2}{3A}, \tag{4.248}$$

where

$$A \equiv \sqrt[3]{-27\lambda^3 + 3\sqrt{81\lambda^6 - 6\lambda^3 t^3} + t^3}, \qquad B \equiv \left(u^3 - 54\lambda^3 + 6\sqrt{3}\sqrt{-u^3\lambda^3 + 27\lambda^6}\right)^{1/3}.$$

IH: Energy

The expectation value of the energy flux as a function of advanced time v is [50],

$$F(v) = -\frac{4\lambda^3 v^4 \left(\lambda^3 + v^3\right)}{\pi \left(v^3 - 8\lambda^3\right)^4}, \tag{4.249}$$

the graphical illustration of which is demonstrated in Fig. (4.94).

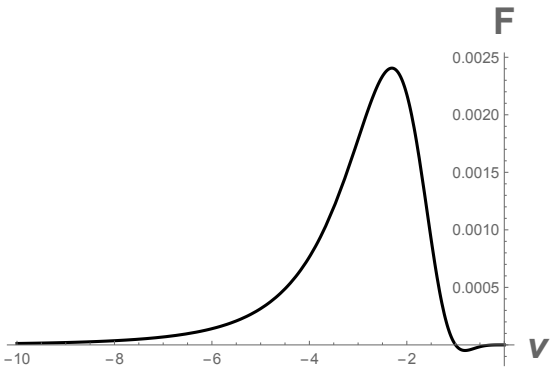

Figure 4.94: Inertial Horizon mirror energy flux, with $\lambda = 1$.

The flux has a considerable positive value and a small negative value at some points in time. The total energy is finite,

$$E = \frac{1}{72\sqrt{3}\lambda}. \tag{4.250}$$

This result is consistent with the numerical verification of the energy found via the beta coefficient using Eq. (3.95).

IH: Particles

The beta Bogolubov coefficient of the Inertial horizon mirror is [50],

$$\beta_{\omega\omega'} = \frac{i}{2\pi^{3/2}\left(\omega+\omega'\right)}\sqrt{\frac{\omega'}{\omega}}G^{3,0}_{0,3}\left(-i\lambda^3\omega\left(\omega+\omega'\right)^2|0,\frac{1}{2},1\right), \tag{4.251}$$

where G is the Meijer G-function. The complex conjugate squaring of Eq. (4.251) yields,

$$|\beta_{\omega\omega'}|^2 = \frac{\omega'|G^{3,0}_{0,3}\left(i\lambda^3\omega(\omega+\omega')^2|0,\frac{1}{2},1\right)|^2}{4\pi^3\omega(\omega+\omega')^2}. \tag{4.252}$$

The numerical result for the IH mirror particle spectrum is demonstrated in Fig. (4.95).

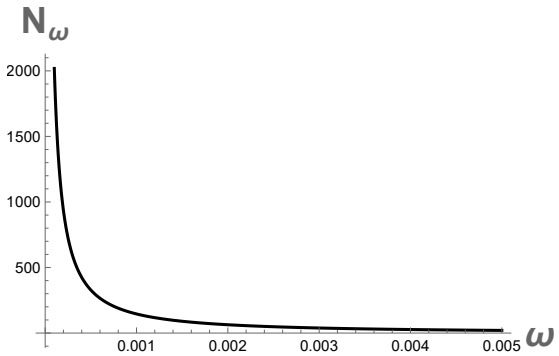

Figure 4.95: Inertial Horizon mirror particle spectrum, with $\lambda = 1$.

The IH mirror particle spectrum is divergent and obeys Meijer-G function distribution.

IH: Entropy

The Inertial horizon mirror entanglement entropy simply is,

$$S(v) = \frac{1}{12} \ln \left(1 - \frac{8\lambda^3}{v^3} \right), \tag{4.253}$$

whose graphical illustration is given in Fig. (4.96).

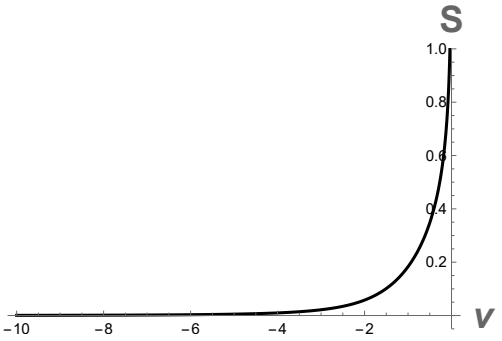

Figure 4.96: Inertial Horizon mirror entropy, with $\lambda = 1$.

Similar to the black hole null mirrors, the IH mirror entropy also monotonically increases over time, diverging at the horizon.

4.7.3 Light-Airy

LA: Dynamics

The trajectory of the Light-Airy moving mirror model is an odd function [52],

$$f(v) = v + \frac{\kappa^2 v^3}{3}, \tag{4.254}$$

whose dynamics is depicted in Fig. (4.97). The trajectory is asymmetric with respect

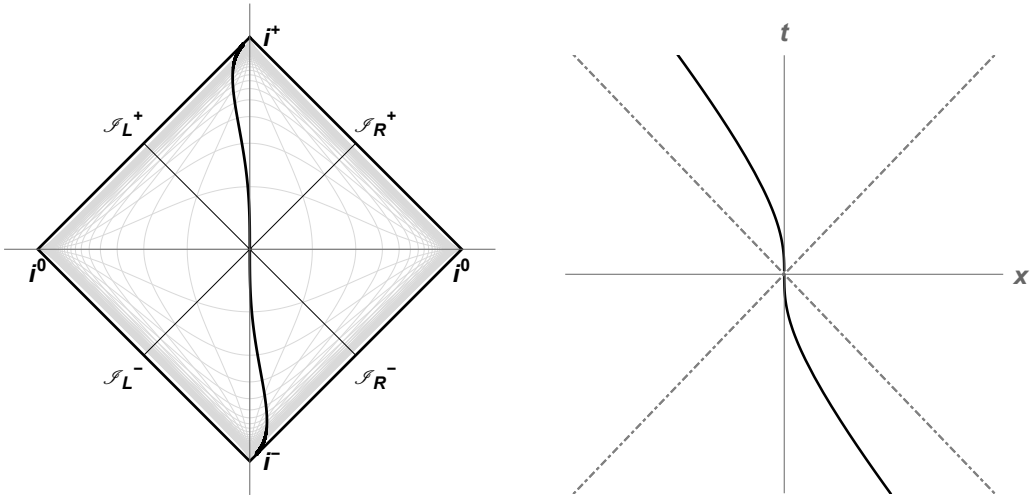

Figure 4.97: a) Penrose and b) Spacetime diagrams for the Light-Airy mirror trajectory.

to time with no horizon. Also, unlike the static mirrors, the LA mirror starts and ends its motion with the speed of light but with zero proper acceleration. This is verified by finding the mirror velocity,

$$V = -\frac{\kappa^2 v^2}{2 + \kappa^2 v^2}, \tag{4.255}$$

which in the $v \to \pm\infty$ limits goes to the speed of light, i.e. $|V| \to 1$. The corresponding proper acceleration,

$$\alpha(v) = -\frac{\kappa^2 v}{\left(\kappa^2 v^2 + 1\right)^{3/2}}, \tag{4.256}$$

where

$$\lim_{v\to\pm\infty} \alpha(v) = 0. \tag{4.257}$$

The trajectories in other coordinates are,

$$p(u) = -\frac{\sqrt[3]{2}}{\mathcal{B}} + \frac{\mathcal{B}}{\sqrt[3]{2}\kappa^2}, \tag{4.258}$$

$$t(x) = -x + \frac{(-6\kappa x)^{1/3}}{\kappa}, \qquad x(t) = -t - \frac{1}{2\kappa}\left(\mathcal{A}_+^{\frac{2}{3}}\mathcal{A}_-^{\frac{1}{3}} + \mathcal{A}_+^{\frac{1}{3}}\mathcal{A}_-^{\frac{2}{3}}\right), \tag{4.259}$$

where $\mathcal{B} \equiv \left(3\kappa^4 u + \sqrt{4\kappa^6 + 9\kappa^8 u^2}\right)^{\frac{1}{3}}$ and $\mathcal{A}_\pm = 3\kappa t \pm \sqrt{9\kappa^2 t^2 + 8}$. So, all ray-tracing functions are transcendentally invertible.

LA: Energy

The expectation value of the energy flux in terms of v coordinate is [52],

$$F(v) = \frac{\kappa^2}{12\pi} \frac{1 - 2\kappa^2 v^2}{\left(\kappa^2 v^2 + 1\right)^4}, \tag{4.260}$$

the graphical illustration of which is demonstrated in Fig. (4.98).

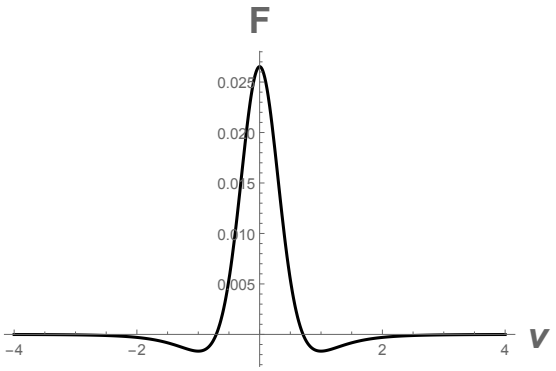

Figure 4.98: Light-Airy mirror energy flux.

The flux is symmetric with respect to the $v = 0$ origin, having a maximum at this point and small negative values at both early and late times. The total energy is finite,

$$E = \frac{\kappa}{96}. \tag{4.261}$$

This result is consistent with the one derived via the beta coefficient using Eq. (3.95).

LA: Particles

The associated beta Bogolubov coefficient is,

$$\beta_{\omega\omega'} = -\frac{1}{\sqrt[3]{\omega\kappa^2}}\sqrt{\frac{\omega'}{\omega}}\mathrm{Ai}\left(\frac{\omega+\omega'}{\sqrt[3]{\omega\kappa^2}}\right), \tag{4.262}$$

where Ai(n) is the Airy function. The complex conjugate squaring of Eq. (4.262) yields,

$$|\beta_{\omega\omega'}|^2 = \frac{\omega'}{\kappa^{4/3}\omega^{5/3}}\mathrm{Ai}^2\left(\frac{\omega+\omega'}{\sqrt[3]{\omega\kappa^2}}\right). \tag{4.263}$$

The numerical result for the LA mirror particle spectrum is demonstrated in Fig. (4.99).

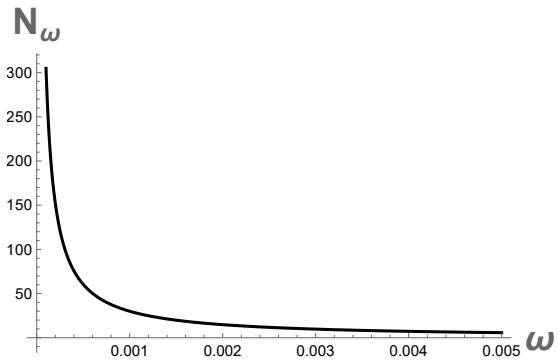

Figure 4.99: Light-Airy mirror particle spectrum.

The LA mirror particle spectrum is divergent and obeys Airy function distribution.

LA: Entropy

The Light-Airy mirror entanglement entropy simply is,

$$S(v) = \frac{1}{12} \ln \left(1 + \kappa^2 v^2\right), \tag{4.264}$$

whose plot is shown in Fig. (4.100).

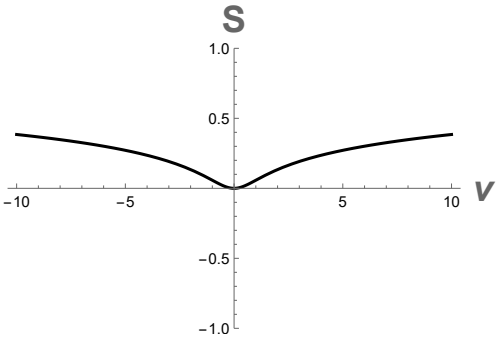

Figure 4.100: Light-Airy mirror entropy.

The Light-Airy mirror entropy is symmetric with respect to the coordinate origin, diverging logarithmically at both far past and far future, $v \to \pm\infty$.

4.8 Drifting

There are 5 beta-known drifting moving mirror models:

- Drifting Schwarzschild
- Drifting CGHS
- Drifting Proex
- Drifting Logex
- Drifting Davies-Fulling

The drifting mirrors are unique models because of the formation of a special object known as the "remnant" when the black hole evaporation process stops. In this case, the energy emission is finite; however, the mirrors suffer from infinite soft particle production. The mirrors coast with a velocity less than the speed of light at late times with zero proper acceleration. In both far past and far future the energy flux is zero.

All five mirrors asymptotically coast at late time with a velocity less than the speed of light. The drifting Davies-Fulling (DDF) mirror is an exception since it also coasts at early time, whereas the other mirrors start off asymptotically static. Interestingly, outside the drifting Schwarzschild (DSch) mirror, the background might not be vacuum as there are particles outside black holes.

Throughout the thesis, κ is a positively defined quantity within a mirror model that has a unit of acceleration in natural units, i.e. $\hbar = c = 1$. The graphs are plotted with $\kappa = 1$ since its value does not affect the general physical properties of the system.

4.8.1 Drifting Schwarzschild

DSch: Dynamics

Explored in [29], [30], [31], [59], the drifting Schwarzschild mirror trajectory is,

$$x(t) = \xi \left(v_H - t - \frac{W(2e^{2\kappa(v_H - t)})}{2\kappa} \right), \tag{4.265}$$

where ξ is the maximum drifting speed of the mirror with range $0 < \xi < 1$. Note when $\xi \to 1$, Eq. (4.265) reduces to the Schwarzschild mirror trajectory, Eq. (4.35).

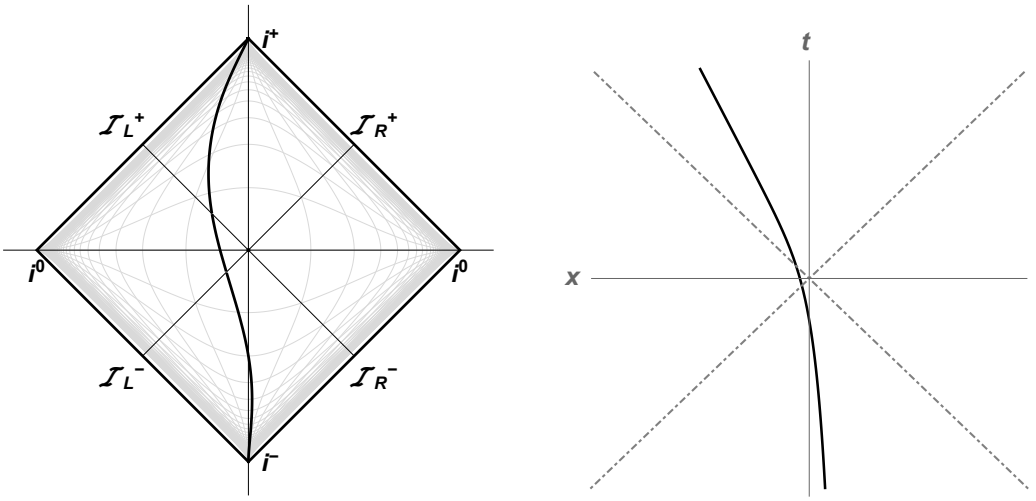

Figure 4.101: a) Penrose and b) Spacetime diagrams for the drifting Schwarzschild mirror trajectory, with $\xi = \frac{1}{2}$ and $v_H = 0$.

The trajectory starts asymptotically static, then goes to time-like future infinity with the velocity less than the speed of light. It can be seen that at late (but not too late) times, the mirror is thermal. The mirror velocity is,

$$\dot{x}(t) = -\frac{\xi}{1 + W(2e^{2\kappa(v_H - t)})}, \tag{4.266}$$

which in the $t \to \infty$ limit coasts with the speed $\dot{x}(t) \equiv |V| \to \xi$. The corresponding proper acceleration is,

$$\alpha(t) = -\frac{2\kappa\xi W(2e^{2\kappa(v_H - t)})}{\left[\left(1 + W(2e^{2\kappa(v_H - t)})\right)^2 - \xi^2 \right]^{3/2}}, \tag{4.267}$$

which in the $t \to \infty$ limit goes to 0. The trajectories in other coordinates are,

$$p(u) = u + \frac{\xi}{\kappa} \ln \left[\frac{\theta}{2} W\left(\frac{2}{\theta} e^{\frac{2}{\theta}\kappa(v_H - u)} \right) \right], \qquad f(v) = v - \frac{\xi}{\kappa} \ln \left[\frac{\epsilon}{2} W\left(\frac{2}{\epsilon} e^{\frac{2}{\epsilon}\kappa(v_H - v)} \right) \right], \tag{4.268}$$

$$t(x) = v_H - \frac{x}{\xi} - \frac{1}{\kappa} e^{2\kappa x/\xi}. \tag{4.269}$$

where $\theta = 1 + \xi$ and $\epsilon = 1 - \xi$. Here we have used the property of the Lambert function, $W(x) = \ln x - \ln W(x)$, to simplify expressions for $p(u)$ and $f(v)$.

DSch: Energy

The expectation value of the drifting Schwarzschild mirror energy flux is [29],

$$F(t)=\frac{\kappa^2\xi W\left(2e^{2\kappa(v_H-t)}\right)\left[\xi^2+2W\left(2e^{2\kappa(v_H-t)}\right)^2+W\left(2e^{2\kappa(v_H-t)}\right)-1\right]}{3\pi\left[1-\xi+W\left(2e^{2\kappa(v_H-t)}\right)\right]^2\left[1+\xi+W\left(2e^{2\kappa(v_H-t)}\right)\right]^4}, \tag{4.270}$$

whose graphical illustration is demonstrated in Fig. (4.102).

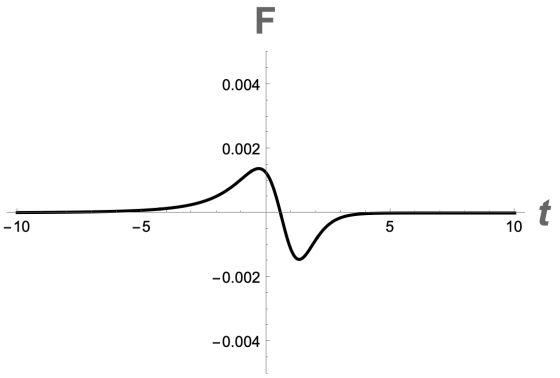

Figure 4.102: Drifting Schwarzschild mirror energy flux, with $\xi=\frac{1}{2}$ and $v_H=0$.

The flux contains negative value at late times. The flux in terms of x is,

$$F(x)=\frac{2\kappa^2\xi e^{\frac{2\kappa x}{\xi}}\left(8e^{\frac{4\kappa x}{\xi}}+2e^{\frac{2\kappa x}{\xi}}+\xi^2-1\right)}{3\pi\left(-2e^{\frac{2\kappa x}{\xi}}+\xi-1\right)^2\left(2e^{\frac{2\kappa x}{\xi}}+\xi+1\right)^4}, \tag{4.271}$$

i.e. as black hole null mirrors, the drifting Schwarzschild mirror flux as a function of space coordinate also does not depend on black hole horizon position, v_H. The total energy emitted is finite,

$$E=\frac{\kappa}{48\pi}\left[\frac{(3-\xi)\eta}{\xi^2}-\frac{(3+2\xi)}{(\xi^2+\xi)}\right], \tag{4.272}$$

where $\eta=\tanh^{-1}(\xi)$ is rapidity. Eq. (4.272) is consistent with the numerical verification of the energy found via the beta Bogolubov coefficient using Eq. (3.95).

DSch: Particles

The beta Bogolubov coefficient for the drifting Schwarzschild mirror is [29],

$$\beta_{\omega\omega'} = -\frac{\xi\sqrt{\omega\omega'}}{2\pi\kappa\omega_p}\left(\frac{i\kappa}{\omega_p}\right)^A \Gamma\left(A\right), \tag{4.273}$$

where $\omega_p \equiv \omega + \omega'$ and $A \equiv \frac{i}{2\kappa}\left[(1+\xi)\omega + (1-\xi)\omega'\right]$. Taking its complex conjugate squaring yields,

$$|\beta_{\omega\omega'}|^2 = \frac{\omega\omega'\xi^2}{\pi\kappa B(\omega+\omega')^2}\frac{1}{e^{\pi B/\kappa}-1}, \tag{4.274}$$

where $B \equiv \left[(1+\xi)\omega + (1-\xi)\omega'\right]$. The numerical result for the DSch mirror particle spectrum is demonstrated in Fig. (4.103).

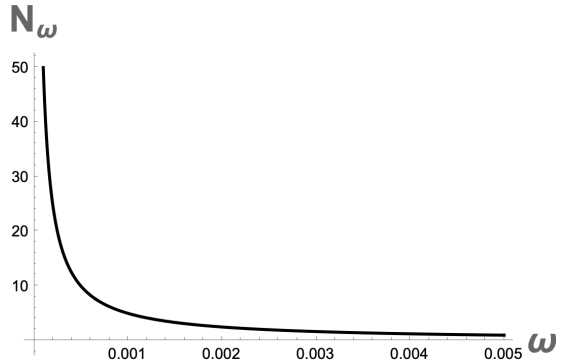

Figure 4.103: Drifting Schwarzschild mirror particle spectrum, with $\xi = \frac{1}{2}$.

The spectrum of the drifting Schwarzschild mirror is thermal (though it never gets to thermality, i.e. to 1) with a leftover remnant, and there is infra-red divergence.

DSch: Entropy

The entanglement entropy of the drifting Schwarzschild mirror simply is [29],

$$S(t) = \frac{1}{6}\tanh^{-1}\left[\frac{\xi}{1+W(2e^{2\kappa(v_H-t)})}\right], \tag{4.275}$$

whose limit in far future is a large number but finite, i.e.

$$\lim_{t\to\infty} S(t) = \frac{1}{6}\tanh^{-1}(\xi) = \frac{\eta}{6} \neq \infty. \tag{4.276}$$

The plot of Eq. (4.275) is shown in Fig. (4.104).

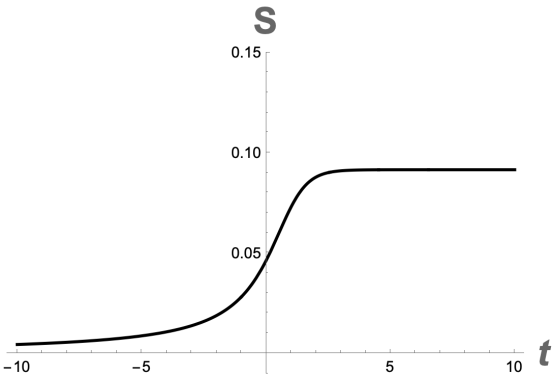

Figure 4.104: Drifting Schwarzschild mirror entropy, with $\xi = \frac{1}{2}$ and $v_H = 0$.

Fig. (4.104) illustrates that the entropy increases at early times and becomes constant at late times, i.e. there is no information loss.

4.8.2 Drifting CGHS

DC: Dynamics

First introduced in [19], the CGHS mirror is multiplicatively shifted to render the energy finite. This drifting trajectory is given as [23],

$$x(t) = -\frac{\xi}{\kappa}\sinh^{-1}\left(\frac{1}{2}e^{\kappa t}\right). \tag{4.277}$$

where ξ is the maximum drifting speed of the mirror with range $0 < \xi < 1$. The dynamics of the DC mirror is depicted in Fig. (4.105).

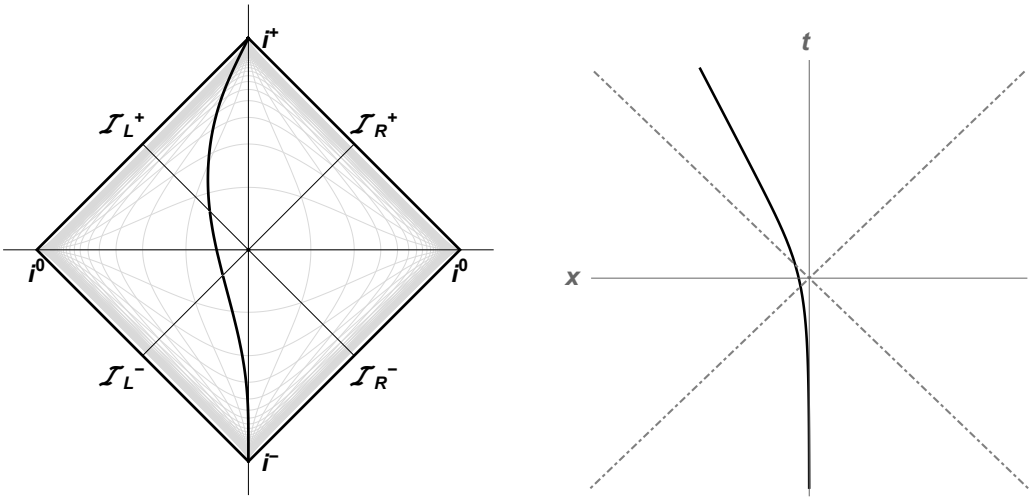

Figure 4.105: a) Penrose and b) Spacetime diagrams for the Drifting CGHS mirror trajectory, with $\xi = \frac{1}{2}$.

Similar to the drifting Schwarzschild mirror, the drifting CGHS mirror trajectory also starts its motion asymptotically static and goes to time-like future infinity with the velocity less than the speed of light. The mirror velocity is,

$$\dot{x}(t) = -\frac{\xi e^{\kappa t}}{\sqrt{4 + e^{2\kappa t}}}, \tag{4.278}$$

which in the $t \to \infty$ limit coasts with the speed $\dot{x}(t) \equiv |V| \to \xi$. The corresponding proper acceleration is,

$$\alpha(t) = -\frac{4\kappa\xi e^{\kappa t}}{[4 + (1-\xi^2)e^{2\kappa t}]^{3/2}}, \tag{4.279}$$

where

$$\lim_{t\to\infty}\alpha(t) = 0. \tag{4.280}$$

The trajectory of the mirror in x space coordinate is,

$$t(x) = \frac{1}{\kappa}\ln\left[-2\sinh\left(\frac{x\kappa}{\xi}\right)\right]. \tag{4.281}$$

So, the trajectories of the drifting CGHS mirror in spacetime coordinates are tractable. However, it is difficult to define the ray-tracing functions in null coordinates.

DC: Energy

The expectation value of the drifting CGHS mirror energy flux is [23],

$$F(t) = \frac{2\kappa^2}{3\pi} \frac{\xi e^{\kappa t}\sqrt{e^{2\kappa t}+4}\left(\left(\xi^2-1\right)e^{2\kappa t}+2\right)}{\left(\sqrt{e^{2\kappa t}+4}-\xi e^{\kappa t}\right)^2\left(\xi e^{\kappa t}+\sqrt{e^{2\kappa t}+4}\right)^4}, \tag{4.282}$$

the graphical illustration of which is demonstrated in Fig. (4.106).

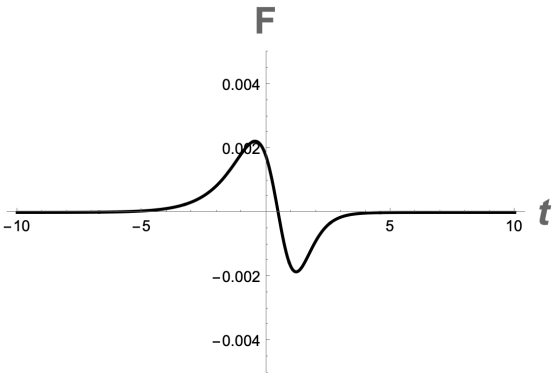

Figure 4.106: Drifting CGHS mirror energy flux, with $\xi = \frac{1}{2}$.

Similar to the Drifting Schwarzschild mirror, the drifting CGHS mirror energy flux also has both positive and negative values. The total energy is finite,

$$E = \frac{\kappa}{96\pi}\left(\frac{3+\xi^2}{2\xi^2}\ln\frac{1+\xi}{1-\xi} - \frac{2\xi^2+3\xi+3}{\xi(1+\xi)}\right). \tag{4.283}$$

This result is consistent with the numerical verification of the energy found via the beta Bogolubov coefficient using Eq. (3.95).

DC: Particles

The beta Bogolubov coefficient of the drifting CGHS mirror is,

$$\beta_{\omega\omega'} = \frac{\xi\sqrt{\omega\omega'}}{\pi\kappa(\omega_p - \xi\omega_n)} B\left[-\frac{i\omega_p}{\kappa}, \frac{i(\omega_p + \xi\omega_n)}{2\kappa}\right], \tag{4.284}$$

where $\omega_p \equiv \omega + \omega'$, $\omega_n \equiv \omega - \omega'$ and $B(m, n)$ is the beta function or the Euler integral of the first kind. The complex conjugate squaring of Eq. (4.284) yields,

$$|\beta_{\omega\omega'}|^2 = \frac{\xi^2\omega\omega'}{\pi^2\kappa^2(\omega_p - \xi\omega_n)^2} \left| B\left[\frac{i\omega_p}{\kappa}, -\frac{i(\omega_p + \xi\omega_n)}{2\kappa}\right]\right|^2. \tag{4.285}$$

The numerical result for the DC mirror particle spectrum is demonstrated in Fig. (4.107).

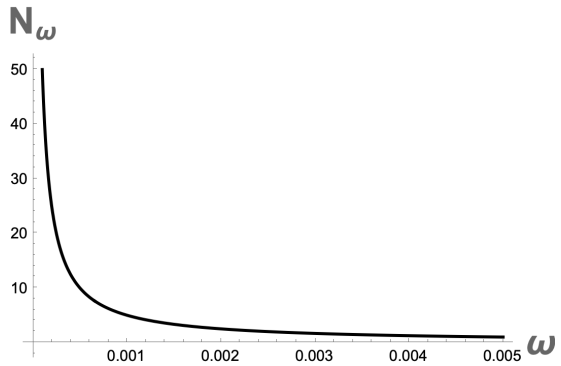

Figure 4.107: Drifting CGHS mirror particle spectrum, with $\xi = \frac{1}{2}$.

The mirror particle spectrum is divergent and obeys beta function distribution.

DC: Entropy

The entanglement entropy of the drifting CGHS mirror is,

$$S(t) = \frac{1}{6}\tanh^{-1}\left(\frac{\xi e^{\kappa t}}{\sqrt{4+e^{2\kappa t}}}\right), \tag{4.286}$$

whose plot is shown in Fig. (4.108).

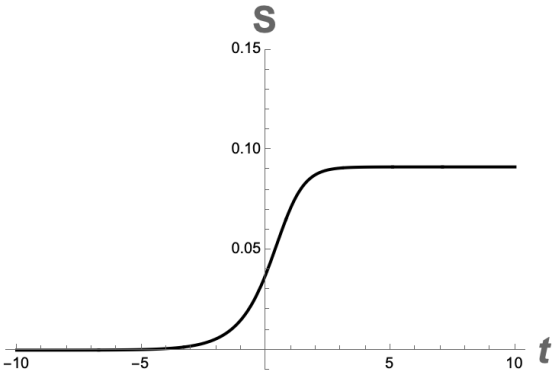

Figure 4.108: Drifting CGHS mirror entropy, with $\xi = \frac{1}{2}$.

Similar to the drifting Schwarzschild mirror case, the drifting CGHS mirror entropy also increases at early times and becomes constant at late times, preserving unitarity.

4.8.3 Drifting Proex

DP: Dynamics

The drifting Proex mirror trajectory reads as [35],

$$x(t) = -\frac{\xi}{\kappa} W\left(e^{\kappa t}\right), \tag{4.287}$$

where ξ is the maximum drifting speed of the mirror with range $0 < \xi < 1$. The dynamics of the DP mirror is depicted in Fig. (4.109).

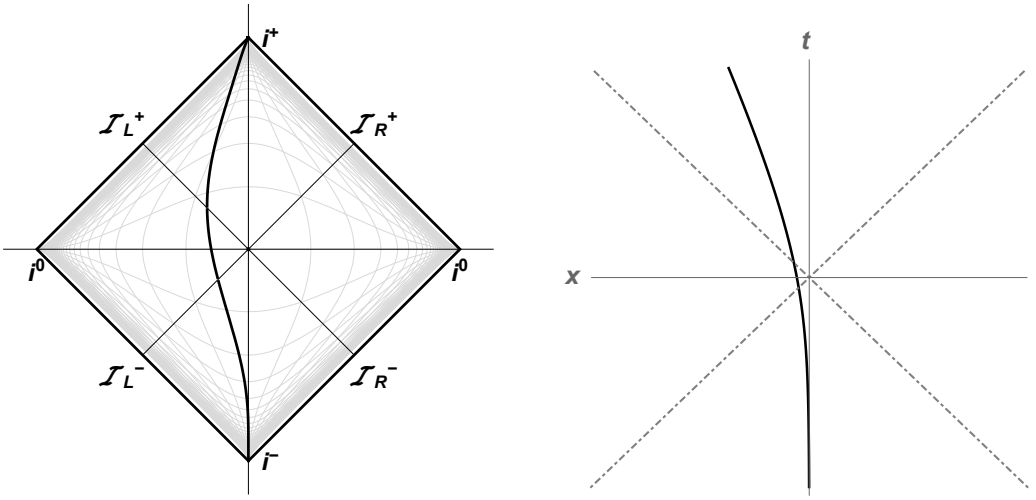

Figure 4.109: a) Penrose and b) Spacetime diagrams for the Drifting Proex mirror trajectory, with $\xi = \frac{1}{2}$.

The drifting Proex mirror trajectory has qualitatively similar behavior as the other drifting mirrors: the trajectory starts asymptotically static and goes to time-like future infinity with the velocity less than the speed of light. The mirror velocity is,

$$\dot{x}(t) = -\frac{\xi W(e^{\kappa t})}{1 + W(e^{\kappa t})}, \tag{4.288}$$

which in the $t \to \infty$ limit coasts with the speed $\dot{x}(t) \equiv V \to \xi$. The corresponding proper acceleration is,

$$\alpha(t) = -\frac{\xi \kappa W(e^{\kappa t})}{[1 + 2W(e^{\kappa t}) + (1 - \xi^2) W^2(e^{\kappa t})]^{3/2}}, \tag{4.289}$$

which in the $t \to \infty$ limit goes to 0. The trajectories in other coordinates are,

$$p(u) = u - \frac{2\xi}{\kappa(1+\xi)} W\left[(1+\xi)e^{\kappa u}\right], \tag{4.290}$$

$$f(v) = v + \frac{2\xi}{\kappa(1-\xi)} W\left[(1-\xi)e^{\kappa v}\right], \tag{4.291}$$

$$t(x) = \frac{1}{\kappa} \ln\left(-\frac{\kappa x}{\xi} e^{-\frac{\kappa x}{\xi}}\right). \tag{4.292}$$

So, all ray-tracing functions are transcendentally invertible.

DP: Energy

The mirror has the remarkable feature of approaching the speed of light while radiating finite total energy with the flux,

$$F(t) = \frac{\kappa^2 \xi W\left(e^{\kappa t}\right)\left[W\left(e^{\kappa t}\right)\left(2\left(\xi^2-1\right)W\left(e^{\kappa t}\right)-1\right)+1\right]}{12\pi\left[(\xi-1)W\left(e^{\kappa t}\right)-1\right]^2\left[(\xi+1)W\left(e^{\kappa t}\right)+1\right]^4}, \tag{4.293}$$

the graphical illustration of which is demonstrated in Fig. (4.110).

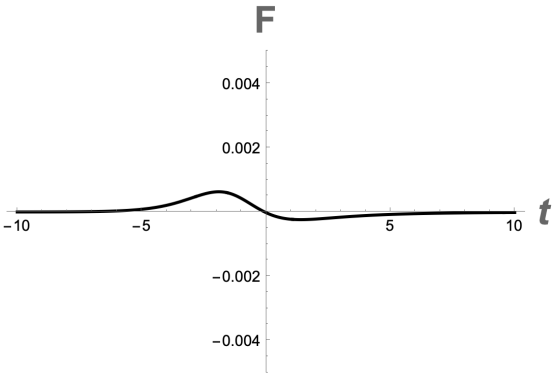

Figure 4.110: Drifting Proex mirror energy flux, with $\xi = \frac{1}{2}$.

Drifting Proex mirror flux has qualitatively similar behavior as the other drifting mirrors. However, the energy flux has very shallow negative emission compared to the positive valued emission. The energy emitted is finite [35],

$$E = \frac{\kappa}{96\pi}\left(\frac{3-2\xi}{\xi} + \frac{(\xi-1)(3+\xi)\eta}{\xi^2}\right), \tag{4.294}$$

where $\eta = \tanh^{-1}(\xi)$. When $\xi = 1$, then Eq. (4.294) reduces to the Proex mirror energy, Eq. (4.239).

DP: Particles

The beta Bogolubov coefficient of the DProex mirror is [35],

$$\beta_{\omega\omega'} = -\frac{i}{\pi}\xi^{i\omega_p}\sqrt{\omega\omega'}(i\omega_\xi)^{i\omega_p-1}\Gamma(-i\omega_p), \tag{4.295}$$

where $\omega_p \equiv \omega + \omega'$, $\omega_n \equiv \omega - \omega'$, $\omega_\xi \equiv \left(\frac{1}{\xi}+1\right)\omega + \left(\frac{1}{\xi}-1\right)\omega'$ and $\kappa = 1$ for simplicity. The complex conjugate squaring of Eq. (4.295) yields,

$$|\beta_{\omega\omega'}|^2 = \frac{\omega'}{\pi\kappa(\omega'+\omega)}\frac{2\omega}{\omega_\xi^2}\frac{1}{e^{\frac{2\pi}{\kappa}(\omega+\omega')}-1}. \tag{4.296}$$

In the limit $\xi \to 1$, Eq. (4.296) leads to the ordinary Proex mirror case, Eq. (4.241). The numerical result for the DP mirror particle spectrum is demonstrated in Fig. (4.111).

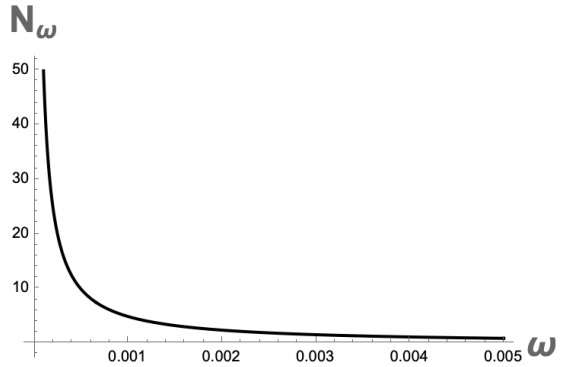

Figure 4.111: Drifting Proex mirror particle spectrum, with $\xi = \frac{1}{2}$.

The particle spectrum obeys Gamma function distribution and is divergent, i.e. there is infinite soft particle production.

The energy found using the beta Bogolubov coefficient is consistent with the energy value found using the flux, Eq. (4.294).

DP: Entropy

The entanglement entropy of the drifting Proex mirror simply is,

$$S(t) = \frac{1}{6} \tanh^{-1} \left[\frac{\xi W\left(e^{\kappa t}\right)}{1 + W\left(e^{\kappa t}\right)} \right], \tag{4.297}$$

whose plot is shown in Fig. (4.112).

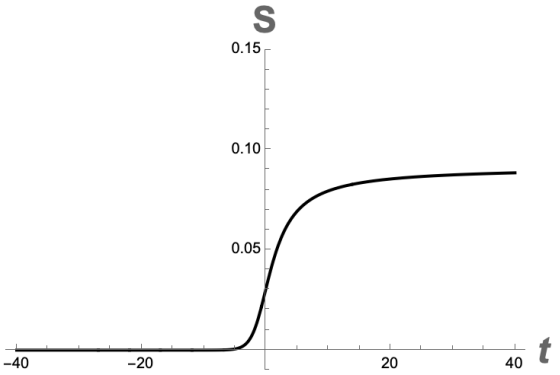

Figure 4.112: Drifting Proex mirror entropy, with $\xi = \frac{1}{2}$.

Similar to the other drifting mirrors, the DP mirror entropy also increases at early-times and monotonically approaches a constant value at late-times, i.e. unitarity is preserved.

It has been demonstrated recently that the drifting Proex mirror trajectory is responsible for a certain case of the beta decay [70].

4.8.4 Drifting Logex

DL: Dynamics

The drifting Logex trajectory, which was studied as a method for validating signatures of energy radiation in particle counts, is [34],

$$x(t) = -\frac{\xi}{2\kappa}\ln\Big(e^{2\kappa t}+1\Big), \tag{4.298}$$

where ξ is the maximum drifting speed of the mirror with range $0 < \xi < 1$. The dynamics of the DL mirror is depicted in Fig. (4.113).

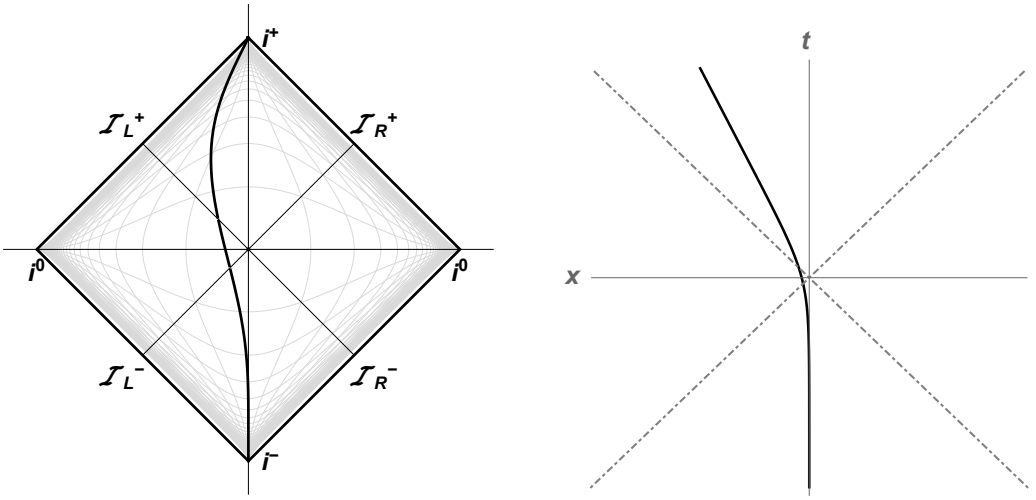

Figure 4.113: a) Penrose and b) Spacetime diagrams for the drifting Logex mirror trajectory, with $\xi = \frac{1}{2}$.

The drifting Logex mirror trajectory has qualitatively similar dynamics as the other drifting mirrors: the trajectory starts asymptotically static and goes to time-like future infinity with the velocity less than the speed of light. The mirror velocity is,

$$\dot{x}(t) = -\frac{\xi e^{2\kappa t}}{1+e^{2\kappa t}}, \tag{4.299}$$

which in the $t \to \infty$ limit coasts with the speed $\dot{x}(t) \equiv |V| \to \xi$. The corresponding proper acceleration is,

$$\alpha(t) = -\frac{2\kappa\xi e^{2\kappa t}(1+e^{2\kappa t})}{\left[(1+e^{2\kappa t})^2 - \xi^2 e^{4\kappa t}\right]^{3/2}}, \tag{4.300}$$

where

$$\lim_{t\to\infty}\alpha(t) = 0. \tag{4.301}$$

The transcendental inversion of Eq. (4.298) is,

$$t(x) = \frac{1}{2\kappa}\ln\left(e^{-\frac{2\kappa x}{\xi}} - 1\right). \tag{4.302}$$

So, the trajectories of the drifting Logex mirror in spacetime coordinates are invertible. However, it is difficult to define the ray-tracing functions in null coordinates.

DL: Energy

The expectation value of the drifting Logex mirror energy flux is [34],

$$F(t) = \frac{\kappa^2 \xi \left(e^{2\kappa t} + e^{4\kappa t}\right) \left[\left(\xi^2 - 1\right) e^{6\kappa t} + \left(2\xi^2 - 1\right) e^{4\kappa t} + e^{2\kappa t} + 1\right]}{3\pi \left[(\xi - 1)e^{2\kappa t} - 1\right]^2 \left[(\xi + 1)e^{2\kappa t} + 1\right]^4}, \tag{4.303}$$

the graphical illustration of which is demonstrated in Fig. (4.114).

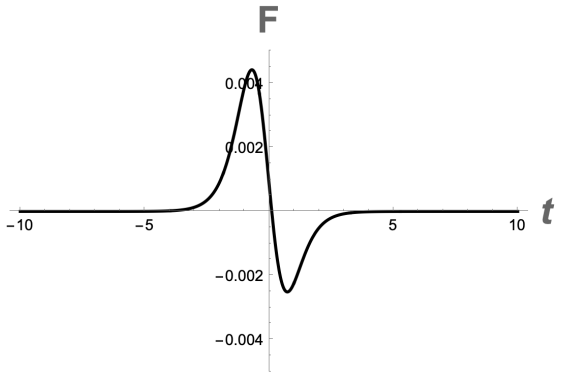

Figure 4.114: Drifting Logex mirror energy flux, with $\xi = \frac{1}{2}$.

The energy flux has a strong initial positive peak at early time and subsequent negative value at late time. This is the first mirror found that has a non-monotonic pulse of emission at high speeds before settling down to thermal equilibrium. The energy emitted is finite,

$$E = \frac{\kappa}{48\pi} \left[\frac{(1+\xi)^2 \tanh^{-1}(\xi) - \xi(1+2\xi)}{\xi(1+\xi)}\right]. \tag{4.304}$$

This result is consistent with the numerical verification of the energy found via the beta Bogolubov coefficient using Eq. (3.95).

DL: Particles

The beta Bogolubov coefficient of the drifting Logex mirror is as follows [34],

$$\beta_{\omega\omega'} = \frac{\sqrt{\omega\omega'}}{2\pi\kappa\omega_n} B\left[-\frac{i\omega_p}{2\kappa}, \frac{i(\omega_p + \xi\omega_n)}{2\kappa}\right]. \tag{4.305}$$

$\omega_p \equiv \omega + \omega'$, $\omega_n \equiv \omega - \omega'$, and $B(m, n)$ is the beta function. The complex conjugate squaring of Eq. (4.305) yields,

$$|\beta_{\omega\omega'}|^2 = \frac{\omega\omega'}{4\pi^2\kappa^2\omega_n^2} \left| B\left[\frac{i\omega_p}{2\kappa}, -\frac{i(\omega_p + \xi\omega_n)}{2\kappa}\right]\right|^2. \tag{4.306}$$

The numerical result for the DL mirror particle spectrum is demonstrated in Fig. (4.115).

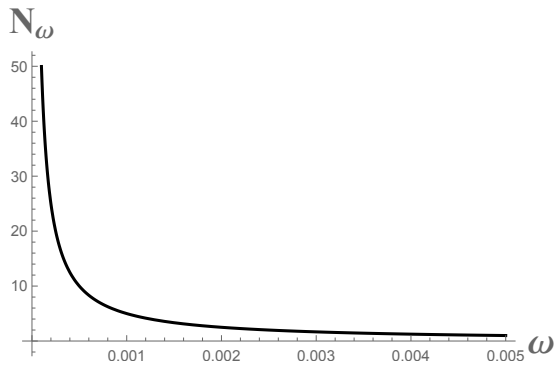

Figure 4.115: Drifting Logex mirror particle spectrum, with $\xi = \frac{1}{2}$.

The spectrum obeys beta function distribution and is divergent, i.e. there is infinite soft particle production.

DL: Entropy

The entanglement entropy of the drifting Logex mirror simply is,

$$S(t) = \frac{1}{6} \tanh^{-1}\left(\frac{\xi e^{2\kappa t}}{1+e^{2\kappa t}}\right), \tag{4.307}$$

whose plot is given in Fig. (4.116).

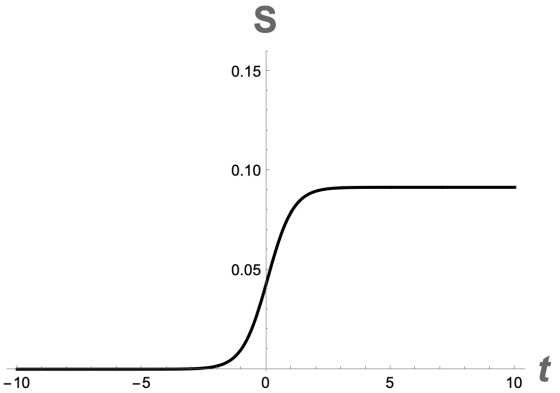

Figure 4.116: Drifting Logex mirror entropy, with $\xi = \frac{1}{2}$.

Similar to the other drifting mirrors, the DL mirror entropy also increases at early-times and becomes constant at late-times, i.e. the unitarity is preserved.

4.8.5 Drifting Davies-Fulling

DDF: Dynamics

The drifting cousin of the Davies-Fulling mirror trajectory is [32, 36],

$$x(t) = -\frac{\xi}{\kappa}\ln[\cosh(\kappa t)], \tag{4.308}$$

where ξ is the maximum drifting speed of the mirror ranging as $0 < \xi < 1$. The dynamics of the DDF mirror is depicted is Fig. (4.117).

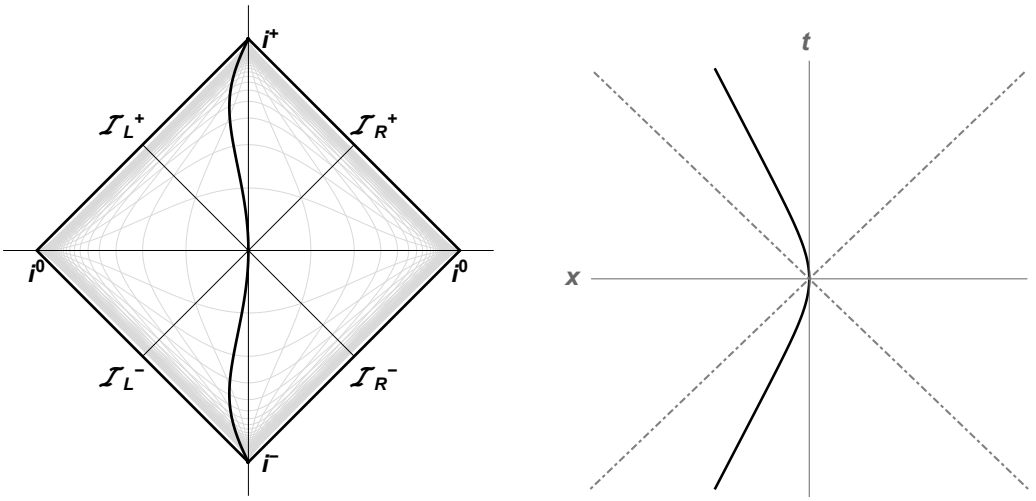

Figure 4.117: a) Penrose and b) Spacetime diagrams for the drifting Davies-Fulling mirror trajectory, with $\xi = \frac{1}{2}$.

As can be seen from the figure, the DDF mirror trajectory looks similar to the Self-dual mirror trajectory, Fig. (4.25). The difference is that the first mirror is drifting on both sides, i.e. it does not start asymptotically static. The mirror velocity is,

$$\dot{x}(t) = -\xi\tanh(\kappa t), \tag{4.309}$$

which in the $t \to \infty$ limit coasts with the speed $\dot{x}(t) \equiv |V| \to \xi$. The corresponding proper acceleration is,

$$\alpha(t) = -\frac{\kappa\xi\,\mathrm{sech}^2(\kappa t)}{\left[1-\xi^2\tanh^2(\kappa t)\right]^{3/2}}, \tag{4.310}$$

where

$$\lim_{t\to\infty}\alpha(t) = 0. \tag{4.311}$$

The transcendental inversion of Eq. (4.308) is,

$$t(x) = \frac{1}{\kappa}\cosh^{-1}\left(e^{-\frac{\kappa x}{\xi}}\right), \tag{4.312}$$

whereas it is difficult to define the ray-tracing functions in null coordinates.

DDF: Energy

The expectation value of the drifting Davies-Fulling mirror energy flux is [32],

$$F(t) = \frac{\kappa^2}{12\pi} \frac{\xi \tanh(\kappa t) \text{sech}^4(\kappa t) \left[2\xi^2 + (\xi^2 - 1)\cosh(2\kappa t) - 1\right]}{\left[\xi \tanh(\kappa t) - 1\right]^2 \left[\xi \tanh(\kappa t) + 1\right]^4}, \tag{4.313}$$

the graphical illustration of which is demonstrated in Fig. (4.118).

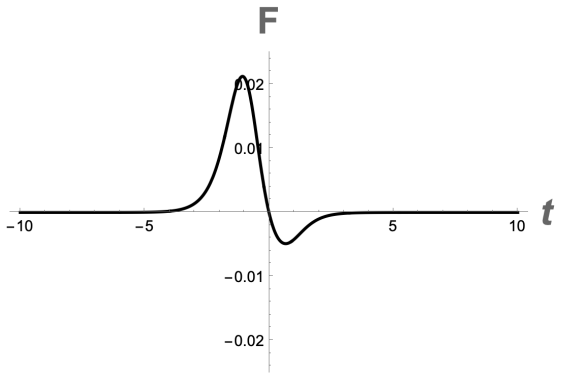

Figure 4.118: Drifting Davies-Fulling mirror energy flux, with $\xi = \frac{1}{2}$.

Similar to other drifting mirrors, the DDF mirror energy flux has a strong initial peak at early time and subsequent negative value at late time. The emitted energy is finite,

$$E = \frac{\kappa}{48\pi} \left[\left(2\gamma^2 - 3\right) + \frac{(4\gamma^2 - 3)\tanh^{-1}\xi}{\gamma^2 \xi} \right], \tag{4.314}$$

where $\gamma \equiv \frac{1}{\sqrt{1-\xi^2}}$. This result is consistent with the numerical verification of the energy found via the beta Bogolubov coefficient using Eq. (3.95).

DDF: Particles

The beta Bogolubov coefficient of the drifting Davies-Fulling mirror is [32],

$$\beta_{\omega\omega'} = \frac{2^{\frac{i\xi\omega_n}{\kappa}}\sqrt{\omega\omega'}}{2\pi\kappa\omega_n} B\left[\frac{i}{2\kappa}\left(\xi\omega_n - \omega_p\right), \frac{i}{2\kappa}\left(\xi\omega_n + \omega_p\right)\right], \tag{4.315}$$

where $\omega_p \equiv \omega + \omega'$, $\omega_n \equiv \omega - \omega'$, and $B(m,n)$ is the beta function. The complex conjugate squaring of Eq. (4.315) yields,

$$|\beta_{\omega\omega'}|^2 = \frac{\xi}{2\pi\kappa\omega_n} \frac{\left(\omega_p^2 - \omega_n^2\right)}{\left(\xi^2\omega_n^2 - \omega_p^2\right)} \frac{\sinh\left(\frac{\pi\xi\omega_n}{\kappa}\right)}{\cosh\left(\frac{\pi\xi\omega_n}{\kappa}\right) - \cosh\left(\frac{\pi\omega_p}{\kappa}\right)}. \tag{4.316}$$

The numerical result for the DDF mirror particle spectrum is demonstrated in Fig. (4.119).

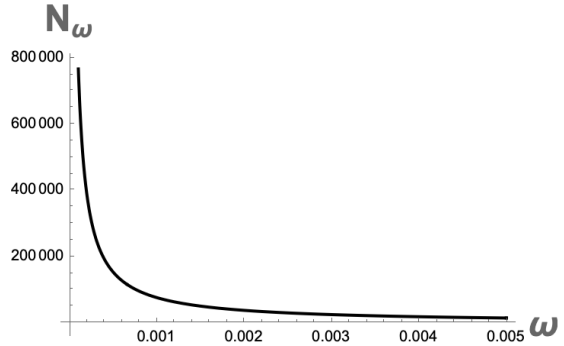

Figure 4.119: Drifting Davies-Fulling mirror particle spectrum, with $\xi = \frac{1}{2}$.

Even though the energy emission of the drifting Davies-Fulling is finite, the particle spectrum is divergent, i.e. there is infinite soft particle production.

DDF: Entropy

The entanglement entropy of the drifting Davies-Fulling mirror simply is,

$$S(t) = \frac{1}{6}\tanh^{-1}[\xi \tanh(\kappa t)], \tag{4.317}$$

whose plot is given in Fig. (4.120).

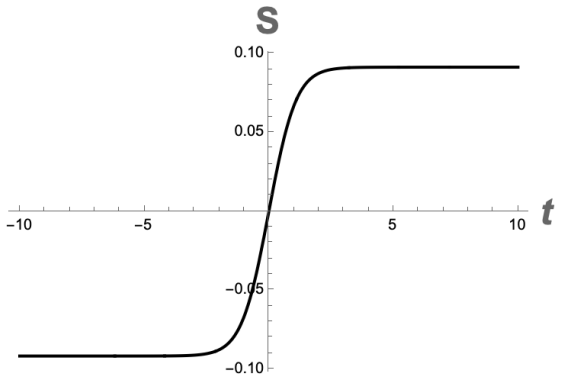

Figure 4.120: Drifting Davies-Fulling mirror entropy, with $\xi = \frac{1}{2}$.

The entropy is negative at early times and becomes positively constant at late times, i.e. there is no information loss.

BLANK

Chapter 5

Conclusions

This dissertation is dedicated to investigating the black hole evaporation process in the framework of the moving mirror model. It was examined both historically and mathematically. The accelerated boundary models were proven to have undergone many changes as well as improvements. The moving mirror was used to explain both the direct explanation of radiation by black holes and the hypothetical processes that emerged as a result of the Hawking effect. The trajectories whose outputs exactly align with the findings of the corresponding physical process, as well as recommendations for a possible solution to the information loss problem, are particularly noteworthy.

The main aspects of the theory of quantum fields in both flat and curved spacetimes are briefly described. The prime quantities of interest used to investigate each mirror model in detail in the main part of the thesis are derived, and some integration formulas for certain physical quantities are provided. The basic derivations include dynamical quantities such as trajectories in spacetime and null coordinates, velocity, rapidity, and acceleration; quantum stress-energy tensor (flux) obtained via two distinct methods (point-splitting and conformal anomaly); radiation energy and particle energy; particle spectrum and total number of particles; the entanglement entropy, formulated in terms of rapidity of a mirror; mirror radiation power; and mirror self-force. The last two quantities were derived relatively recently in the framework of the moving mirrors and are presented here as a guide for understanding some relevant recent works on mirror/electron equivalence and future research direction. Moreover, it is interesting to note that some mirror trajectories are well-defined in both spacetime and null coordinates. In contrast, some trajectories are tractable only in certain coordinates (t, x, u, or v), or coordinate systems: null or spacetime.

The fourth chapter, the main part of this thesis work, presented a complete collection of trajectories with solved beta Bogolubov coefficients. Also, the graphs of all the trajectories, the corresponding energy fluxes, particle spectrum, and entanglement entropy of a system were given. Therefore direct behavioral comparison becomes possible. In total, 30 moving mirror trajectories are classified according to their dynamical behavior and similar radiation scenarios. The analysis and summary of the detailed study of each of these mirror models and the corresponding classifications bring us to the following insights and some new results:

The ***canonical*** mirrors, historically the first trajectories proposed, have global particle and energy counts that are infinite, with the information loss during the evaporation

process. All four mirrors move with the speed of light in the far future with an infinite acceleration. The mirror ray-tracing functions are all tractable in both null and spacetime coordinates. This set is supplemented by adding the trajectories in x space coordinate for the DF and CW mirrors, Eqs. (4.5) and (4.25), respectively. The DF and UA mirrors' trajectories have symmetric behavior with respect to the x space coordinate. The Schwarzschild mirror energy flux as a function of x space coordinate is independent of the black hole horizon location, Eq. (4.41). All four mirrors have the entanglement entropy that diverges at late times. Moreover, it is found that the CW mirror entropy density has a one-to-one correspondence with the thermodynamic entropy density, Eq. (4.34).

The ***static*** mirrors are arguably the most physical in the moving mirror model since they solve the problems associated with the Hawking radiation. Namely, static mirrors have finite total particles and finite energy emission, and unitarity is preserved. No null horizons and mirrors move with a velocity less than the speed of light, becoming asymptotically static in the past and future. The energy flux for all five solutions contains, at some point, a negative value. The WD and SP mirrors are well defined in (x, v) coordinates, where for the first mirror, the trajectory in v coordinate is found, Eq. (4.48). For the Arctx, SD, and GL mirrors, the trajectories are well defined in spacetime coordinates, which is supplemented by adding the trajectories in x space coordinate, Eqs. (4.58), (4.73) and (4.83), respectively. The key feature of the SD mirror is that it has a symmetric behavior in time that results in the same energy on both the left and right sides of the mirror. The key feature of the SP mirror is that it is the only asymptotically static mirror that has thermal radiation at some periods in time, with the flux radiation and finite energy as presented in Eqs. (4.94) and (4.95). The WD mirror's $f(v)$ trajectory allows us to find the corresponding energy flux and the beta coefficient in slightly simpler forms, Eqs. (4.50) and (4.52), compared to the same quantities found using the original $t(x)$ trajectory. Moreover, the analytic form of the SD mirror beta coefficient is presented, Eq. (4.76). A numerical calculation of the particle count for all five mirrors gives a finite but small number relative to 1. The entanglement entropy has no divergence over all times. However, each of these five mirrors has different entropy behavior with respect to each other.

The ***null*** mirrors stand out because of having thermal radiation at some periods in time, with infinite energy $\&$ particle production and information loss. The DT mirror is unique because it emits radiation at two different temperatures, corresponding to thermal equilibrium at late times and non-thermal transition states. The radiation occurring near the horizon is hotter than the radiation occurring early. For the Logex and Evans mirrors, the trajectories are well defined in both null and spacetime coordinates, which is supplemented by adding the trajectories in x space coordinate, Eqs. (4.105) and (4.113). For the DT mirror, the trajectories are well defined in null coordinates, which

is supplemented by adding the trajectory is u coordinate, Eq. (4.121). However, the ray-tracing functions in spacetime coordinates are intractable. Moreover, the analytic form of the DT mirror beta coefficient is presented in Eq. (4.127). The entanglement entropy of the mirrors is shown to be divergent at late or early times.

The ***black hole null*** mirrors are the most interesting ones since they correspond to the well-known black hole models approximated to (1+1)-dimensions, except the CGHS and Taub-NUT cases, which are themselves simplified (1+1)D black hole toy models. All mirrors have a monotonic approach to thermal equilibrium at late times, with infinite energy, particle production, and information loss. The CGHS and Taub-NUT mirrors are one-parameter systems, while the RN and Kerr mirror models have two parameters that complicate the calculations of some significant quantities. All black hole null mirrors have qualitatively similar dynamics: trajectories start asymptotically static and go to infinite acceleration in the far future. All these mirrors have an event horizon. The CGHS mirror ray-tracing functions are tractable in both null and spacetime coordinates. However, the RN, Kerr, and Taub-NUT mirrors' trajectories are tractable only in v null coordinate. The original RN mirror trajectory is rewritten more compactly, Eq. (4.145). Similar to the Schwarzschild mirror case, the CGHS mirror flux as a function of x coordinate is independent of the horizon location, Eq. (4.140). It can be assumed that this fact is true for all black hole null mirrors. The analytic forms of the Kerr and Taub-NUT mirrors' beta coefficients are presented in Eqs. (4.158) and (4.166). All the mirrors have qualitatively similar entropy behavior: monotonic increase at early times and divergence at the horizon.

The ***extremal null*** mirrors' key feature is that they emit finite energy. However, there is infinite soft particle production, and information is lost. The mirrors have qualitatively similar dynamics: trajectories start motion inertial at rest, then approach uniform acceleration asymptotically. All the mirrors are tractable only in v null coordinate; the exception is the extremal Reissner-Nordström mirror trajectory, which is also tractable in x space coordinate. The original extremal Kerr mirror trajectory is rewritten in terms of the black hole analog moving mirror quantity, Eq. (4.181). The energy flux for all the mirrors vanishes near the horizon. The analytic forms of the extremal Kerr and extremal Kerr-Newman mirrors' beta coefficients are presented, Eqs. (4.187) and (4.197). The mirrors have qualitatively similar entropy as the other black hole null mirrors.

The ***cosmo null*** mirrors are unusual since they have two asymptotic null horizons with thermal radiation emission overall times, infinite particle production, and information loss. The Schwarzschild de Sitter mirror is unique because it has thermal flux for the past and future periods separately. Surprisingly, the AdS mirror travels to the right with the asymptotic uniform acceleration in the far past and future, Eq. (4.214). The dS and AdS mirrors are well-defined in null coordinates. This set is supplemented by adding the AdS mirror ray-tracing function in u coordinate, Eq.

(4.211). However, the trajectories in spacetime coordinates are not tractable. For the dS mirror, the radiation energy is infinite, while the energy of particles is finite. For the AdS mirror, the radiation energy is finite but negative, Eq. (4.216), due to the corresponding constant negative flux over all times. Due to the complex form of the trajectory, the SdS mirror ray-tracing function is tractable only in v coordinate. All three mirrors have entanglement entropy that diverges at their horizons, with the AdS mirror entropy being negative over the whole region bounded by its horizons.

The ***inertial null*** mirrors resemble usual black hole and extremal null mirrors. The difference is that the first mirrors have zero proper acceleration in the asymptotic future. All three inertial null solutions admit negative energy flux at some point and have finite total energy emission with thermal radiation. However, the mirrors suffer from soft infinite particle production, and information is lost. The mirrors are well-defined in both null and spacetime coordinates. For the Proex mirror, this set is supplemented by adding the trajectory in x coordinate, Eq. (4.237). For the Inertial horizon mirror, this set is supplemented by adding the trajectories in (u, t) coordinates, Eqs. (4.247) and (4.248b). For the Light-Airy mirror, this set is supplemented by adding the trajectory in u coordinate, Eq. (4.258). All three solutions have divergent entropy in future times.

The ***drifting*** mirrors are unique models because of the formation of a special object known as the "remnant" when the black hole evaporation process stops. In this case, the energy emission is finite, and the unitarity is preserved. However, the mirrors suffer from infinite soft particle production. The mirrors coast with a velocity less than the speed of light at late times with zero proper acceleration. The ray-tracing functions of the drifting Schwarzschild mirror can be written in more compact forms, Eq. (4.268). It is seen that $p(u)$ and $f(v)$ trajectories have unexpected symmetry. Drifting Schwarschild and drifting Proex mirrors are well-defined in both spacetime and null coordinates. This set is supplemented by adding the trajectories in (u, v) coordinates for the DProex mirror, Eqs. (4.290) and (4.291). However, the drifting CGHS, drifting Logex and drifting Davies-Fulling solutions are tractable only in spacetime coordinates. This set is supplemented by adding the trajectories in x coordinate for the respective mirrors, Eqs. (4.281), (4.302) and (4.312). The drifting CGHS mirror beta coefficient is derived in a slightly simplified form, Eq. (4.284). All the drifting mirror models have non-divergent entropy, indicating no information loss.

Overall, a comprehensive analysis and investigation of all the known existing moving mirror models have been accomplished. One can use this collection of trajectories as a handbook with all the noteworthy descriptions of their features and importance.

As a direction for future studies, it is possible to extend the work done in this thesis by investigating further the correspondence between the particular moving mirror and an electron. Namely, where possible, the quantities of interest here will be Larmor power and self-force for the moving mirror models. Another possible direction

to study is to investigate the drifting cases of all the moving mirror models. This might help further find mirror solutions to the issues associated with the black hole evaporation process. Moreover, finding a Lagrangian and the action corresponding to the mirror models will be interesting. In this case, one needs to use the moving backward technique, starting from a mirror trajectory to a corresponding Lagrangian or an action. The exception will be the well-known black hole and extremal black hole models whose actions and Lagrangians are already known. In these cases, the straightward method finds the analog moving mirror trajectories, starting from the corresponding line element. Furthermore, an interesting but challenging investigation will be the study of the mirror analog of the more complicated cosmological models such as the Schwarzschild Anti-de Sitter, Reissner-Nordström de Sitter, Reissner-Nordström Anti-de Sitter, Kerr de Sitter, and Kerr Anti-de Sitter backgrounds. Captivatingly, studying the right-hand side of the Einstein field equations with matter, i.e. the stress-energy tensor, in the framework of the moving mirror, is another idea for future research direction. In addition, it will be particularly important to find a relation between different formulations of entropy, including the von Neumann entanglement entropy of a moving mirror, Bekenstein-Hawking entropy and et. al. Finally, it will be fascinating to study more comprehensively a relation between the conformal field theory and a moving mirror as the first has particularly significant physical effects in (1+1) dimensions. Understanding the implications of the CFT in mirror models might help one to explain more rigorously the black hole near-horizon physics as the boundary of the black hole is described by quantum physics. Globally, this means we might come one step closer to understanding quantum gravity since black holes are considered quantum gravitational objects.

BLANK

Bibliography

[1] S. W. Hawking, "Particle creation by black holes," *Communications In Mathematical Physics*, vol. 43, no. 3, pp. 199–220, 1975.

[2] S. A. Fulling and P. C. W. Davies, "Radiation from a moving mirror in two dimensional space-time: Conformal anomaly," *Proceedings of the Royal Society A: Mathematical, Physical and Engineering Sciences*, vol. 348, no. 1654, pp. 393–414, 1976.

[3] P. C. W. Davies and S. A. Fulling, "Radiation from moving mirrors and from black holes," *Proceedings of the Royal Society A: Mathematical, Physical and Engineering Sciences*, vol. 356, no. 1685, pp. 237–257, 1977.

[4] H. Casimir, "On the attraction between two perfectly conducting plates," *Proceedings of the KNAW*, vol. 51, no. 7, p. 793–795, 1948.

[5] G. T. Moore, "Quantum theory of the electromagnetic field in a variable-length one-dimensional cavity," *Journal of Mathematical Physics*, vol. 11, no. 9, pp. 2679–2691, 1970.

[6] S. A. Fulling, "Nonuniqueness of canonical field quantization in riemannian space-time," *Physical Review D*, vol. 7, no. 10, pp. 2850–2862, 1973.

[7] N. D. Birrell and P. C. W. Davies, *Quantum fields in curved space*. Cambridge University Press, 1982.

[8] A. Fabbri and J. Navarro-Salas, *Modeling black hole evaporation*. London, UK: Imperial College Press, 2005.

[9] B. S. DeWitt, "Quantum field theory in curved spacetime," *Physics Reports*, vol. 19, no. 6, pp. 295–357, 1975.

[10] W. G. Unruh, "Notes on black hole evaporation," *Physical Review D*, vol. 14, no. 4, p. 870, 1976.

[11] W. R. Walker and P. C. W. Davies, "An exactly soluble moving-mirror problem," *Journal of Physics A: Mathematical and General*, vol. 15, no. 9, pp. L477–L480, 1982.

[12] W. R. Walker, "Particle and energy creation by moving mirrors," *Physical Review D*, vol. 31, no. 4, pp. 767–774, 1985.

[13] W. G. Unruh and R. M. Wald, "Acceleration radiation and the generalized second law of thermodynamics," *Physical Review D*, vol. 25, no. 4, pp. 942–958, 1982.

[14] W. R. Walker, "Negative energy fluxes and moving mirrors in curved space," *Classical and Quantum Gravity*, vol. 2, no. 2, pp. L37–L40, 1985.

[15] R. D. Carlitz and R. S. Willey, "Reflections on moving mirrors," *Physical Review D*, vol. 36, no. 8, pp. 2327–2335, 1987.

[16] M. Reuter, "Hawking radiation and the virasoro algebra," *Classical and Quantum Gravity*, vol. 6, no. 8, pp. 1149–1158, 1989.

[17] S. M. Christensen and S. A. Fulling, "Trace Anomalies and the Hawking Effect," *Physical Review D*, vol. 15, pp. 2088–2104, 1977.

[18] F. Wilczek, "Quantum purity at a small price: Easing a black hole paradox," in *International Symposium on Black holes, Membranes, Wormholes and Superstrings*, pp. 1–21, 1993.

[19] M. Hotta, M. Shino, and M. Yoshimura, "Moving mirror model of hawking evaporation," *Progress Of Theoretical Physics*, vol. 91, no. 5, pp. 839–870, 1994.

[20] N. Obadia and R. Parentani, "Notes on moving mirrors," *Physical Review D*, vol. 64, no. 4, p. 044019, 2001.

[21] N. Obadia and R. Parentani, "Uniformly accelerated mirrors. i. mean fluxes," *Physical Review D*, vol. 67, no. 2, p. 024021, 2003.

[22] N. Obadia and R. Parentani, "Uniformly accelerated mirrors. ii. quantum correlations," *Physical Review D*, vol. 67, no. 2, p. 024022, 2003.

[23] M. R. R. Good, P. R. Anderson, and C. R. Evans, "Time dependence of particle creation from accelerating mirrors," *Physical Review D*, vol. 88, no. 2, p. 025023, 2013.

[24] M. R. R. Good and Y. C. Ong, "Are black holes springlike?," *Physical Review D*, vol. 91, no. 4, p. 044031, 2015.

[25] P. R. Anderson, M. R. R. Good, and C. R. Evans, "Black hole - moving mirror i: An exact correspondence," in *Proceedings, 14th Marcel Grossmann Meeting*, vol. 2, pp. 1701–1704, 2017.

[26] M. R. R. Good, P. R. Anderson, and C. R. Evans, "Black hole - moving mirror ii: Particle creation," in *Proceedings, 14th Marcel Grossmann Meeting*, vol. 2, pp. 1705–1708, 2017.

[27] M. R. R. Good, P. R. Anderson, and C. R. Evans, "Mirror reflections of a black hole," *Physical Review D*, vol. 94, p. 065010, 2016.

[28] M. R. R. Good, "Reflections on a black mirror," in *Proceedings, 2nd LeCosPA Symposium*, pp. 560–565, 2017.

[29] M. R. R. Good, K. Yelshibekov, and Y. C. Ong, "On horizonless temperature with an accelerating mirror," *Journal of High Energy Physics*, vol. 2017, no. 3, p. 13, 2017.

[30] M. R. R. Good, Y. C. Ong, A. Myrzakul, and K. Yelshibekov, "Information preservation for null shell collapse: a moving mirror model," *General Relativity and Gravitation*, vol. 51, no. 7, p. 92, 2019.

[31] A. Myrzakul and M. R. R. Good, "Unitary evaporation via modified Regge-Wheeler coordinate," in *Proceedings, 15th Marcel Grossmann Meeting*, World Scientific, 7 2022.

[32] M. R. R. Good and E. V. Linder, "Slicing the Vacuum: New Accelerating Mirror Solutions of the Dynamical Casimir Effect," *Physical Review D*, vol. 96, no. 12, p. 125010, 2017.

[33] M. R. R. Good and E. V. Linder, "Finite energy but infinite entropy production from moving mirrors," *Physical Review D*, vol. 99, no. 2, p. 025009, 2019.

[34] M. R. R. Good and Y. C. Ong, "Signatures of energy flux in particle production: A black hole birth cry and death gasp," *Journal Of High Energy Physics*, vol. 07, no. 7, p. 145, 2015.

[35] M. R. R. Good, "Reflecting at the speed of light," in *Memorial Volume for Kerson Huang* (K. K. Phua, H. B. Low, and C. Xiong, eds.), pp. 113–116, 2017.

[36] M. R. R. Good and E. V. Linder, "Eternal and evanescent black holes and accelerating mirror analogs," *Physical Review D*, vol. 97, no. 6, p. 065006, 2018.

[37] W. Cong, E. Tjoa, and R. B. Mann, "Entanglement harvesting with moving mirrors," *Journal of High Energy Physics*, 2019.

[38] Y. C. Ong and M. R. R. Good, "Quantum atmosphere of Reissner-Nordström black holes," *Physical Review Research*, vol. 2, no. 3, p. 033322, 2020.

[39] M. R. R. Good and Y. C. Ong, "Particle spectrum of the Reissner–Nordström black hole," *European Physical Journal C*, vol. 80, no. 12, p. 1169, 2020.

[40] M. R. R. Good, J. Foo, and E. V. Linder, "Accelerating boundary analog of a Kerr black hole," *Classical and Quantum Gravity*, vol. 38, no. 8, p. 085011, 2021.

[41] M. R. R. Good, "Extremal Hawking radiation," *Physical Review D*, vol. 101, no. 10, p. 104050, 2020.

[42] J. Foo and M. R. R. Good, "Hawking radiation particle spectrum of a Kerr-Newman black hole," *Journal of Cosmology and Astroparticle Physics*, vol. 01, p. 019, 2021.

[43] J. Foo, M. R. R. Good, and R. B. Mann, "Analog Particle Production Model for General Classes of Taub-NUT Black Holes," *Universe*, vol. 7, no. 9, p. 350, 2021.

[44] A. Myrzakul, C. Xiong, and M. R. R. Good, "CGHS Black Hole Analog Moving Mirror and Its Relativistic Quantum Information as Radiation Reaction," *Entropy*, vol. 23, no. 12, p. 1664, 2021.

[45] M. R. R. Good, A. Zhakenuly, and E. V. Linder, "Mirror at the edge of the universe: Reflections on an accelerated boundary correspondence with de Sitter cosmology," *Physical Review D*, vol. 102, no. 4, p. 045020, 2020.

[46] D. Fernández-Silvestre, J. Foo, and M. R. R. Good, "On the duality of Schwarzschild de Sitter spacetime and moving mirror," *Classical and Quantum Gravity*, vol. 39, no. 5, p. 055006, 2022.

[47] M. R. R. Good, E. V. Linder, and F. Wilczek, "Moving mirror model for quasithermal radiation fields," *Physical Review D*, vol. 101, no. 2, p. 025012, 2020.

[48] M. R. R. Good and E. V. Linder, "Modified Schwarzschild metric from a unitary accelerating mirror analog," *New Journal of Physics*, vol. 23, no. 4, p. 043007, 2021.

[49] A. Moreno-Ruiz and D. Bermudez, "Optical analogue of the Schwarzschild–Planck metric," *Classical and Quantum Gravity*, vol. 39, no. 14, p. 145001, 2022.

[50] M. Good and E. Abdikamalov, "Radiation from an Inertial Mirror Horizon," *Universe*, vol. 6, no. 9, p. 131, 2020.

[51] M. R. R. Good, A. Mitra, and V. Zarikas, "Dual-Temperature Acceleration Radiation," *Astronomy Reports*, vol. 65, no. 10, pp. 942–946, 2021.

[52] M. R. R. Good and E. V. Linder, "Light and Airy: a simple solution for relativistic quantum acceleration radiation," *Universe*, vol. 7, no. 3, p. 60, 2021.

[53] S. M. Carroll, *Spacetime and geometry: An introduction to general relativity*. San Francisco, USA: Addison-Wesley, 2004.

[54] E. Bianchi and M. Smerlak, "Entanglement entropy and negative energy in two dimensions," *Physical Review D*, vol. 90, p. 041904, 2014.

[55] A. Zhakenuly, M. Temirkhan, M. R. R. Good, and P. Chen, "Quantum power distribution of relativistic acceleration radiation: classical electrodynamic analogies with perfectly reflecting moving mirrors," *Symmetry*, vol. 13, no. 4, p. 653, 2021.

[56] L. H. Ford and A. Vilenkin, "Quantum radiation by moving mirrors," *Physical Review D*, vol. 25, p. 2569, 1982.

[57] M. R. R. Good, *Quantized Scalar Fields Under the Influence of Moving Mirrors and Anisotropic Curved Spacetime*. PhD thesis, The University of North Carolina at Chapel Hill, 2011.

[58] S. Mukohyama and W. Israel, "Moving-mirror entropy," *Physical Review D*, vol. 62, no. 12, p. 121501, 2000.

[59] M. R. R. Good, "Spacetime continuity and quantum information loss," *Universe*, vol. 4, no. 11, 2018.

[60] M. R. R. Good, E. V. Linder, and F. Wilczek, "Finite thermal particle creation of Casimir light," *Modern Physics Letters A*, vol. 35, no. 03, p. 2040006, 2020.

[61] B. A. Juárez-Aubry, *Asymptotics in the time-dependent Hawking and Unruh effects*. PhD thesis, Nottingham U., 2017.

[62] S. Liberati, T. Rothman, and S. Sonego, "Nonthermal nature of incipient extremal black holes," *Physical Review D*, vol. 62, p. 024005, 2000.

[63] T. Rothman, "Nonthermal nature of extremal kerr black holes," *Physics Letters A*, vol. 273, no. 5, pp. 303–309, 2000.

[64] G. W. Gibbons and S. W. Hawking, "Cosmological event horizons, thermodynamics, and particle creation," *Physical Review D*, vol. 15, pp. 2738–2751, 1977.

[65] S. Bhattacharya, "Particle creation by de sitter black holes revisited," *Physical Review D*, vol. 98, p. 125013, 2018.

[66] M. R. R. Good and E. V. Linder, "Stopping to Reflect: Asymptotic Static Moving Mirrors as Quantum Analogs of Classical Radiation," *Physics Letters B*, vol. 138124, p. 2023, 2023.

[67] E. Ievlev, M. R. R. Good, and E. V. Linder, "Thermal radiation from an electron with schwarzschild-planck acceleration," *arXiv:2304.04412*, 2023.

[68] A. H. Taub, "Empty space-times admitting a three parameter group of motions," *Annals of Mathematics*, vol. 53, pp. 472–490, 1951.

[69] E. Newman, L. Tamburino, and T. Unti, "Empty space generalization of the Schwarzschild metric," *Journal of Mathematical Physics*, vol. 4, p. 915, 1963.

[70] M. R. R. Good and P. C. W. Davies, "Infrared Acceleration Radiation," *Foundations of Physics*, vol. 53, no. 3, p. 53, 2023.